AMBIENT MEASUREMENTS OF THE NO_X RESERVOIR SPECIES N_2O_5 USING CAVITY RING-DOWN SPECTROSCOPY

A Dissertation

by

JUSTINE NICOLE GEIDOSCH

Submitted to the Office of Graduate Studies of
Texas A&M University
in partial fulfillment of the requirements for the degree of

DOCTOR OF PHILOSOPHY

August 2011

Major Subject: Chemistry

Ambient Measurements of the NO_x Reservoir Species N_2O_5 using

Cavity Ring-down Spectroscopy

AMBIENT MEASUREMENTS OF THE NO_X RESERVOIR SPECIES N_2O_5 USING CAVITY RING-DOWN SPECTROSCOPY

A Dissertation

by

JUSTINE NICOLE GEIDOSCH

Submitted to the Office of Graduate Studies of
Texas A&M University
in partial fulfillment of the requirements for the degree of

DOCTOR OF PHILOSOPHY

Approved by:

Chair of Committee,	Simon W. North
Committee Members,	Robert R. Lucchese
	Emile Schweikert
	Donald Collins
Head of Department,	David H. Russell

August 2011

Major Subject: Chemistry

ABSTRACT

Ambient Measurements of the NO_x Reservoir Species N_2O_5 Using Cavity Ring-down Spectroscopy. (August 2011)

Justine Nicole Geidosch, B.S., Duquesne University

Chair of Advisory Committee: Dr. Simon W. North

The regulated control of pollutants is essential to maintaining good air quality in urban areas. A major concern is the formation of tropospheric ozone, which can be especially harmful to those with lung conditions and has been linked to the occurrence of asthma. Ozone is formed through reactions of oxidized volatile organic compounds with nitrogen oxides, and the accurate modeling of the process is necessary for smart and effective regulations. Ambient measurements are important to understanding the mechanisms involved in tropospheric chemistry.

This dissertation describes the characterization of a novel instrument for the ambient measurement of dinitrogen pentoxide, N_2O_5, and the results of several field studies. This is an important intermediate in the major nighttime loss pathway of nitrogen oxides. The understanding of this process requires correct modeling formation, as any nitrogen oxides not removed at night will result in increased ozone formation at sunrise.

Calibration studies have been performed in order to quantify the loss of reactive species within the instrument, and the sampling flow and N_2O_5 detection have been well characterized. The results of the laboratory measurements are presented.

Results are presented from the SHARP Field Study in Houston, TX in the spring of 2009. N_2O_5 measurements are compared to measurements of other species, including nitric acid and nitryl chloride, which were performed by other research groups. Mixing ratios exceeding 300 ppt were observed following ozone exceedance days, and a dependence of the concentration on both wind speed and direction was noticed. There was a strong correlation determined between N_2O_5 with HNO_3 and $ClNO_2$ indicating both a fast heterogeneous hydrolysis and N_2O_5 as the primary source of the species. Observed atmospheric lifetimes for N_2O_5 were short, ranging from several seconds to several minutes.

We have also investigated the presence of N_2O_5 in College Station, TX. Low mixing ratios peaking at approximately 20 ppt were observed, with longer atmospheric lifetimes of up to several hours. The role of biogenic emissions in the NO_3-N_2O_5 equilibrium is discussed.

Per mio nonno

ACKNOWLEDGEMENTS

This work has certainly been a collaborative effort and would not have been possible without the support of many people. I, first and foremost, must thank my advisor, Dr. Simon North. His knowledge and advisement in the subject area were essential, but his patience and compassion certainly have made him an exceptional person for whom to work. The members of my committee, Dr. Don Collins, Dr. Robert Lucchese, and Dr. Emile Schweikert, have been consistently supportive and always willing to give their advice.

I must express my gratitude to Prof. Barry Lefer and his research group at the University of Houston. Their advice, assistance, and crash courses in meteorology have made me feel like an adopted group member, and I appreciate their acceptance of a chemist into the group.

The members of the North Research Group have taught me much about myself. It is strange to have seen the evolution of the group over the past five years; going from the new young kid to the jaded old lady seems to have happened overnight. The motivation of the current generation is unmatched, and I am excited to see what they bring to the future.

I would have never made it this far if not for the support of my family and friends. They have put up with my missed holidays and unreturned phone calls, and still have continued to be my biggest cheerleaders. Thank you.

NOMENCLATURE

CIMS	Chemical Ionization Mass Spectrometry
CRDS	Cavity Ring-down Spectroscopy
DMS	Dimethyl Sulfide
DMSO	Dimethyl Sulfoxide
DOAS	Differential Optical Absorption Spectroscopy
EPA	Environmental Protection Agency
FEP	Fluorinated Ethylene Polypropylene
HRVOC	Highly Reactive Volatile Organic Compound
LIF	Laser-induced Fluorescence
MFC	Mass Flow Controller
NAAQS	National Ambient Air Quality Standards
NBL	Nocturnal Boundary Layer
NOAA	National Oceanic and Atmospheric Administration
NO_X	Nitrogen Oxides
PBL	Planetary Boundary Layer
PMT	Photomultiplier Tube
ppb	Parts per Billion
ppt	Parts per Trillion
PTFE	Polytetrafluoroethylene
sccm	Standard Cubic Centimeters Per Minute

SIP	State Implementation Plan
SLPM	Standard Liters Per Minute
TCEQ	Texas Commission on Environmental Quality
TexAQS	Texas Air Quality Study
VOC	Volatile Organic Compound
YAG	Yttrium Aluminum Garnet

TABLE OF CONTENTS

CHAPTER Page

LIST OF FIGURES

FIGURE Page

FIGURE Page

FIGURE Page

FIGURE Page

FIGURE Page

LIST OF TABLES

CHAPTER I

INTRODUCTION

I.1 Motivation for Ambient Measurements of N_2O_5

With increased industrialization and the continued use of fossil fuels as an energy source, air quality analysis and an understanding of tropospheric processes has become a challenge especially in urban and industrial areas. In 1990, Congress amended the Clean Air Act to require the Environmental Protection Agency (EPA) to regulate the concentrations of certain pollutants deemed harmful to human health. The atmospheric mixing ratio of multiple species is limited to certain values, known as National Ambient Air Quality Standards (NAAQS), and the current values are shown in Table 1.1. Nitrogen oxides (NO_X) are the sum of both nitric oxide (NO) and nitrogen dioxide (NO_2). The photochemical cycling between NO and NO_2 is important in the formation of another tropospheric pollutant, ozone. Ozone (O_3) is a highly regulated species as it is detrimental to human respiratory systems. It especially affects those in already sensitive groups such as those with asthma or other lung diseases [*Finlayson-Pitts and Pitts*, 1999].

This dissertation follows the style of *Journal of Geophysical Research*.

Table 1.1. Current National Ambient Air Quality Standards as regulated by the EPA.

Pollutant	Standard	Averaging Time
Carbon Monoxide	9 ppm	8 hour
	35 ppm	1 hour
Lead	0.15 μg/m^3	3 month
	1.5 μg/m^3	Quarterly
Nitrogen Dioxide	53 ppb	Annual
	100 ppb	1 hour
Particulate Matter, PM_{10}	150 μg/m^3	24 hour
Particulate Matter, $PM_{2.5}$	15.0 μg/m^3	Annual
	35 μg/m^3	24 hour
Ozone	75 ppb	8 hour
	120 ppb	1 hour
Sulfur Dioxide	30 ppb	Annual
	140 ppb	24 hour
	75 ppb	1 hour

Dintrogen pentoxide, or N_2O_5, chemistry is especially important to the understanding, and subsequently regulation, of two of these compounds, NO_2 and ozone. N_2O_5 is a key intermediate involved in the primary nocturnal NO_X removal pathway and thus will also impact the subsequent day ozone formation [*Brasseur et al.*, 1999]. It is therefore important to understand the chemistry of N_2O_5.

Species regulated through the NAAQS are all primary pollutants emitted directly from sources with the exception of ozone. Ozone is formed through the oxidation of volatile organic compounds (VOCs), represented as RH, initiated by reaction with hydroxyl radical producing alkyl radicals.

$$RH + OH \rightarrow R + H_2O \qquad (1.1)$$

This reaction determines the atmospheric lifetime of VOCs. Typically the VOC is a non-methane hydrocarbon (NMHC) emitted through either vehicle exhaust or industrial processing. The resulting alkyl radical reacts rapidly with an oxygen molecule to produce an alkyl peroxy radical, RO_2. The alkyl peroxy radical reacts with nitric oxide emissions to produce nitrogen dioxide.

$$RO_2 + NO \rightarrow RO + NO_2 \tag{1.2}$$

This results in an alkoxy radical, RO, which will react with oxygen, forming a hydroperoxy radical.

$$RO + O_2 \rightarrow HO_2 + RCHO \tag{1.3}$$

The hydroperoxy radical behaves similar to RO_2 and produces another molecule of nitrogen dioxide.

$$HO_2 + NO \rightarrow OH + NO_2 \tag{1.4}$$

Nitrogen dioxide photolyzes at wavelengths shorter than 420 nm and results in the production of a ground state oxygen atom, $O(^3P)$.

$$NO_2 + h\upsilon \rightarrow NO + O \tag{1.5}$$

The oxygen atom will then quickly react with an oxygen molecule, forming ozone.

$$O + O_2 + M \rightarrow O_3 + M \tag{1.6}$$

This leaves an overall net production of two ozone molecules along with an oxidized VOC as an aldehyde or ketone [*Brasseur et al.*, 1999].

$$RH + 4O_2 + h\upsilon \rightarrow RCHO + H_2O + 2O_3 \qquad (1.7)$$

The NO_X compounds act as a catalyst in this cycle, and are generated to go on and react with additional peroxy or alkyl peroxy radicals. This means that the ozone production cycle can continue as long as there are significant emissions of VOCs and OH. A major source of OH is the photolysis of ozone to form $O(^1D)$, which then reacts with water form two more hydroxyl radicals [*Singh et al.*, 1995].

The regulation of harmful pollutants relies on the ability to successfully model tropospheric processes. The photochemical cycle is not active at night which gives the atmosphere a chance to remove nitrogen oxides. However, any NO_X compounds that are not removed from the gas phase at night will remain to catalyze the ozone cycle the following day and can do so with increased efficiency of up to three total ozone molecules per NO_x [*Ryerson et al.*, 2001]. It is therefore important to understand and have to ability to successfully model NO_X loss at night.

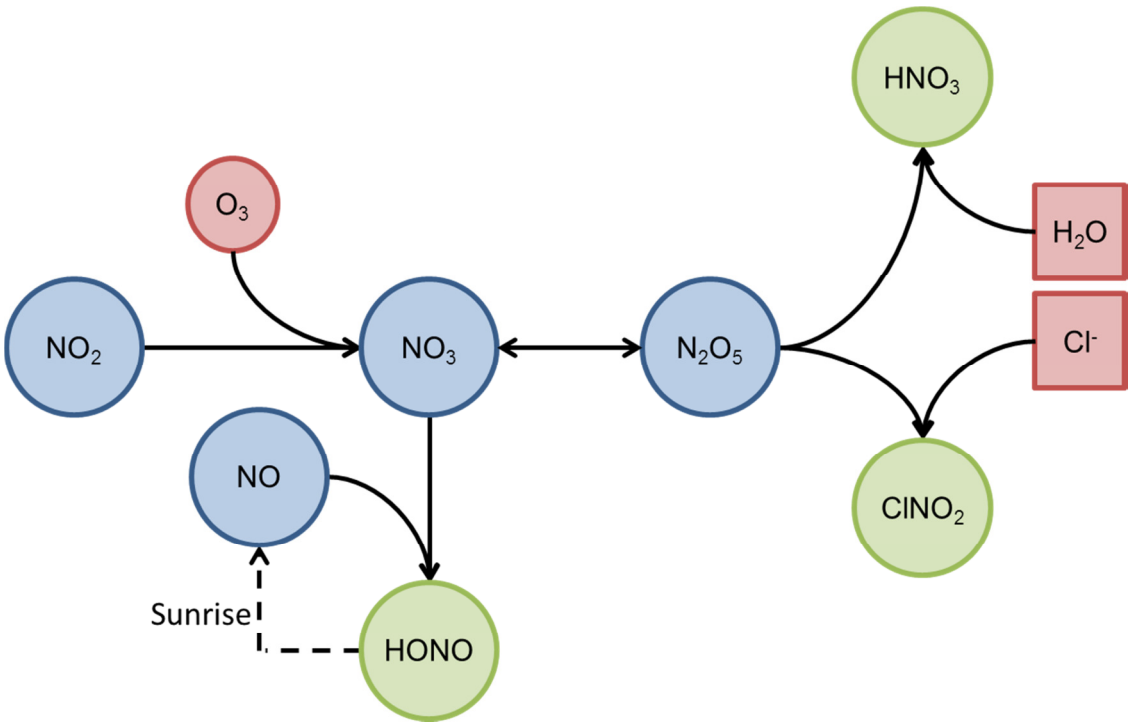

Figure 1.1. Nighttime loss and storage pathways of nitrogen oxides in the troposphere. Nitrogen-containing intermediate species are shown in blue, with sinks in green, and other species shown in red. Gaseous species are indicated by circles and aerosol particles in squares.

I.2 Nighttime Loss Pathways of Nitrogen Oxides

It is important that the nighttime loss pathways of nitrogen oxides are well understood in order to ensure efficient modeling of daily ozone formation and effective pollutant regulation. As shown in Figure 1.1, NO_3 and N_2O_5 are key intermediates in the destruction of nitrogen oxides. While the fast photolysis of NO_3 during the day prevents appreciable loss through the mechanism, in the absence of the photolytic pathways at night up to one third of total daily NO_X removal can occur in this way, with the remaining lost during daytime reactions with hydroxyl radical [*Brown et al.*, 2004; *Dentener and Crutzen*, 1993; *Platt et al.*, 1984; *Wayne et al.*, 1991].

Initially, ozone oxidizes NO_2 forming NO_3 [*Sander et al.*, 2006].

$$NO_2 + O_3 \rightarrow NO_3 + O_2 \qquad (1.8)$$

$$k_1 = 3.5 \times 10^{-17}\ cm^3\ s^{-1}$$

During the day, the atmospheric lifetime of the nitrate radical is short and typically less than 5 seconds [*R Atkinson*, 2000; *Stark et al.*, 2007; *Wayne et al.*, 1991]. Most often, the short lifetime is due to the fast photolysis where the wavelength is shorter than 635 nm resulting in 90% NO_2 and 10% NO.

$$NO_3 + h\upsilon \rightarrow NO_2 + O \qquad 90\% \qquad (1.9)$$

$$NO_3 + h\upsilon \rightarrow NO + O_2 \qquad 10\% \qquad (1.10)$$

However, in urban environments where the NO mixing ratio is greater than 5 ppb, the fast titration of NO_3 by NO can be dominant [*Asaf et al.*, 2010; *R Atkinson et al.*, 2004; *Stutz et al.*, 2004].

$$NO_3 + NO \rightarrow 2NO_2 \qquad (1.11)$$

$$k_2 = 2.6 \times 10^{-11} \text{cm}^3 \text{ s}^{-1}$$

Under typical atmospheric conditions, a temperature-dependent equilibrium with N_2O_5 is established within minutes of the formation of NO_3.

$$NO_2 + NO_3 + M \leftrightarrow N_2O_5 + M \quad (1.12)$$

N_2O_5 is a thermally unstable compound, so it will dissociate back into NO_2 and NO_3.The temperature-dependent equilibrium constant, K_{eq}, is given by Equation 1.13.

$$K_{eq} = \frac{[N_2O_5]}{[NO_3][NO_2]} \quad (1.13)$$

$$K_{eq}(298\text{K}) = 2.9 \times 10^{-11} \text{cm}^3 \text{ molecule}^{-1}$$

The laboratory investigation and determination of the equilibrium constant as a function of temperature will be discussed further in Section I.7 of this chapter.

N_2O_5 is an important intermediate in the major NO_X loss mechanism at night through reaction with water to form soluble nitric acid [*Dentener and Crutzen*, 1993]. This hydrolysis reaction has been shown to occur both homogeneously in the gas phase and heterogeneous with liquid water adsorbed on a aerosol surfaces.

$$N_2O_{5(g)} + H_2O_{(g)} \rightarrow 2HNO_{3(g)} \quad (1.14)$$

$$N_2O_{5(g)} + H_2O_{(l)} \rightarrow 2HNO_{3(aq)} \quad (1.15)$$

While Equation 1.14 has been observed in the laboratory, it has been shown that the homogeneous reaction is too slow to impact the N_2O_5 lifetime and have atmospheric significance [*R Atkinson*, 2000; *Brown et al.*, 2009; *Dentener and Crutzen*, 1993; *Morris and Niki*, 1973]. The heterogeneous reaction has been shown to be much faster and is believed to be the dominant mechanism for N_2O_5, and in most cases NO_X, removal

[*Bertram et al.*, 2009; *Dentener and Crutzen*, 1993; *Riemer et al.*, 2003; *Russell et al.*, 1985; *Snyder et al.*, 1999].

Table 1.2. Heterogeneous reaction probabilities, $\gamma(N_2O_5)$, of N_2O_5 hydrolysis on several common aerosols.

Particle Type	Reaction Probability, $\gamma(N_2O_5)$	Reference
$NaNO_3$	0.02	[*Mentel et al.*, 1999]
Sulfuric Acid	0.1	[*Hanson and Ravishankara*, 1991] [*Robinson et al.*, 1997]
Organic Carbon	0.03, RH≥57%	[*Evans and Jacob*, 2005]
	RH x (5.2×10^{-4}), RH<57%	[*Evans and Jacob*, 2005]
Black Carbon	0.005	
Sea Salt	0.005 RH<62%	
	0.03, RH≥62%	
Na_2SO_4	0.04	[*Mentel et al.*, 1999]

As shown in Table 1.2, there is a large variability in the uptake coefficient, γ, for Equation 1.15 on different compositions of aerosol particles and relative humidity, RH. There have been several proposed mechanisms to explain the details of the N_2O_5 heterogeneous hydrolysis mechanism in order to characterize the reaction over a range of atmospheric particle types. The ionic hydrolysis mechanism was proposed in 1988 as a four-step process initiated by N_2O_5 dissolving in water and dissociating to form NO_3^- which then reacts with the water to form nitric acid [*Mozurkewich and Calvert*, 1988]. This mechanism is consistent with many studies, however there are still uncertainties in the role of nitrate aerosol in the process [*Griffiths et al.*, 2009; *Hallquist et al.*, 2003; *Wahner et al.*, 1998].

In regions with high concentration of alkene or sulfur emissions, the oxidation by the nitrate radical of these compounds can also be a significant nocturnal sink of nitrogen oxides [*Stutz et al.*, 2009]. NO_3 will react with unsaturated hydrocarbons through addition to the carbon-carbon double bond [*Wayne et al.*, 1991].

$$R'-C=C-R''+NO_3 \rightarrow R'-C-C(NO_3)-R'' \quad (1.16)$$

Nitrate radical will also react rapidly with sulfur containing compounds, such as dimethyl sulfide (DMS) [*Brasseur et al.*, 1999].

$$NO_3 + CH_3SCH_3 \rightarrow HNO_3 + CH_3SCH_2 \quad (1.17)$$

If either alkenes or DMS are present in high concentrations typical in urban areas, Equations 1.16 and 1.17 must be considered as significant NO_X sinks and addressed in nocturnal models.

Although not yet fully understood, the heterogeneous reaction of NO_2 with water produces nitrous acid (HONO), which acts as a NO_x reservoir during the night [*Finlayson-Pitts et al.*, 2003].

$$2NO_2 + H_2O \xrightarrow{\text{heterogeneous}} HONO + HNO_3 \quad (1.18)$$

Because HONO is readily photolyzed in sunlight, half of the NO_2 is returned to gas phase and along with the OH produced is used in for photochemical ozone production.

$$HONO + h\upsilon \rightarrow OH + NO \quad (1.19)$$

This can be a major early morning source of OH radicals, affecting ozone formation and therefore must be understood to be modeled correctly [*Alicke et al.*, 2003; *Platt et al.*, 1980].

Recently, it has been shown that the reaction of N_2O_5 with heterogeneous chloride ions to form $ClNO_2$ maybe be of significance in the marine boundary layer.

$$N_2O_{5(g)} + Cl^-_{(aq)} \rightarrow ClNO_{2(g)} + NO^-_{3(aq)} \quad (1.20)$$

Although this reaction had been observed in the laboratory for many years, it was only recently observed atmospherically in the mid-latitude marine boundary layer [*Bertram and Thornton*, 2009; *Osthoff et al.*, 2008]. Simultaneous ambient measurements performed in the Gulf of Mexico near Houston, TX have shown efficient conversion of N_2O_5 to $ClNO_2$ at yield of 10-65%. $ClNO_2$ was observed in mixing ratios of up to 1 ppb and to occupy up to seven percent of the total NO_y budget. This pathway can have significant effects on morning ozone formation, as $ClNO_2$ is photolyzed after sunrise and can produce appreciable amounts of chlorine atoms. Reactive halogen atoms efficiently oxidize volatile organic compounds, leading to the acceleration of ground level ozone production. This also occurs in the early morning when hydroxyl radical concentrations are low, and therefore can contribute to an otherwise dark pathway [*Chang et al.*, 2011; *Finlayson-Pitts and Pitts*, 1999; *Osthoff et al.*, 2008]. As this can possibly be a significant pathway in daily ozone formation that is not currently addressed by most models, further investigation, including additional simultaneous N_2O_5 and nitryl chloride measurements, is necessary into the relevance of Equation 1.20 in the marine atmosphere [*Chang et al.*, 2011].

I.3 Analysis of N_2O_5 Atmospheric Lifetime

The atmospheric lifetime of species provides insight into the balance in the sources and sinks for a species. With N_2O_5, the lifetime can provide information as to the

local aerosol composition through the degree of N_2O_5 hydrolysis and thus total NO_X loss. In order to calculate the atmospheric lifetime, the continuity equation for the concentration of a species must be calculated as in Equation 1.21.

$$\frac{dC}{dt} = P - L + F \tag{1.21}$$

where C is the concentration, P is the local production rate, L is the local loss rate, and F is the net flux [*Ravishankara and Lovejoy*, 1994]. Because N_2O_5 is a reactive species, any changes is concentration due to transport are likely to be small relative to chemical changes and therefore the net flux can be treated as negligible. The lifetime of the species, τ, can then be represented by Equation 1.22.

$$\tau = \frac{C}{P - \frac{dC}{dt}} \tag{1.22}$$

The sources of N_2O_5 are nitrogen dioxide and ozone through Equation 1.8, and the atmospheric steady-state lifetime, τ, and non-steady-state lifetime, τ^*, can be calculated through the ambient concentrations of these three species along with the NO_3 formation rate constant [*Brown et al.*, 2003a].

$$\tau_{N_2O_5} = \frac{[N_2O_5]}{k_1[O_3][NO_2]} \tag{1.23}$$

$$\tau^*_{N_2O_5} = \frac{[N_2O_5]}{k_1[O_3][NO_2] - \frac{d[N_2O_5]}{dt}} \tag{1.24}$$

Although it has been shown that the mixing ratios of NO_3 and N_2O_5 may deviate from those calculated steady-state analysis, for typical ambient conditions the analysis of the

atmospheric lifetime will still be valid. Typical lifetimes for N_2O_5 range from several minutes to an hour in polluted urban areas, and tens of minutes to several hours in more rural locations [*Brown et al.*, 2006; *Brown et al.*, 2007b; *Stutz et al.*, 2004; *Wood et al.*, 2005]. The N_2O_5 lifetime was measured to be less than eight minutes when studied in Houston, TX in 2000 and ranged up to four hours in a study in Fairbanks, AK in 2002 [*Ayers and Simpson*, 2006; *Stutz et al.*, 2004].

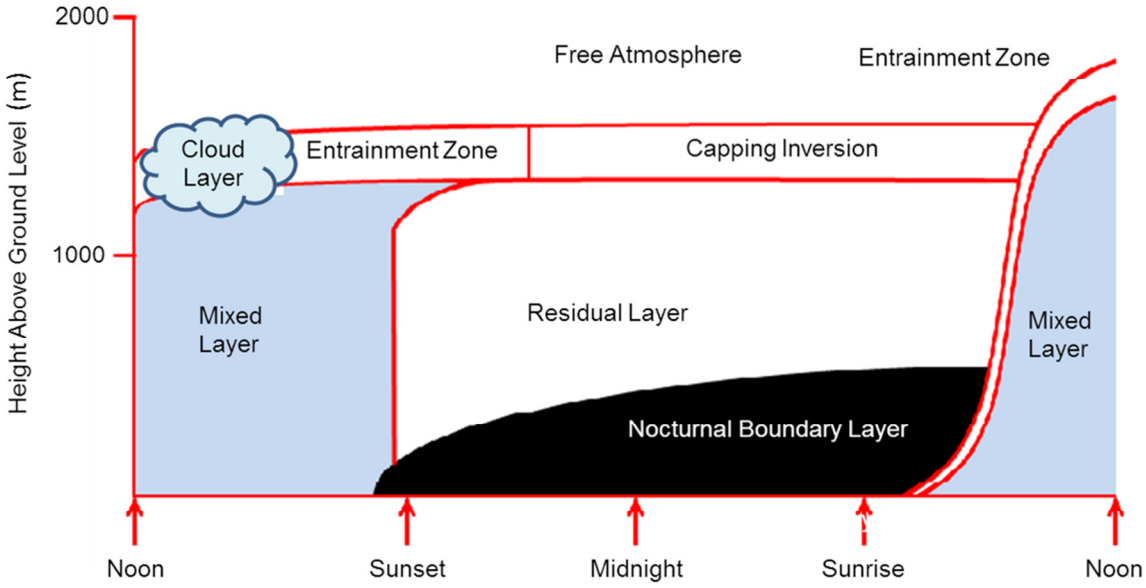

Figure 1.2. Characteristics and regions of the planetary boundary layer over the course of a day, showing the beginning of the nocturnal boundary layer after sunset.

I.4 Nocturnal Boundary Layer Characteristics

The lowest 100 m to 3000 m of the atmosphere is referred to as the planetary boundary layer (PBL), and the characteristics of this region are shown in Figure 1.2. This region differs from the region of the atmosphere above 3000 m, known as the free

atmosphere, in that it is influenced by the surface of the earth on a rapid (< 1 hour) time scale. The most noticeable forcing is the diurnal change in temperature near the earth's surface. Temperatures are much warmer during the day and cool down considerably at night, which is caused by the absorption of solar radiation by the ground and then the transference of this energy as heat to the surrounding air. However, after a height of approximately 1000 m, this phenomenon is no longer observed and ambient temperature no longer varies based on a diurnal cycle [*Stull*, 1988].

The transfer of heat from the surface of the earth into the boundary layer results in a turbulent mixing of the air, which is due to the thermals of warmer air rising away from the earth and thermals of cool air sinking from the cloud layer. This mixing results in a nearly homogenous mixture of chemical species vertically. However after the sun sets and the ground surface cools, a temperature inversion is created characterized by a decrease in temperature with increasing altitude. The nocturnal boundary layer (NBL) is characterized by a mass of air in which little to no mixing occurs leading to distinct vertical profiles in several reactive chemical species, and typically extends to about 0.1-0.5 km in height.

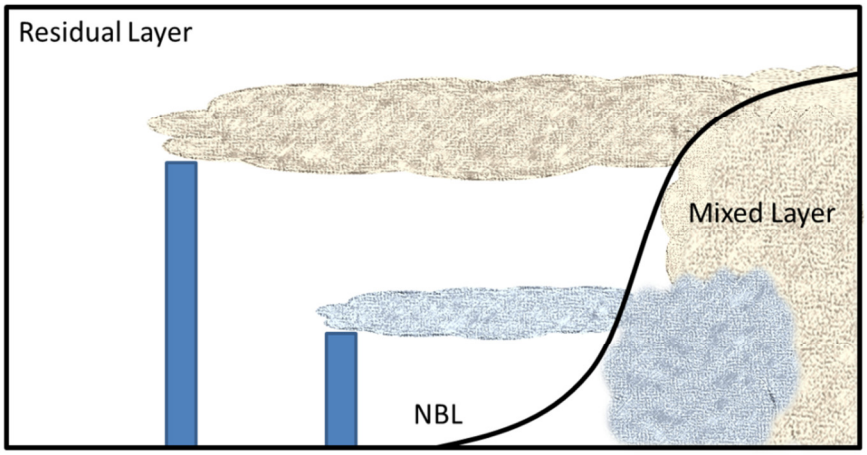

Figure 1.3. Mixing of species emitted during the night within the nocturnal boundary layer and mixing in the morning hours.

As the ground warns in the hours proceeding sunrise, convective mixing will eliminate the stratification of species. Any species emitted above the nocturnal boundary layer during the night will then mix to the ground layer, as shown in Figure 1.3. In urban outflow areas, this may result an increase in measured pollutants in the early morning hours. However, this is not due to local emissions but rather a consequence of the downward mixing of aged emissions. It is important that it is recognized that single-point ambient measurements and night and in the early morning hours are not taken as representative of the total concentration of species vertically.

The absence of turbulent vertical mixing in the nocturnal boundary layer leads to the stratification of reactive species in the troposphere and the existence of distinct vertical profiles in reactive species [*Allan et al.*, 2002; *Brown et al.*, 2007a; *Brown et al.*, 2007b; *Singh et al.*, 2007; *Stutz et al.*, 2004]. Gases emitted near the surface, such as NO_x, will stay near the ground throughout the night and dictate the lower altitude chemistry [*Doran et al.*, 2003]. The ozone concentration profile is determined by the NO

mixing ratio at various altitudes [*Wang et al.*, 2006]. The fast titration of ozone with nitric oxide results in a lower ozone concentration near the surface that increases linearly with altitude. The NO gradient is also reflected in the NO_3, and therefore N_2O_5, vertical profiles. Since NO reacts very quickly with NO_3 ($k = 2.6 \times 10^{-11}$ s^{-1}), high levels of nitric oxide will result in a short atmospheric lifetime of NO_3 and prevent the buildup of appreciable NO_3 and N_2O_5 concentrations [*Stutz et al.*, 2004]. Consequently, N_2O_5 concentrations near ground level in an area with high emissions are expected to be negligible.

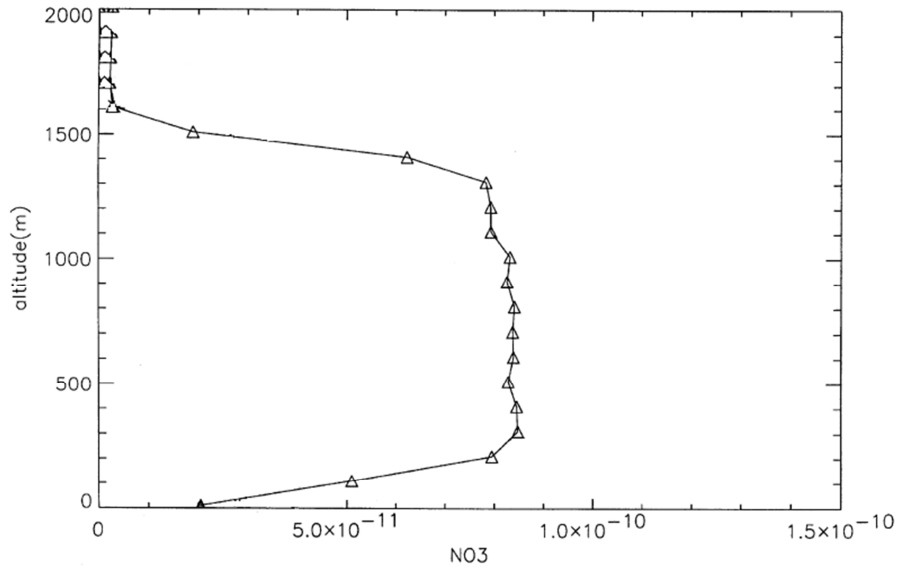

Figure 1.4. Modeled vertical distribution of the nitrate radical concentration in the nocturnal boundary layer below 2 km [*Fish et al.*, 1999].

There have been several modeling studies simulating distinct vertical distributions of N_2O_5 and NO_3 [*Fish et al.*, 1999; *Geyer and Stutz*, 2004; *Riemer et al.*, 2003]. As shown in Figure 1.4, the NO_3 concentration is expected to be low near the

surface and linearly increase to a maximum at the top of the nocturnal boundary layer. This profile makes *in situ* measurements on the ground difficult, as the N_2O_5 concentration will be small at low altitudes.

The N_2O_5 vertical profile has been investigated experimentally or calculated from NO_3 data in several field studies [*Brown et al.*, 2007a; *Brown et al.*, 2007b; *Stutz et al.*, 2004]. All these studies showed higher mixing ratios of N_2O_5 aloft, although the paper by *Stutz et al.* showed concentration gradients which were not as strong as expected. It was noted by *Brown et al.* that there is a large variability in the vertical distribution of NO_3 and N_2O_5, and the variability is greater than that of both nitrogen dioxide and ozone [2007b]. This observation was attributed to an inhomogeneous mixture of NO_X emissions and N_2O_5 sinks.

I.5 Ambient Detection with CRDS

Cavity ring-down spectroscopy (CRDS) was first developed in the 1980s as a technique for determining the reflectivity of optical mirrors [*Herbelin et al.*, 1980]. First published by O'Keefe and Deacon in 1988, CRDS now has wide range of applications in environmental measurements [*O'Keefe and Deacon*, 1988]. The method is based on the Beer-Lambert Law whereby the intensity of light absorb by a medium is proportional to the concentration of the absorber.

$$I = I_0 \exp(-\sigma l N) \tag{1.25}$$

where I_0 is the initial intensity of light and I is the intensity of transmitted after passing through a medium with absorption coefficient and number density, σ and N, and with pathlength, l. Typically the sensitivity of detection is limited by the pathlength.

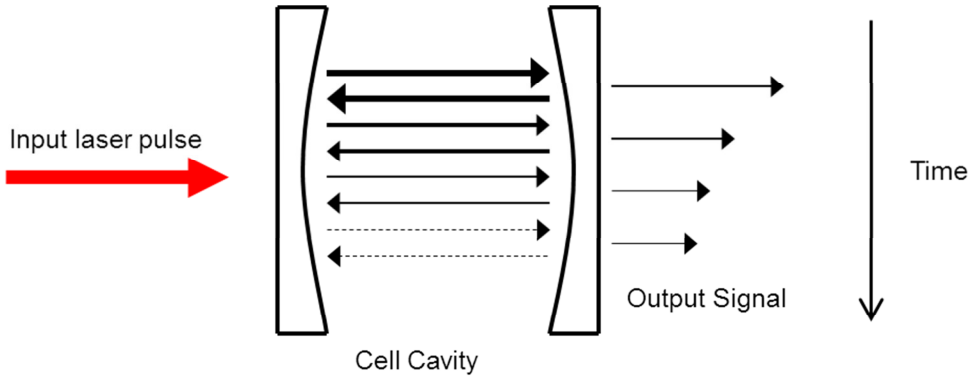

Figure 1.5. Schematic outline of the exponential decay of light within the system cavity over the measurement time.

By injecting coherent light into a high-finesse optical cavity, this pathlength can be extended in excess of several kilometers while contained within a small footprint. The light is transmitted into the cavity through a single entrance mirror and the intensity is measured through a separate exit mirror. The light intensity will exponentially decay over time, and a schematic is shown in Figure 1.5. The intensity of the light decays with each reflection and can be modeled according to Equation 1.26.

$$I(t) = I_0 \exp\left[-\left(\frac{\#\text{ of reflections}}{\text{round trip}}\right)\left(\frac{\text{loss}}{\text{reflection}}\right)(\#\text{ of round trips})\right] \qquad (1.26)$$

While systems with multiple (greater than two) mirrors have been used in various detection methods, the instrument employed by this work uses two mirrors, so the mathematical derivations presented here will assume simple cavity consisting of two mirrors. The terms in Equation 1.27 can then be defined by Equations 1.27-1.29.

$$\frac{\#\text{ of reflections}}{\text{round trip}} = 2 \qquad (1.27)$$

$$\#\text{ of round trips at t} = \frac{tc}{2L} \tag{1.28}$$

$$\frac{\text{loss}}{\text{reflection}} = 1 - R \tag{1.29}$$

where t is the time, c is the speed of light, L is the cavity length, and R is the reflectivity of the mirrors. Equation 1.26 can then be simplified to yield Equation 1.30.

$$I(t) = I_0 \exp(-(2)(1-R)\left(\frac{tc}{2L}\right) = I_0 \exp\left(-(1-R)\frac{tc}{L}\right) \tag{1.30}$$

Equation 1.30 assumes an empty cavity and that the decrease of light intensity within the cavity is solely due to incomplete mirror reflections. In the presence of an absorbing species in the cavity there will an additional term for absorption loss:

$$\text{total absorption loss} = \left(\frac{\text{absorption loss}}{\text{round trip}}\right)(\#\text{ of round trips}) = (2\alpha L)\left(\frac{tc}{2L}\right) \tag{1.31}$$

where α is the absorption coefficient multiplied by the absorber concentration, σ[A]. The total exponential decay of the light intensity within the cavity is therefore described by Equation 1.32.

$$I(t) = I_0 \exp\left(-[(1-R)+\alpha L]\frac{tc}{L}\right) \tag{1.32}$$

The time constant for decay with an absorber present is given by τ and the decay in an empty cavity by τ_0.

$$\tau = \frac{t_r}{2[(1-R)+\alpha L]} \tag{1.33}$$

$$\tau_0 = \frac{t_r}{2(1-R)} \tag{1.34}$$

The variable t_r is the round trip transit time and determined by the distance L between the two mirrors. If both the intrinsic decay time of the cavity and the decay lifetime with an absorber present are measured, the difference in the decay lifetime can be used to determine the concentration of the absorber. For an absorbing species, A, the concentration is then given by Equation 1.35.

$$[A] = \frac{R_L}{\sigma c}\left(\frac{1}{\tau} - \frac{1}{\tau_0}\right) \tag{1.35}$$

Typically, the experimental setup will include a buffer region between the sample flow and the mirrors that is purged with dry gas to inhibit the loss of reflectivity due to deposition on the mirror. The constant, R_L, reflects this null region, and is defined as the ratio of the pathlength between the mirrors to the pathlength the sample is present.

Cavity ring-down spectroscopy has become a widely used technique for both kinetics and in situ tropospheric measurements of various species [*D B Atkinson*, 2003; *Brown*, 2003; *Scherer et al.*, 1997; *Vallance*, 2005]. CRDS is the most widely applied technique in in situ measurements of N_2O_5 and NO_3. The first use was published in 2001 and since the initial publication there has been significant work into the characterization of the instrument and multiple improvements to the sensitivity. [*Brown et al.*, 2002a; *Brown et al.*, 2001; *Brown et al.*, 2002b; *Dubé et al.*, 2006; *Fuchs et al.*, 2008]. Pulsed cavity ring-down based systems have been used in both urban and rural studies, as well as ship-based and airborne campaigns with typical detection limits ranging from 1-10 ppt.

I.6 Previous N_2O_5 Measurements

Before 2000, quantifying ambient N_2O_5 mixing ratios required the measurement of NO_3 and the calculation of N_2O_5 assuming the equilibrium shown in Equation 1.12 is in steady-state. The nitrate radical was first measured stratospherically in 1978 using Differential Optical Absorption Spectroscopy (DOAS) , and this method is now commonly used to measure NO_3 in the troposphere [*McLaren et al.*, 2010; *Noxon et al.*, 1978; *Stutz et al.*, 2004; *Stutz et al.*, 2009]. In tropospheric DOAS to measure NO_3, and xenon lamp is used as a light source over an optical path of several kilometers. The visible spectra of NO_3 is then used as a fingerprint to determine the concentration after the broadband light is collected by a detector [*Heard*, 2006]. Recently it has been suggested through simultaneous measurements that while the NO_3-N_2O_5 equilibrium is quickly established it may take several hours to reach a steady-state and may not reach this point in a single night [*Benton et al.*, 2010; *Brown et al.*, 2003a; *Wood et al.*, 2005]. It has therefore been shown necessary to directly measure N_2O_5 without relying on indirect calculation.

As discussed in the previous section, cavity ring-down spectroscopy is one method that has been used in ambient N_2O_5 detection by multiple research groups [*Benton et al.*, 2010; *Brown et al.*, 2004; *Nakayama et al.*, 2008; *Simpson*, 2003]. Field instrument employing laser-induced fluorescence (LIF) and chemical ionization mass spectrometry (CIMS) have also been developed for N_2O_5 quantification [*Matsumoto et al.*, 2005; *Slusher et al.*, 2004; *Wood et al.*, 2003; *Zheng et al.*, 2008]. These instruments

have been used in various field campaigns, and a summary of several of these studies along with the maximum observed N_2O_5 concentration is shown in Table 1.3.

Table 1.3. Summary of ambient N_2O_5 measurements using various techniques.

Measurement Location	Measurement Time	Maximum [N_2O_5]	Site Description	Reference
San Francisco, CA	January 2004	150 ppt	Urban Outflow	[*Wood et al.*, 2005]
Gulf of Mexico	August-September 2006	500 ppt	Various	[*Osthoff et al.*, 2008]
London, England	October-November 2007	800 ppt	Urban	[*Benton et al.*, 2010]
Toyokawa, Japan	February 2006	20 ppt	Rural	[*Nakayama et al.*, 2008]
New Hampshire Coastline	July-August 2004	120 ppt	Various	[*Brown et al.*, 2007b]
Fairbanks, AK	December 2002	20 ppt	Rural	[*Simpson*, 2003]
Tokyo, Japan	March 2004	400 ppt	Urban	[*Matsumoto et al.*, 2005]
Kleiner Feldberg, Germany	May 2008	70 ppt	Urban Outflow	[*Crowley et al.*, 2010]
Boulder, CO	October-November 2001	3 ppb	Urban	[*Brown et al.*, 2003b]
Houston, TX*	August-September 2000	300 ppt	Urban	[*Stutz et al.*, 2004]
Vancouver, Canada*	August 2001	300 ppt	Rural	[*McLaren et al.*, 2004]

* Calculation of steady-state N_2O_5 following measurement of NO_3 by DOAS

It is important to note that the measurements presented in Table 1.1 were performed in different regions at varying time periods and multiple measurement altitudes and should not be directly compared. It does however present the range of concentrations at which N_2O_5 can exist. Nearly all of these studies also noted that there was no N_2O_5 observed on many, if not most, of the days that measurements were

attempted [*Benton et al.*, 2010; *Brown et al.*, 2007b; *Simpson*, 2003]. As expected, higher levels of N_2O_5 were observed in more urban and industrialized areas, although low concentrations can be an indication of extremely strong sinks and fast processing.

I.7 Physical Properties of NO_3 and N_2O_5

As the nitrate radical is such an important atmospheric species, the absorbance spectrum has been the focus of many studies and therefore well characterized [*Wayne et al.*, 1991; *Yokelson et al.*, 1994]. A recent study using high-resolution Fourier transform spectroscopy measured the absorbance spectrum is the visible region between 465 and 797 nm to calibrate the energy of observed transitions to an uncertainty of 0.02 cm^{-1} [*Orphal et al.*, 2003].

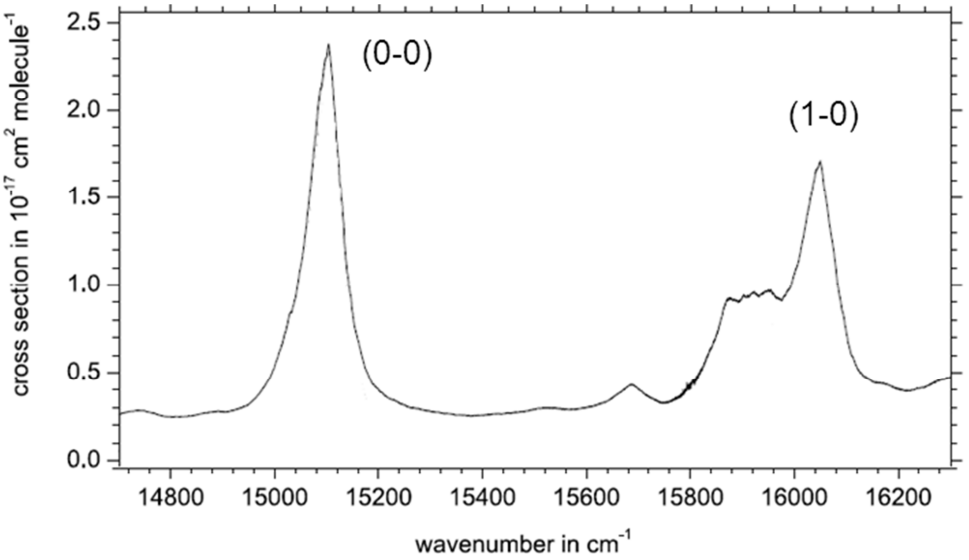

Figure 1.6. Absorbance spectrum of NO_3 as measured by *Orphal et al.*[2003]. The strong band at 15100 cm^{-1} (662 nm) is typically used in cavity ring-down studies.

As shown in Figure 1.6. there are two distinct transitions in the NO_3 absorbance spectrum. The peaks in the NO_3 absorption spectrum are broad due to strong predissociation [*Kim et al.*, 1992; *Marinelli et al.*, 1982]. Most detection techniques, including CRDS and LIF, take advantage of the strong band centered near 662 nm (15100 cm^{-1}) corresponding to the (0-0) transition. This is a non-dissociative electronic transition with a peak width of approximately 80 cm^{-1}. The peak at 623 nm (approximately 16000 cm^{-1}) is due to the (1-0) hot band and is less popular in spectroscopic studies due to its wide width and additional possibility of interferences.

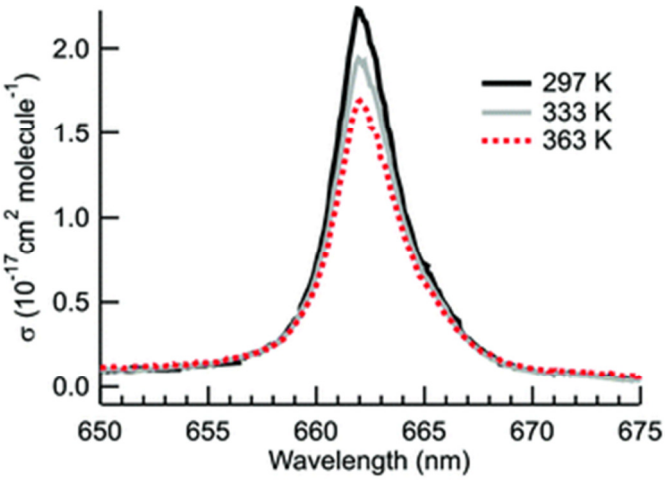

Figure 1.7. NO_3 absorption peak at 662 nm over varying temperatures [*Osthoff et al.*, 2007].

The absorption cross section of NO_3 at 662 nm, σ_{662nm} , has shown to vary significantly with temperature, and therefore has been the subject of numerous studies [*Cantrell et al.*, 1987; *Orphal et al.*, 2003; *Osthoff et al.*, 2007; *Sander*, 1986; *Yokelson et al.*, 1994]. The temperature dependence of the NO_3 absorption cross-section in the (0-

0) transition is has been proven to be due to the increase in the population of the ground vibrational state caused by the depopulation of the degenerate in-plane bending vibration with increasing temperature [*Orphal et al.*, 2003]. As shown in Figure 1.7, the cross section can vary by more than 20% over atmospherically relevant temperatures [*Osthoff et al.*, 2007].

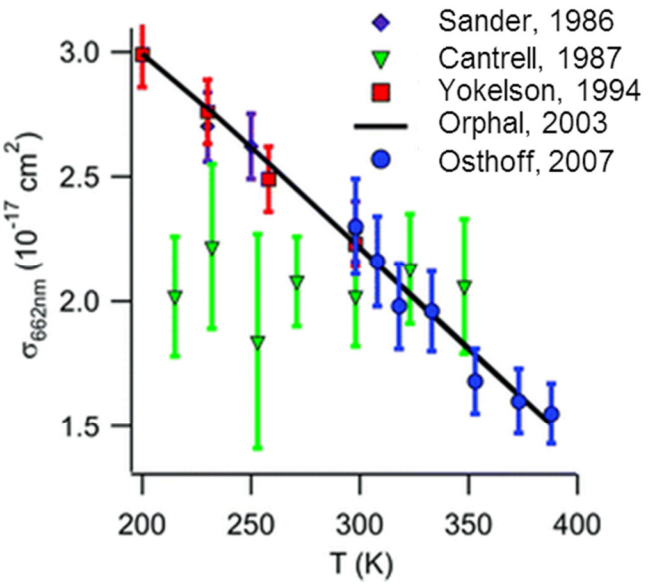

Figure 1.8. Comparison of the various measurements of the temperature dependence of the NO_3 (0-0) transition [*Osthoff et al.*, 2007].

A comparison of results from the various temperature dependence studies is shown in Figure 1.8. *Orphal, et al.* predicted the cross section through the calculation of the population density in the ground vibrational states of NO_3, and this method has shown good agreement with most of the experimental studies [2003]. Most recently, *Osthoff, et al.* determined the cross section from 298-388 K using cavity ring-down spectroscopy in a very similar experimental design to the ambient measurements [2007].

Their data combined with the previous measurements at lower temperature was used to determine the cross section as a function of the temperature using a least-squares fit, as shown in Equation 1.36.

$$\sigma_{662\,\mathrm{nm}}(\mathrm{T}) = [(4.582 \pm 0.096) - (0.00796 \pm 0.00031) \times \mathrm{T}] \times 10^{-17}\ \mathrm{cm}^2\ \mathrm{molecule}^{-1} \tag{1.36}$$

In the TAMU CRDS system, NO_3 is measured above room temperature and closely resembles the system used by *Osthoff, et al.* Their evaluation of the cross section is therefore most appropriate and used throughout this work.

Because the N_2O_5 absorption spectrum is broad, it is difficult to detect optically due to the presence of interfering species. When measured with cavity ringdown spectroscopy, N_2O_5 is first quantitatively thermally converted to NO_3, and the resulting NO_3 is measured. This means that understanding the $N_2O_5 - NO_3$ equilibrium in Equation 1.12 must be well understood, and has been the focus of several studies [*Ide et al.*, 2008; *Osthoff et al.*, 2007; *Wängberg et al.*, 1997]. The NASA/JPL recommendation for the equilibrium constant, K_{eq} has a large error and is only valid from 200-300 K [*Sander et al.*, 2006]. In calculating the steady-state concentrations of NO_3 and N_2O_5 throughout this work, the temperature often exceed this range. The equilibrium constant determined by *Osthoff, et al.* has been used, which is valid from 278-321 K [2007].

$$\mathrm{K_{eq}}(\mathrm{T}) = (5.1 \times 10^{-27}) \exp\left(\frac{10871 \pm 46\mathrm{K}}{\mathrm{T}}\right) \mathrm{cm}^3\ \mathrm{molecule}^{-1} \tag{1.37}$$

I.8 Summary of Remaining Chapters

The proceeding chapters describe the development and calibration of the Texas A&M cavity ring-down instrument and some field measurements with the instrument.

Chapter II details the instrument specifics including both the sampling and detection methods. This chapter also contains the results of laboratory measurements performed in order to calibrate the loss of reactive species within the instrument and ensure accurate quantitative measurements. Chapter III outlines measurements of N_2O_5 performed in Houston, TX as part of a large field study to access air quality especially relating to atmospheric radicals. Chapter IV contains measurements performed near Texas A&M in College Station, TX from a rural site. Finally, Chapter V summarizes all data presented and makes suggestions for future directions.

CHAPTER II

INSTRUMENT DESCRIPTION AND CHARACTERIZATION

II.1 Experimental Setup

The Texas A&M cavity ring-down instrument is based on the designed originally proposed by Brown and Ravishankara at the National Oceanic and Atmospheric Administration (NOAA) in Boulder, CO [*Brown et al.*, 2002a; *Brown et al.*, 2001; *Brown et al.*, 2002b]. Our instrument has been entirely home-built and specific for the detection of N_2O_5 and NO_3, and a photograph of the current instrument is pictured in Figures 2.1 and 2.2. The layout of the optical system, shown in Figure 2.3, has been designed to be compact and reliable in the field. A 532 nm Nd:YAG laser (Big Sky, Ultra-CFR) produces 6 ns laser pulses at 10 Hz, which pumps a Sirah Dye Laser (CBR-P). DCM laser dye ($C_{19}H_{17}N_3O$, MW 303.37 g/mol, Exciton) in dimethylesulfoxide (DMSO) is used to produce optimum laser power at the 662 nm, the peak of the NO_3 absorption band. Typical laser output power is 3.5-4.5 mJ/pulse. The beam is directed through an optical periscope system shown in Figure 2.1 to the upper level of the instrument containing the detection cavities. The laser light is then directed through a 50/50 beamsplitter and aligned through both the heated and the ambient temperature cavities along the detection axes. Two 99.995% reflective, 0.8 in diameter, 6 m radius of curvature dielectric coated mirrors (Los Gatos Research) are mounted on either end of each cavity, enclosing a 94 cm long detection region with a 29.7 mL volume. Dry

nitrogen purge gas is injected onto each mirror at a rate of 25 sccm (standard cubic centimeters per minute) through a mass flow controller (MKS 1179A) in

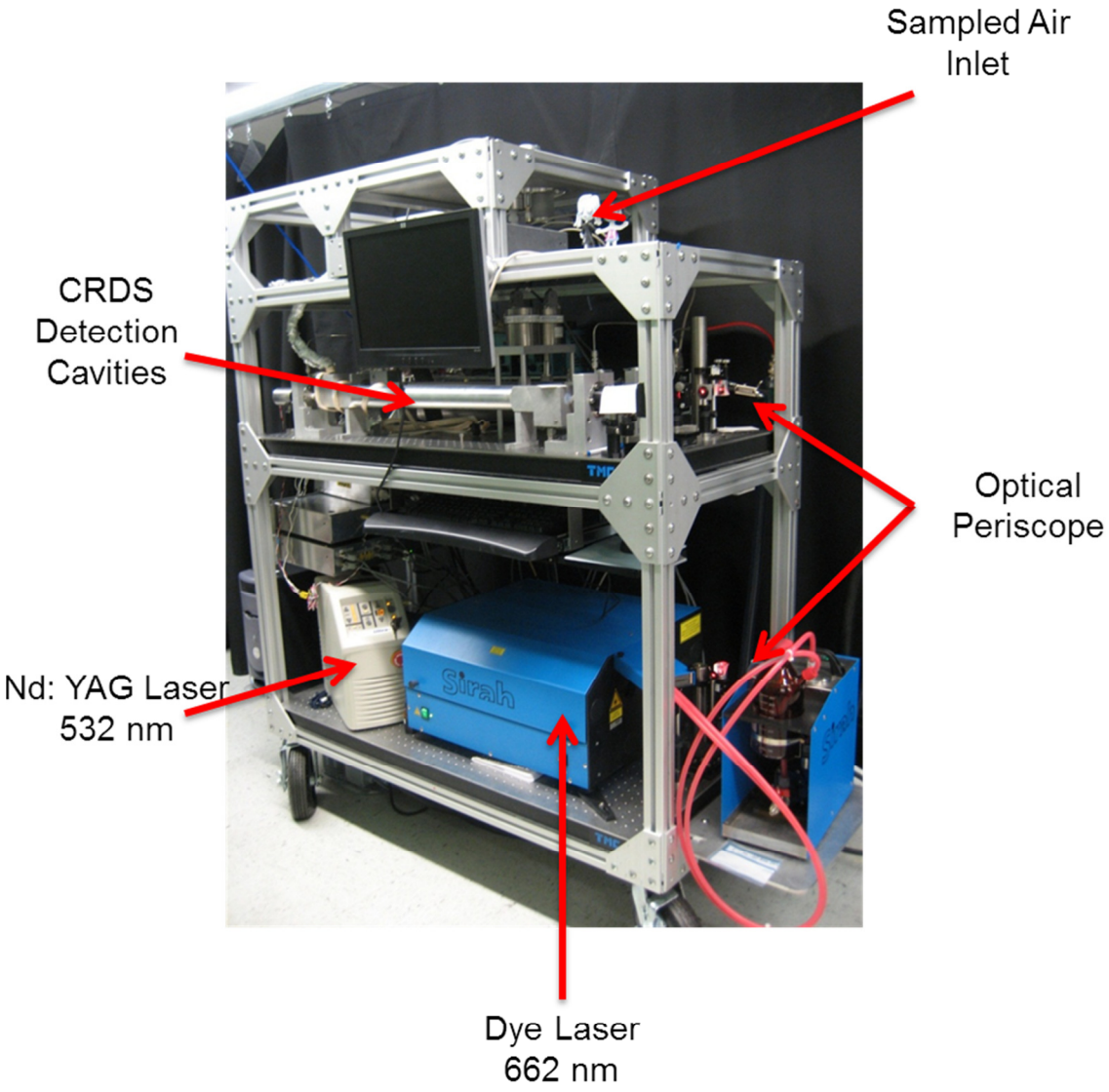

Figure 2.1. Photograph of the TAMU cavity ring-down spectrometer.

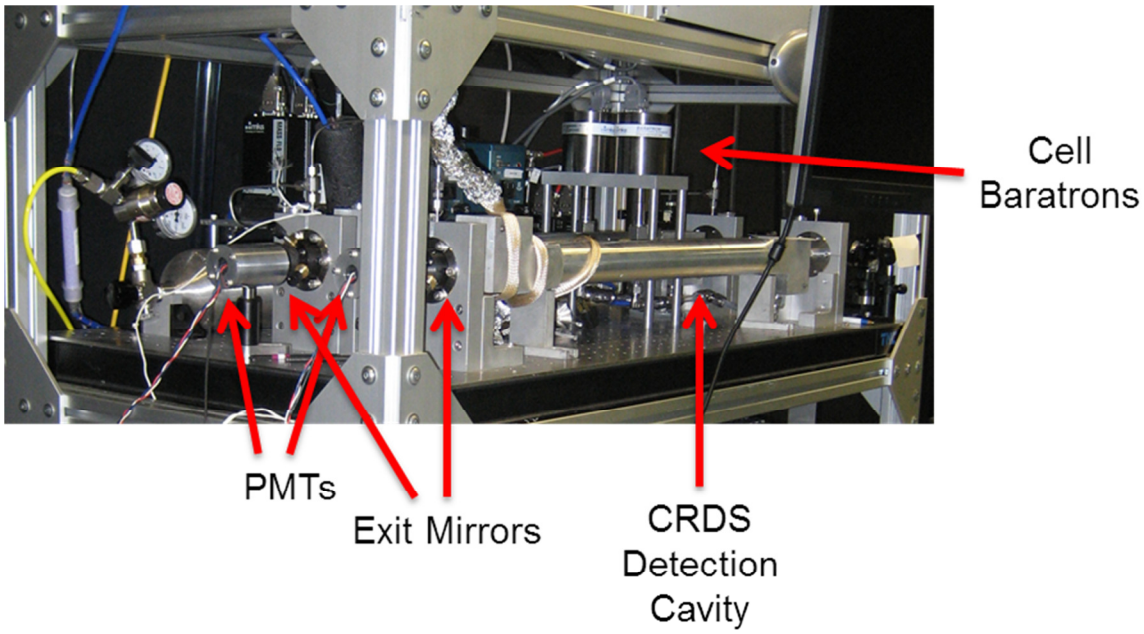

Figure 2.2. Photograph of the top section of the instrument showing the detection cavities along with the mounted mirrors, PMT detectors, and cell Baratrons.

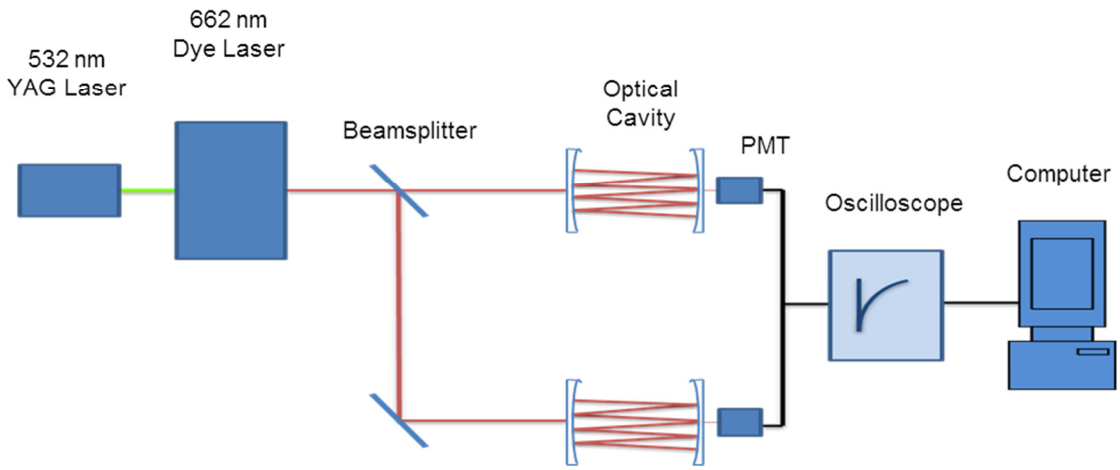

Figure 2.3. Optical setup of the cavity ring-down spectrometer.

order to keep the mirror clean and dry to maintain reflectivity during experiments. The light transmitted through the exit mirror passes through a 610 nm longpass colored glass filter (Thorlabs, FGL610) and the exponential decay of the laser power within the cavities is monitored by two photomultiplier tubes (PMTs, Hamamatsu, H6780-20). The signal is digitalized using a 14-bit PCI oscilloscope (Gage Applied Technologies, 14100) and analyzed on a computer using custom-designed software in Labview 8.0 (National Instruments).

The air sampling system for the CRDS spectrometer has been specially designed to minimize in situ losses in measuring reactive and radical species, and a schematic layout in shown in Figure 2.4. The entire system is constructed of FEP Teflon, including the inlet, filter and filter holder, detection cavities, and all fittings. With the exception of the thermal conversion region, the sampling portion of the instrument is maintained at ambient temperature. This is to prevent the condensation of water when the instrument is located in a climate-controlled environment and to minimize an artificial bias through the thermal decomposition of N_2O_5 when the instrument is warmer than the ambient temperature. Care has been taken to effectively insulate the instrument using fiberglass insulation, and the temperature is monitored in four separate places using K-type thermocouples and recorded by the computer. The sampling inlet is protected from rain and wind by a FEP Teflon funnel and the gas sample enters a fast-flow system consisting

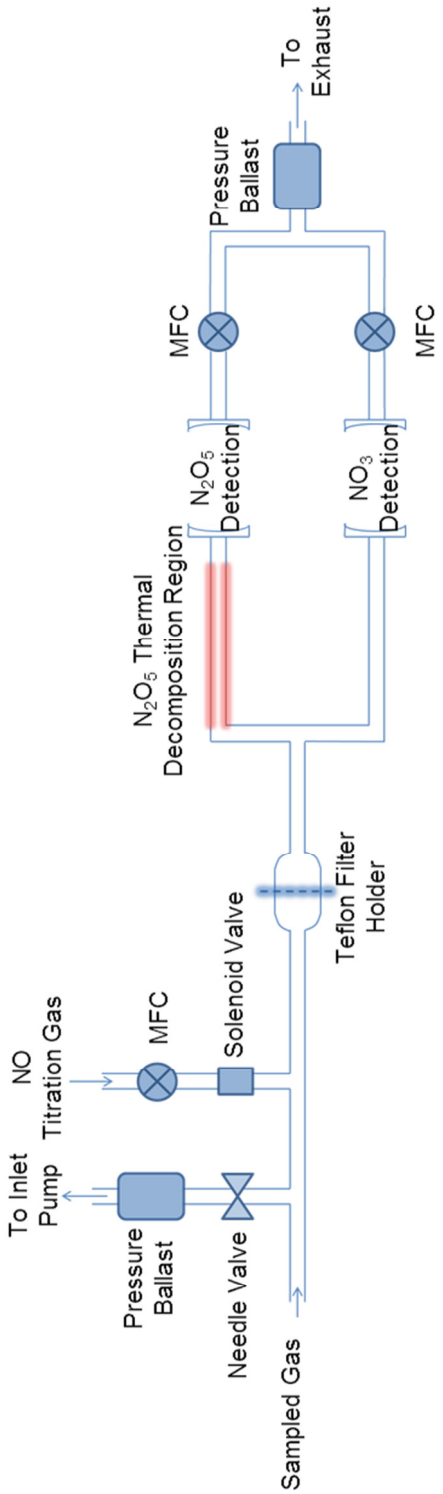

Figure 2.4. Gas sampling setup of the cavity ring-down spectrometer.

of 0.25" O.D., 0.125" I.D. FEP Teflon tubing designed to deliver the sample rapidly to the CRDS instrument. The inlet length can range from 1.5 m to 6.0 m in length and is minimized depending on the sampling location to lessen sample wall reactions. The majority of the sampled air is exhausted through a needle valve by diaphragm pump (Vacuubrand, ME4 NT). A large volume pressure ballast was constructed and inserted into the system before the inlet pump to reduce continuous fluctuations in the pumping speed and therefore reduce fluctuations in the inlet pressure. The ballasts were constructed using PVC tubing and fittings and have an approximate volume of 16.5 L. The fast flow inlet pressure is monitored by a Baratron capacitance manometer (MKS, 722B, 1000 torr), and is typically in the range of 330 – 375 torr.

A small portion of the sampled gas then enters the slow flow region where it is quantitatively analyzed for N_2O_5 and NO_3 concentrations. A sample with a total flow rate of 8.0 standard liters per minute (SLPM) passes through a Teflon 25 μm wide micropore filter (Pall Life Sciences) with a 2 μm pore size to effectively remove particulates. Aerosols within the sampled flow will refract the laser light which will lead to a loss in the decay lifetime and an increase in the detection limit. Also, particulates in the system can build up on the cavities mirrors and decrease reflectivity over time. Both of these issue result in the necessity to filter the sample however both the analyzed species will react with aerosols contained on the filter. This results in the need to change to a fresh filter often, and the filter is manually replaced with every one hour of sampling time. The determination of filter losses has been thoroughly investigate and described in the literature [*Fuchs et al.*, 2008].

After passing through the filter, the gas sample is divided into two channels each with a flow of 4 SLPM. One channel measures absorption due to NO_3 and the second channel to thermally decompose N_2O_5 to NO_3 and NO_2 and measures the resulting NO_3 combined with the ambient NO_3.

$$N_2O_5 \xleftrightarrow{\Delta} NO_3 + NO_2 \qquad (2.1)$$

There are three distinct temperature regions in the instrument. The shared slow flow inlet and the entire NO_3 channel and detection region, Section A, is maintained at the ambient temperature of sampling to prevent water condensation when the instrument is located in climate-controlled environment. In the heated N_2O_5 channel, the sampled air first passes through an N_2O_5 thermal decomposition region, where N_2O_5 is quantitatively converted to NO_3 at a temperature between 388 and 393 K. The optimum temperature has been carefully calibrated, and is described further in Section V of this chapter. The third temperature region, Section C, contains the N_2O_5 detection region and is heated to 348 – 353 K to maintain stability in the gas sample.

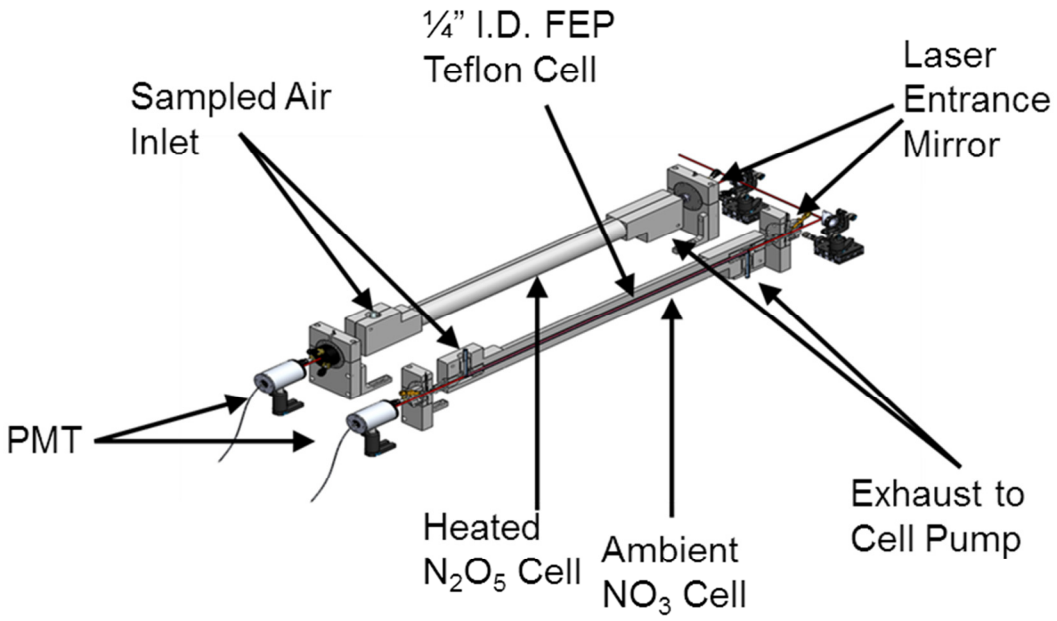

Figure 2.5. Optical setup and sampling manifold in the CRDS instrument.

The coupling of the optical and flow systems in the detection region is shown in Figure 2.5. The mirrors are mounted on either end of each cavity using a three-point adjustment cavity ring-down mount (Los Gatos Research). The FEP Teflon cells are housed in a home-built aluminum manifold to maintain alignment and allow for consistent heating of the cells. The PMTs are positioned parallel to the detection axis at the exit mirror to monitor the laser light transmitted, and are mounted in aluminum housing and secured to the optical breadboard. Light-insulating material is used minimize background light entering the PMTs.

The pressure in the detection cavities is typically 300-315 torr and is monitored by two Baratron capacitance manometers (MKS 628B). The air in each cavity then

passes through a calibrated mass flow controller (MKS 1179A) at 4 SLPM and is exhausted through a pressure ballast and second diaphragm pump (Vacuubrand ME4).

In order to determine the intrinsic lifetime of the laser pulse within the cavity, NO_3 must be effectively and quickly removed from the system. This is accomplished by the addition of nitric oxide gas to titrate NO_3 [*R Atkinson et al.*, 2004].

$$NO + NO_3 \rightarrow 2NO_2 \qquad (2.2)$$

$$k = 2.6 \times 10^{-11}\ cm^3\ molecule^{-1}\ s^{-1}$$

Nitric oxide gas with a concentration of 0.02% in nitrogen gas is passed through a sodium hydroxide (Ascarite) trap to remove NO_2 and is then injected into the instrument with a flow of 50 sccm through a mass flow controller (MKS 1179A). An automated Teflon solenoid valve (Parker Hannifin) controls the delivery of NO titration gas, and titration scheme and characterization is described further in Section II.3 of this chapter.

II.2 Data Analysis

The exponential decay signal from the PMTs are digitalized on a PCI oscilloscope card within the computer. The oscilloscope is triggered externally by the Q-switch of the laser, and the oscilloscope trace is analyzed in Labview 8.0. Signal is acquired for several hundred microseconds after each pulse which represents greater than two times the intrinsic ring down time of the cavity. However, only a subset of the data is used in the analysis, typically 50-100 μs. The initial 30-50 μs after each pulse is excluded due to interferences with signal acquisition. The software performs a natural logarithm of the exponential decay signal measured in each cavity and linearly fits the resulting data. The slope of the fit corresponds to the inverse lifetime of the laser pulse in

each cell and represents either $1/\tau$ or $1/\tau_0$, depending on whether an NO_3 absorption measurement is being performed or if the system has been titrated with NO gas for a background measurement. Typically a 25-50 shot average of the exponential decay time is performed to reduce noise in the signal.

The Labview 8.0 program also records the output of four thermocouples which measure ambient, heated inlet, heated cell, and ambient cell temperature and records the output of three Baratrons measuring the pressure in the inlet, heated cell, and ambient cell. This data is averaged and recorded at the same time scale as the exponential decay lifetimes along with an indicator as to whether the instrument is currently taking an absorption or a background measurement.

Background measurements are performed frequently because the intrinsic exponential decay of the light within the cavity drifts throughout the course of a night, and can be due to several causes. Slight changes in temperature can cause an alignment drift of the laser pulse. Although the gas sample is filtered and the mirrors are purged with dry nitrogen gas, any debris on the mirrors can cause a decrease in reflectivity. Also, the background measurement is taken by injected NO to titrate the NO_3 is the gas sample. However, NO_2 absorbs weakly at 662nm, and dramatic changes ambient concentrations of NO_2 will also affect the background exponential lifetime.

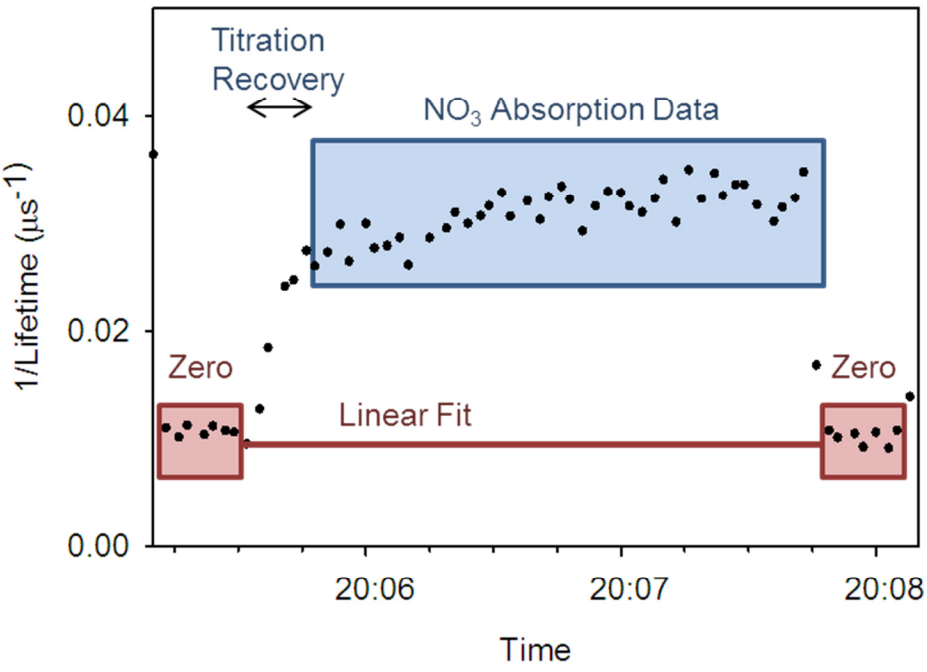

Figure 2.6 Average exponential decay lifetimes as recorded by the CRDS instrument with the absorption data highlighted in blue and the zeroed background measurement data highlighted in red.

After the lifetime measurements are acquired, calculations are performed to determine the concentration of absorbed species along with the instrument sensitivity and detection limit. The concentration of NO_3 is each cavity is calculated through Equation 2.3.

$$[NO_3] = \frac{R_L}{\sigma_{662nm} c}\left(\frac{1}{\tau} - \frac{1}{\tau_0}\right) \qquad (2.3)$$

where τ is the exponential lifetime with NO_3 present and τ_0 is the intrinsic lifetime found by zeroing with NO.As shown in Figure 2.6, a linear fit is performed for the two zero measurements adjacent the absorption measurement to extrapolate the background

lifetime at the time of each absorption measurement. The value of the linear fit at the time of each absorption measurement is used as τ_0. R_L is the ratio of the distance between the mirrors and the distance occupied by the gas sample and for the TAMU CRDS instrument is equal to 1.45.

The concentration of NO_3 present in the cavity is calculated based on the temperature dependent cross-section at 662 nm (σ_{662nm}) for both the ambient and the heated cavities.

$$\sigma_{662\,nm}(10^{-17}\,cm^2\,molecule^{-1}) = (4.582 \pm 0.096) - (0.00796 \pm 0.00031) \times T(K) \qquad (2.4)$$

as determined by Osthoff, et al. [2007]. This value will vary between the ambient and the heated cell, and will also affect the ambient cell analysis if there is any temperature drift throughout the night. Due to this, the absorption cross-section is calculated for each data point based on the current measured cell temperature.

The concentration is determined in units of molecule cm^{-3}, however the pressure and temperature inside of the instrument differs greatly from ambient temperature and pressure. Concentrations are converted to ppt at standard ambient temperature and pressure using the measured pressure and temperature within the cavities. Similar to the cross-section, the temperature and pressure can drift throughout the night and is therefore calculated individually for each data point.

The sensitivity of the instrument to NO_3 is dependent on the error within the zero measurement and will change with every NO titration. Therefore, the detection limit and

error is calculated individually for each data point, where $\Delta\tau$ is the standard deviation of the fluctuations within the zero measurement [*Brown et al.*, 2001].

$$[NO_3]_{min} = \frac{R_L}{c\sigma}\frac{\Delta\tau}{\tau_0^2} \qquad (2.5)$$

II.3 Implementation of Automated Zeroing

The original design of the instrument included the manual on/off switching of the NO titration gas to remove NO_3 by reaction 2.2. This method proved to be inaccurate in timing for data analysis as well as creating error due to the slow initial delivery of gas by the mass flow controller. This issue was resolved through the addition of a solenoid valve for the automated addition of titration gas which can be synchronized and recorded with the NO_3 absorption data to provide an absolute record of timing in the data analysis.

The solenoid valve had a PTFE coated interior to prevent corrosion, and is position down flow of the mass flow controller on the instrument. The MFC is set to be always open to prevent the time delay for the flow to reach the full set value, with the flow rate set to 50 sccm. The solenoid is interfaced with the data collection software, and the opening and closing times are manually programmable.

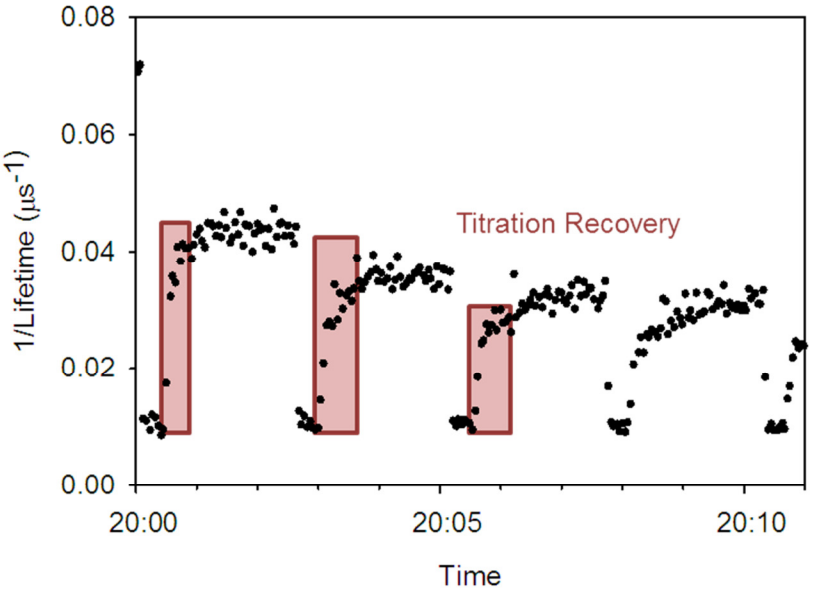

Figure 2.7. Chemical zeroing of NO_3 with NO titration gas. Note the recovery time in the NO_3 absorption lifetime due to the time of complete removal of the titration gas.

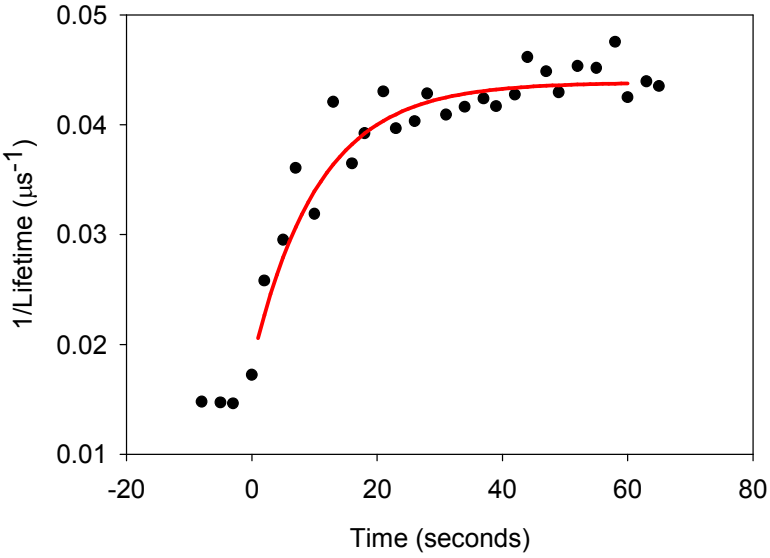

Figure 2.8. Example data shown from 30 s on, 90 s off titration scheme in black dots with modeled fit shown in red.

The volume of the sampling system creates a delay in the complete removal of NO titration gas from the instrument and therefore the recovery of the NO_3 absorption lifetime after the solenoid valve is closed. As shown in Figure 2.7, it is essential that only the data points after the complete removal nitric oxide be included in the data analysis. In order to characterize the recovery time, several laboratory measurements were made using synthesized solid N_2O_5 as a calibration source and varying timing schemes for solenoid titration. The N_2O_5 sample was kept at dry ice in acetone temperature (-68°C) and delivered to the system using argon carrier gas at a flow rate of 50 sccm.

The laboratory data was modeled using the data analysis program GENPLOT and a nonlinear least-squares fit to the exponential example Equation 2.6.

$$\tau(t) = A_0(1 - \exp(-\frac{k_0}{t - t_0})) + A_1 \qquad (2.6)$$

Data collection and fitting initiates when the solenoid is closed, defined at time zero. Example data is shown with the NLS fit normalized to data points in Figure 2.8. Using the determined k_0 from the fit, the average recovery time after titration was 10.5 ± 1.89 s, with a minimum of 7.49 s and a maximum of 14.9 s throughout all trials. However the maximum recovery time occurred infrequently and it was determined that a recovery time allotment of 15 s would be sufficient to exclude biased data. These values are consistent with the time required to evacuate the injected gas based on the flow rate and instrument volume.

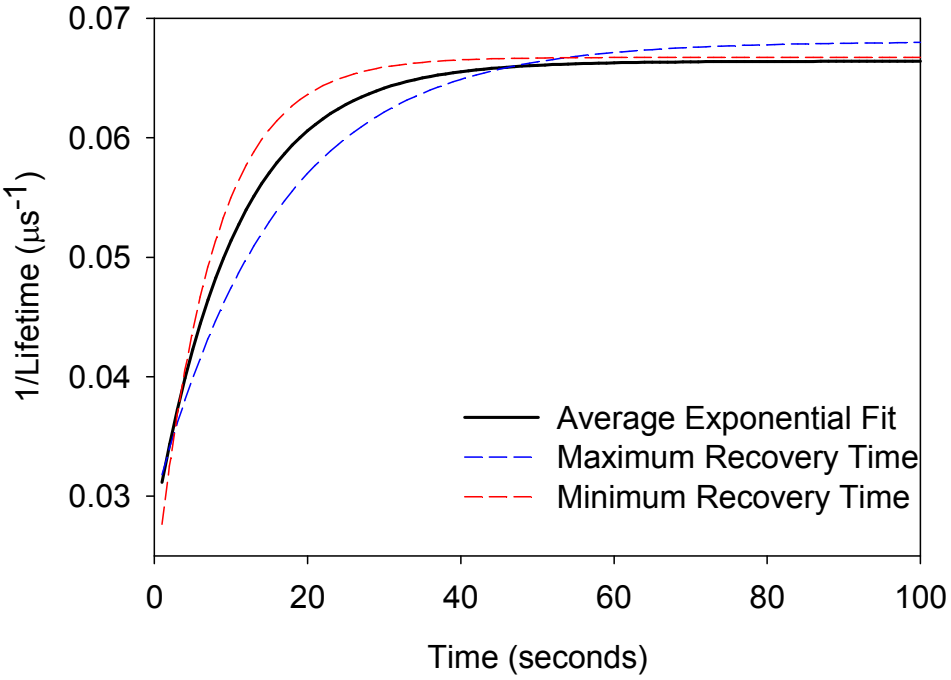

Figure 2.9. Exponential fit of titration recovery data shown with minimum and maximum recovery times.

Figure 2.9 shows the modeled exponential fit to Equation 2.6. The recovery time was independent of the titration zeroing time as was expected. A titration scheme of 30 s of NO titration followed by 90 s of NO_3 absorption measurements. The frequent zeroing is necessary to monitor the background drift due to changes in the sampled gas, such as nitrogen dioxide concentration. Due to the recovery time necessary to completely remove NO from the instrument, the first 15 s of NO_3 absorption data is discarded and not used for absorber concentration analysis.

II.4 Characterization of Instrument Flow

The first part of the CRDS instrument is a fast flow region designed to quickly bring the sampled air outside to the instrument to be analyzed. The length of the inlet is kept at a minimum in order to decrease the residence time of the sample and therefore the least amount of sample wall losses. The pumping speed through the fast flow region was characterized through laboratory analysis with the goal of determining the inlet residence time based on inlet length.

The fast flow inlet pump (Vacuubrand ME4 NT) operates at a maximum pumping speed of 19.4 L s^{-1}. However, the pumping rate is restricted by the addition of a needle valve between the instrument and the pump. The aperture of the needle valve is adjusted in order to achieve an optimum pressure in the inlet of 330-350 torr for the length of inlet used. The inlet flow rate was measured by connecting a closed 5 L bulb to the instrument and monitoring the exponential rate of decrease in the pressure of the system, with results shown in Figure 2.10.

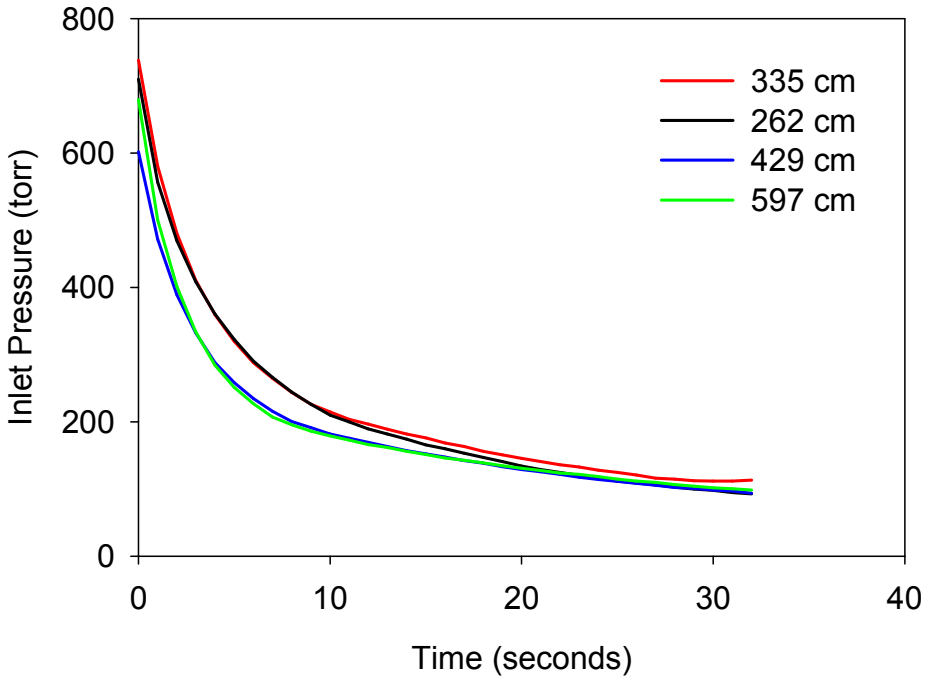

Figure 2.10. Inlet pressure decrease in a closed 5 L system with varying inlet lengths.

The pressure decrease as the system evacuated the 5 L bulb was modeled to an exponential function using a nonlinear least-squares fit in GENPLOT to Equation 2.7.

$$\text{pressure}(t) = A_0 \exp\left(-\frac{k_0}{t - t_0}\right) + A_0 \qquad (2.7)$$

The pumping speed was confirmed to be the same for the varying inlet lengths, and a fit corresponding to a pumping rate of 1.04 L s^{-1} was determined. With a typical inlet consisting of a 0.0125" I.D. Teflon tube with a length of 16 ft, this corresponds to an inlet residence time of only 0.037 s. The conductance of the inlet tube far exceeds the

sampling rate, as the maximum flow through the inlet system is over 10 L s^{-1}, and is therefore not an issue.

II.5 N_2O_5 Thermal Decomposition

N_2O_5 is thermally decomposed into NO_2 and NO_3 in order to analyze optically as NO_3. The absorption spectrum of N_2O_5 is very broad without any distinct peaks, and therefore it is extremely difficult to differentiate the absorption signal of interfering species from that of N_2O_5. Instead, the temperature dependent equilibrium that exists between N_2O_5 and NO_3 is exploited, and N_2O_5 is quantitatively converted and measured as NO_3.

As shown in Figure 2.3, the air sample is heated after the split between the two channels in the slow flow region. The heated section consists of a 47 cm section of FEP Teflon tubing that is wrapped several times with heating tape and insulted with woven fiberglass. The detection cavity is also heated to maintain temperature stability in the sample, and the aluminum manifold surrounding the FEP Teflon cavity is also wrapped with heating tape. The temperature is controlled manually by two Variac autotransformers.

Although the temperature dependent equilibrium of Equation 2.1 has been well characterized, calibration measurements were performed specifically for the TAMU CRDS instrument to insure complete conversion of N_2O_5 [*Ide et al.*, 2008]. Solid N_2O_5 was synthesized from ozone and nitrogen dioxide and delivered to the CRDS instrument by argon carrying gas at 20.0 sccm. The concentration of N_2O_5 and NO_3 was measured in each cavity while varying the temperature of the heated conversion region in the N_2O_5

channel. The conversion was measured at seven different temperatures of the heated inlet, ranging from approximately 330K to 394K. Concentrations of N_2O_5 and NO_3 were measured in respective cavities five times at each temperature through chemical titration by the injection of NO gas.

As shown in Figure 2.11, it is extremely difficult to maintain a consistent concentration of N_2O_5 delivered to the instrument for long periods of time (up to ten hours) required to perform these calibration measurements. The NO_3 observed in the system is the result of conversion of N_2O_5 at room temperature between the sample bubbler and the detection cavity, and should be relatively consistent given the consistent temperature of the laboratory. However, as seen in Figure 2.11, this is not the case. Although the argon carrier gas is delivered to the sample bubbler accurately through a mass flow controller, it is difficult to maintain the temperature of bubbler in a dry ice/acetone mixture. Also, N_2O_5 is a solid at this temperature and sublimes to a gas rather than evaporating from a liquid. As the experiment progresses, the surface area of the N_2O_5 exposed to the carrier gas can change dramatically causing a change in the concentration of N_2O_5 delivered to the system. It is therefore better to determine the degree of N_2O_5 thermal conversion through the observed $[N_2O_5]/[NO_3]$ ratio in the CRDS instrument.

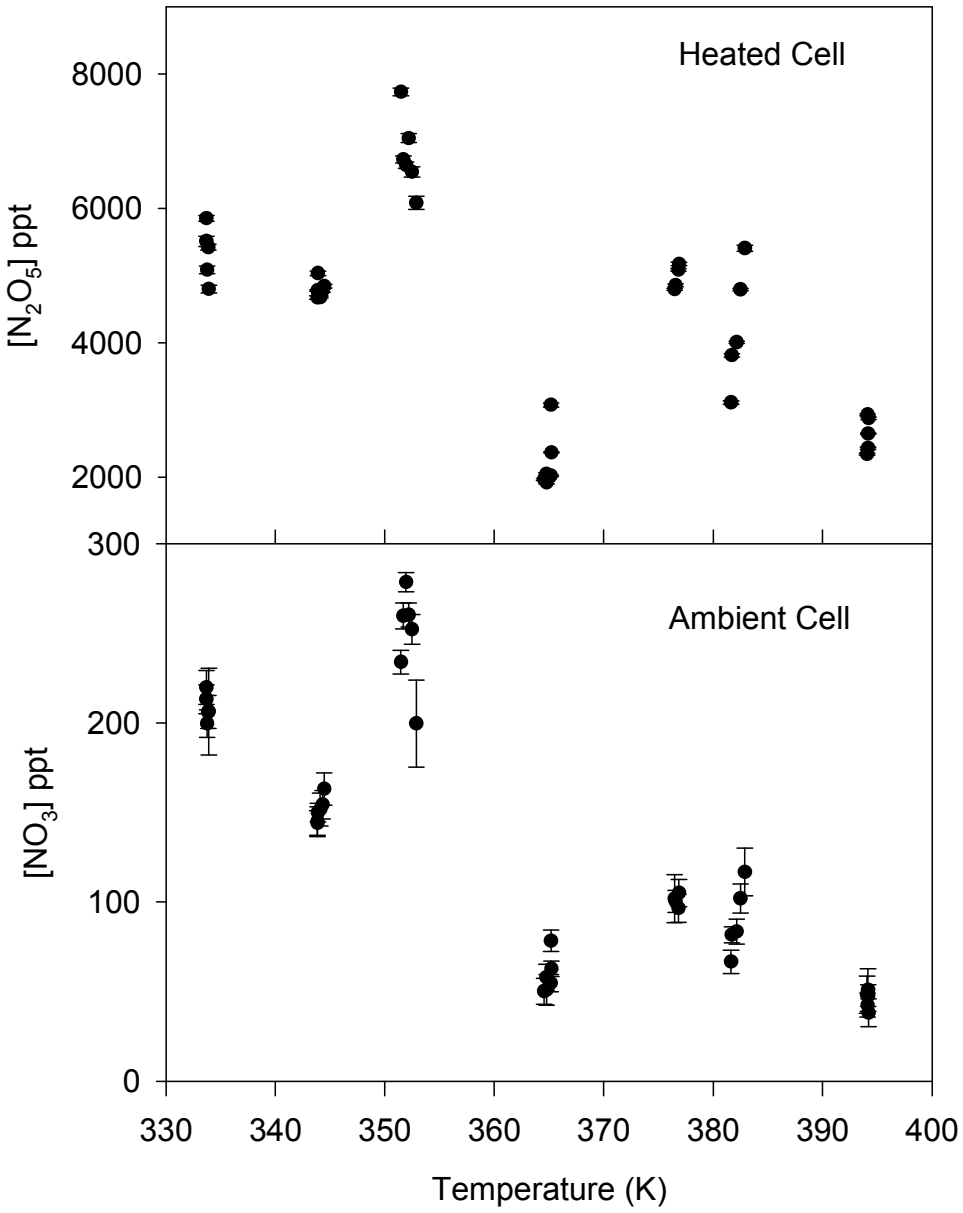

Figure 2.11. N_2O_5 and NO_3 concentrations at varying heated inlet temperatures.The ambient cell is maintained at 298K.

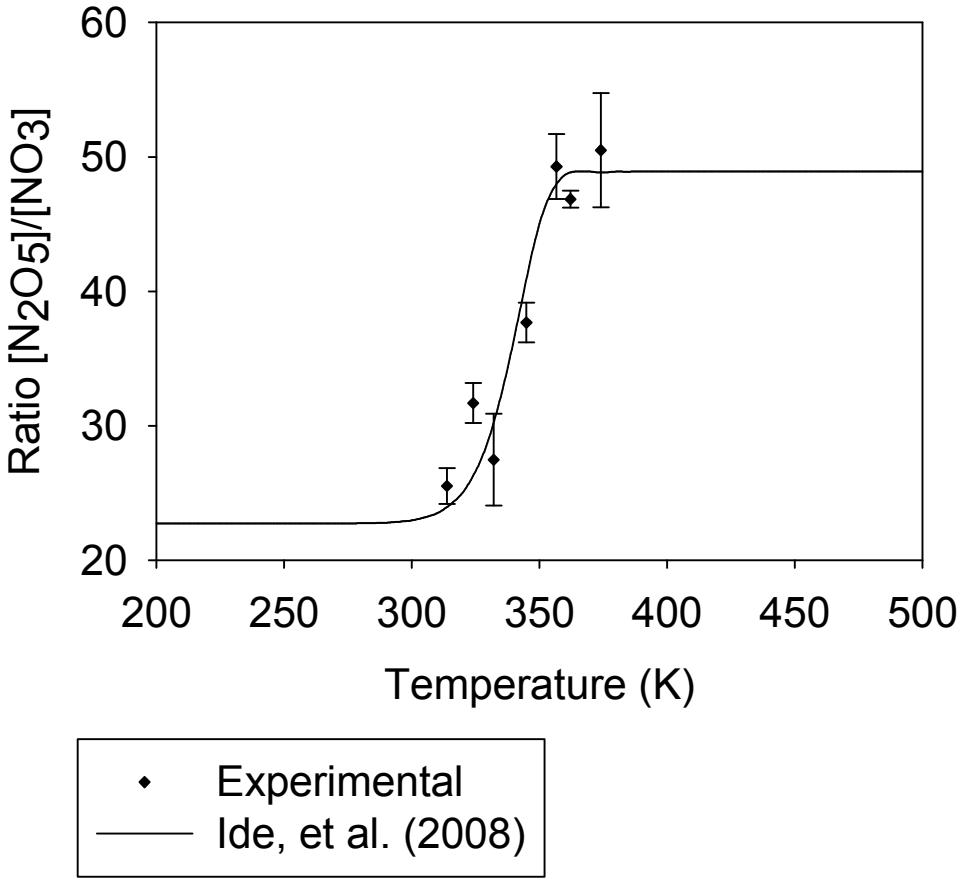

Figure 2.12. Ratio of observed $[N_2O_5]/[NO_3]$ compared with the calculated ratio using temperature equilibrium data by Ide, *et al*. 2008.

The ratio of $[N_2O_5]/[NO_3]$ was calculated at each measured temperature, and results are shown in Figure 2.12. Confirmation of the data was also performed by calculating the theoretical ratio $[N_2O_5]/[NO_3]$ using the temperature dependent equilibrium constant of Equation 2.1 published by Ide, et al. and shown in Equation 2.8.

$$K_{eq} = 1.36 \times 10^{15} \exp(\frac{-11300}{T}) s^{-1} \qquad (2.8)$$

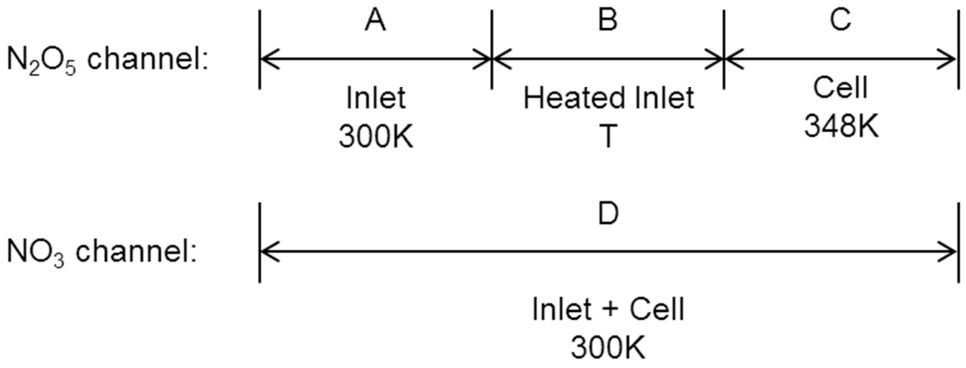

Figure 2.13. Temperature regions of each channel as defined in the temperature conversion model.

The theoretical ratio is calculated using a simple kinetics model based on the residence time and temperature of each section leading to the two detection cavities as shown in Figure 2.13. The model determines the quantity of N_2O_5 converted to NO_3 in each section and calculates the ratio according to Equations 2.9-2.16.

A:
$$[N_2O_5]_A = [N_2O_5]_0 \exp(-k_{300K} t_A)$$
$$[NO_3]_A = 1 - [N_2O_5]_A \qquad (2.9, 2.10)$$

B:
$$[N_2O_5]_B = [N_2O_5]_A \exp(-k_T t_B)$$
$$[NO_3]_B = 1 - [N_2O_5]_B \qquad (2.11, 2.12)$$

C:
$$[N_2O_5]_C = [N_2O_5]_B \exp(-k_{348K} t_C)$$
$$[NO_3]_C = 1 - [N_2O_5]_C \qquad (2.13, 2.14)$$

D:
$$[NO_3]_D = 1 - [N_2O_5]_0 \exp(-k_{300K} t_D) \qquad (2.15)$$

$$\frac{[N_2O_5]}{[NO_3]} = \frac{[NO_3]_A + [NO_3]_B + [NO_3]_C}{[NO_3]_D} \qquad (2.16)$$

where t_A is the residence time of the sample in Region A, etc. As shown in Figure 2.12, the calculated ratio based on literature values agrees very well with the observed ratio in the TAMU CRDS instrument. It is important to operate the system in the high temperature plateau region to ensure complete conversion of N_2O_5, and the instrument is typically operated with the heated inlet at 383-393K. At temperatures higher than this it is difficult to maintain stability in the exponential decay time. Additionally, NO_3 wall losses increase with increasing temperature, so the ideal temperature will be as low as possible to ensure complete N_2O_5 decomposition and minimum NO_3 wall loss [*Fuchs et al.*, 2008]

II.6 Determination of NO_3 Losses

NO_3 is an extremely reactive radical species, and will react on even the inert Teflon used in the CRDS instrument. It is therefore important to characterize the loss rates of NO_3 on the inlet in order to determine ambient concentrations.

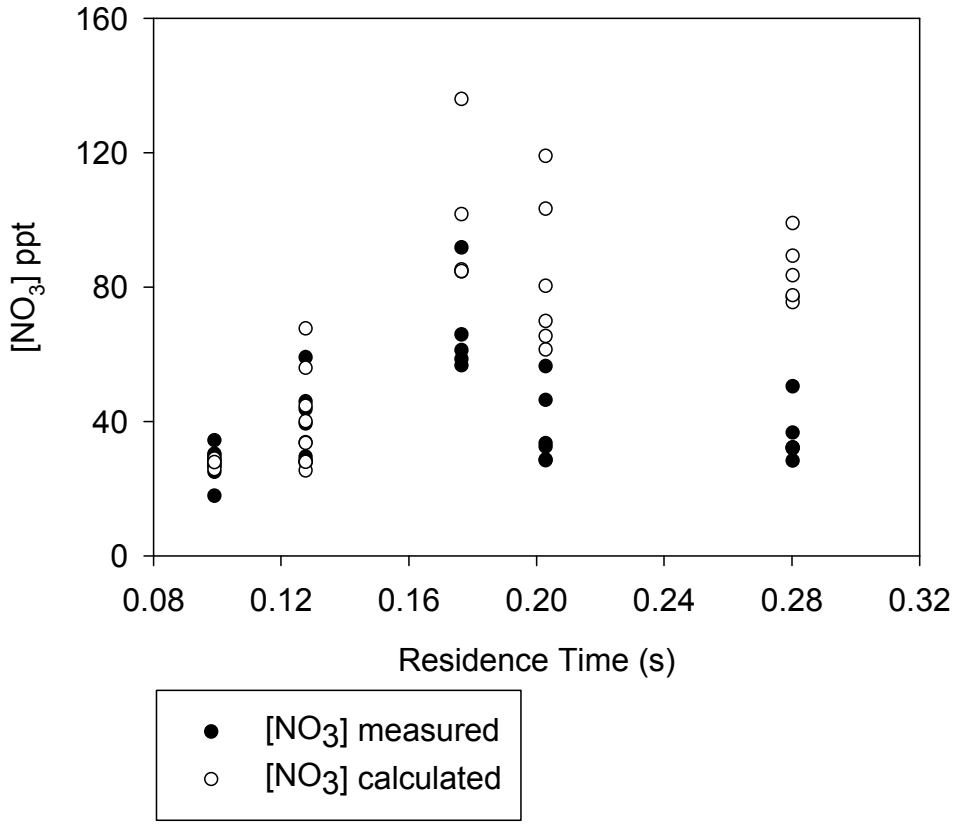

Figure 2.14 Concentration of NO_3 observed by the CRDS instrument compared to calculated NO_3 converted based of observed N_2O_5 concentration.

Experiments were performed using varying lengths of 0.125" I.D. PTFE Teflon tubing similar to what is used in the field for ambient measurements. Solid N_2O_5 sample was delivered to instrument using argon carrier gas at a flow rate of 20 sccm. Inlet lines ranging in length from 3.5 – 10 m and corresponding to an inlet residence time of approximately 0.1-0.3 seconds were used to determine the loss rate of NO_3 on the PTFE inlet. N_2O_5 has been shown to be unreactive on the Teflon inlet surface, so the absorption due to N_2O_5 measured in the heated channel can be used to calculate the concentration of NO_3 in the flow at the time of entry into the inlet [*Fuchs et al.*, 2008].

This was then compared to the observed concentration of NO_3 measured in the ambient temperature cavity to determine the loss rates. Consequently, the experiment is independent of any fluctuations in the concentration of sample gas delivered to the instrument throughout the experiment.

Results of the experiments are shown in Figure 2.14 and confirm that at longer inlet residence times less NO_3 is observed than expected. In order to model the loss rate of NO_3 on the inlet as a function of residence time, a first-order exponential decay rate was calculated based on the ratio of $[NO_3]_{measured}$ compared to $[NO_3]_{ambient}$ according to Equation 2.17 and 2.18.

$$NO_{3,ambient} \xrightarrow{k} NO_{3,measured} \tag{2.17}$$

$$\ln\left(\frac{[NO_3]_{measured}}{[NO_3]_{ambient}}\right) = -kt \tag{2.18}$$

$$k = 5.7 s^{-1} \tag{2.19}$$

where the time, t, is the residence time of the air sample in the inlet line. The loss rate constant, k, has been determined to be 5.7 s^{-1}.

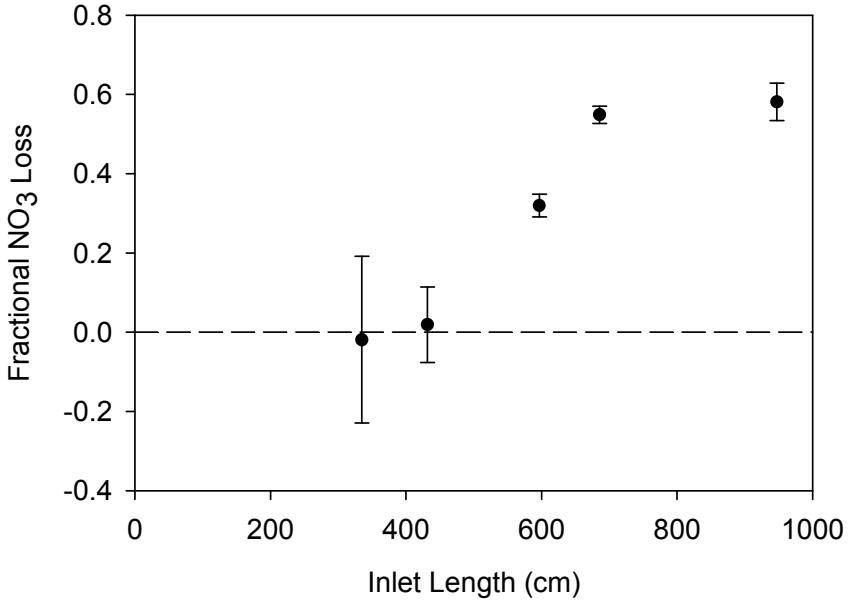

Figure 2.15. Fractional loss of NO_3 on varying inlet lengths.

Also interesting to note is the fractional loss of NO_3 on the inlet with increasing inlet lengths as shown in Figure 2.15. The length of the inlet is often dependent on the site logistics of the instrument in the field, and the inlet length is kept at the minimum possible. With respect to the loss of NO_3 on the inlet, it is important to be certain that the inlet is less than 600 cm (approximately 20 ft) and ideally less than 500 cm (approximately 16.5 ft) in order to detect ambient concentrations of NO_3.

CHAPTER III

NOCTURNAL NITROGEN CHEMISTRY IN HOUSTON, TX

III.1 Motivation

The large population density in urban areas leads to an increase in emissions and typically a poor air quality. As many urban centers are located in coastal regions, the tropospheric chemistry can be even more complicated by the presence of marine species. The large amount of emissions from both industrial processing and vehicular traffic has resulted in a history of ozone exceedance days in the city of Houston, TX. The history of poor air quality has made the region the subject of several large air quality studies to characterize the urban tropospheric chemistry of the area.

The first Texas Air Quality Study (TexAQS) took place in 2000 involving over 300 researchers at was located at three individual sites throughout the Houston area in a response to extremely high ozone concentrations that had been identified throughout the city. The focus of this study was to identify both chemical and physical processes that lead to atypical ozone events. A major finding of this study was the role of highly reaction volatile organic compounds (HRVOCs) and identified the need for the revision of the current state implementation plan (SIP) for the regulation of emitted compound. These reactive emissions, mainly ethylene, propylene, butenes, and butadiene, were found to be more detrimental in the formation of ground level ozone that emitted NO_x and were previously unregulated. The study was an excellent example of how

researchers in the scientific community were able to affect regulation and policy making for the betterment of air quality [*Allen et al.*, 2001].

The second major Houston field study was the second Texas Air Quality study, or TexAQS II, and took place from August-October of 2006. The goal during this project was to better understand ozone formation and distribution and establish the influence of background ozone in southeastern Texas. It was determined that although HRVOC emissions had been regulated due to the 2000 study, the emissions inventory still did not account for all observed HRVOCs. Also of note was the fact that a large amount of background ozone was observed, making it unlikely that local regulations could lead to the attainment of the current 75 ppb ozone NAAQS [*Parrish et al.*, 2009].

During the spring of 2009, the TAMU CRDS instrument was involved in a large Houston-based field study. The main focus of this study was to better understand tropospheric radical chemistry, and was known as the Study of Houston Atmospheric Radical Precursors, or SHARP. The goals of this project were to investigate the following processes:

1. The contribution of direct emissions of radical precursors HCHO and HONO from flares, stacks, and other point and mobile sources.
2. The identification of formation pathways of HONO including differences in night and day formation, heterogeneous and surface reactions, and gas-phase formation.
3. Impact of both fresh and aged soot on chemistry, climate, and dynamics.
4. The ambient levels of $ClNO_2$ in Houston and potential as a radical source.

5. The relative importance of measured radicals and other "missing" radical sources.

6. Identify important spring ozone formation mechanisms in Houston.

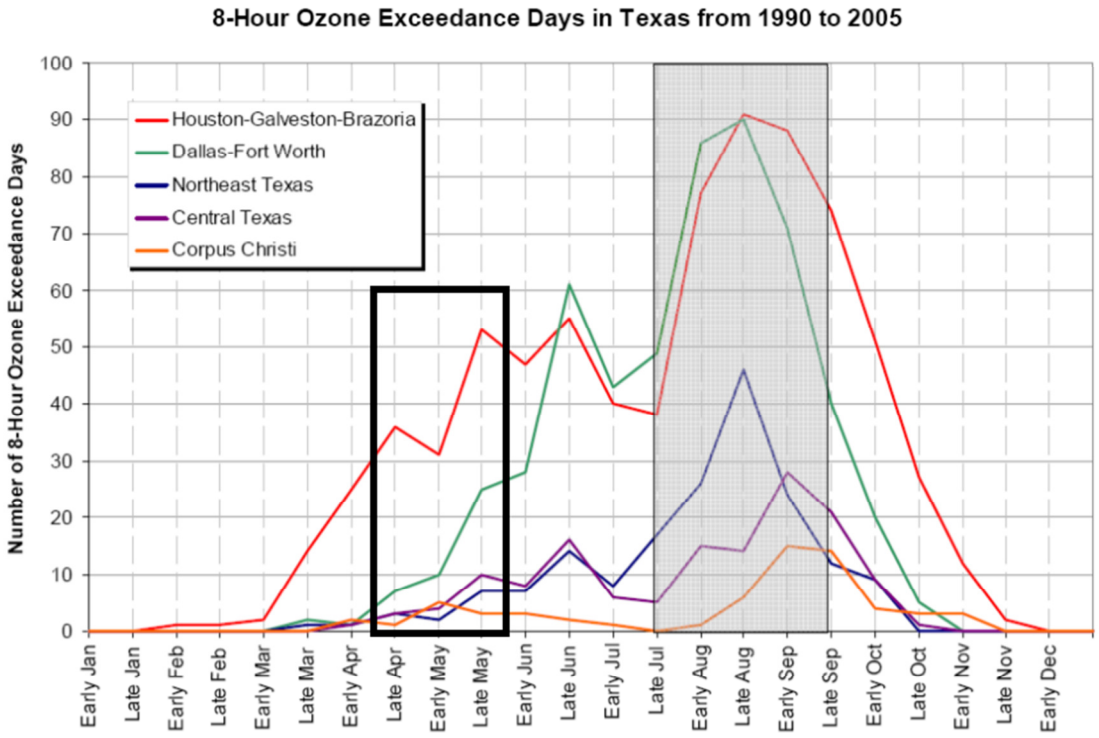

Figure 3.1. Number of exceedance days based on calendar month in several Texas regions from 1990 to 2005. The focus of the previous Houston field studies is highlighted in gray and the time period of the SHARP campaign is outlined in black.

The SHARP field study involved over 50 researchers from universities and government laboratories throughout the United States, and was also the first large field study in which the TAMU CRDS instrument participated. The majority of the measurements were performed from 15 April to 30 May 2009 on the North Moody Tower on the University of Houston campus. Additional measurements were performed

in other locations and in mobile and airborne laboratories. However, this data was not used in comparison to the TAMU CRDS measurements and will not be discussed here. This time period was chosen specifically to study the cause of ozone exceedance days in the spring, as most previous concentrated campaigns in Houston studied the ozone formation in the late summer and early fall months.

As shown in Figure 3.1, there has been a larger number of ozone exceedance days in the late summer in the Houston region, however there are also a significant number in the spring. Typically, ozone is higher in the late summer months because an increase in the temperature and sunlight creates favorable conditions for ozone production. This is also coupled with northerly winds that are typical of that season and bring an increase in the background ozone. The spring conditions favor ozone production as well. The wind direction is typically southerly to southeasterly, and while this does not provide a large amount of background ozone, the wind direction does provide transport for the emitted precursor compounds from industrial processing centers. There is also tendency to have a high amount of stratospheric ozone entrainment in the late spring. However, with a lower temperature and background ozone, the springtime does not normally provide as much ozone production as the late summer. There is a decrease in the ozone exceedance days in the early summer because the meteorological conditions do not favor ozone production or the delivery of background ozone.

Notable in this field study was the abundance of nighttime nitrogen species that were measured. Collaborative efforts between individual researchers encompassed the

measurements of NO_x, HONO, N_2O_5, and HNO_3, meaning the nocturnal fate of nitrogen in the troposphere can be observed. This was especially important in the understanding of the processing of N_2O_5, as both source and sink terms were measured in addition to the concentration of N_2O_5.

Nitryl chloride was first observed ambiently during TEXAQS II in 2006 on the NOAA research vessel, *Ronald H. Brown*, in the Gulf of Mexico and Houston ship channel. It was determined through analysis of this data that the reaction of N_2O_5 with heterogeneous chloride ions is the major source of $ClNO_2$ with possible implications in the formation of additional tropospheric ozone. Scientists from the Georgia Institute of Technology in Atlanta, GA performed nitryl chloride measurements on Moody Tower during the SHARP campaign. The comparison of the ambient concentration to that of N_2O_5 was analyzed to determine the prevalence of this pathway in the fate of N_2O_5 and nocturnal nitrogen oxides.

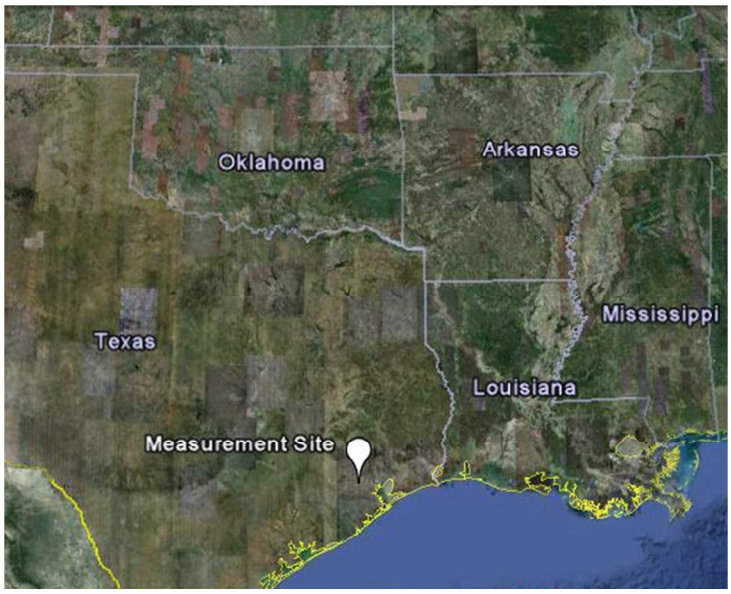

Figure 3.2. Location of measurement site in Houston, TX in relation to the Southern United States and Gulf of Mexico coastline.

III.2 Site Description

The city of Houston is located near the Gulf of Mexico coastline in Southeastern Texas and the regional location is shown in Figure 3.2.The measurement site was approximately 65 km from the shore of the Gulf of Mexico. Galveston Bay, an estuary with a mixture of salt water and fresh water, extends inland approximately 30 km from the measurement site. Houston is the fourth largest city in the United States in population, and the area also contains a significant number of oil refineries and chemical processing plants. This results in a large amount of emissions from both industrial and vehicular sources. Because of this, legislation has been difficult as both individual and industrial pollutant sources must be regulated. A high amount of ship traffic also leads to significant emissions, and is concentrated along what is known as the Houston Ship Channel to the northwest of the Galveston Bay.

Figure 3.3. Location of Moody Tower in Houston, TX in relation to Galveston Bay and Houston Ship Channel.

Figure 3.4. View of Downtown Houston to the Northwest from the measurement site on the roof of the Moody Tower.

Figure 3.5. View of the Houston Ship Channel to the East from the measurement site on the roof of the Moody Tower.

Measurements of N_2O_5 were taken from the roof of the North Moody Tower on the University of Houston campus (29.718, -95.342). The Moody Tower is an eighteen story dormitory located in southeastern Houston just inside of the 610 traffic loop. The geographical location in relation to the city is show in Figure 3.3. The University of Houston is located approximately 5 km to the southeast of Downtown Houston, pictured from the top of the tower in Figure 3.4, and approximately 25 km from the entrance to the Houston Ship Channel from Galveston Bay. The view of the ship channel from the top of the tower is shown in Figure 3.5. Typical Spring wind direction is southerly to south-easterly, and puts the Moody Tower in a good position to observe emissions from industrial sources along the Gulf of Mexico coastline.

Figure 3.6. The North Moody Tower on the University of Houston campus. Measurement trailers can be seen on the roof along with the scaffolding for meteorological measurements.

The measurement trailer was located approximately 70 m above ground in the southeast corner of the Moody Tower. The immediate area surrounding the measurement site is a university campus with very few emission sources to provide a local bias in the measurements. A second tower of equal height, the South Moody Tower, is adjacent to the building where the measurements were performed and is shown in Figure 3.6. However, with the exception of this tower all surrounding buildings are significantly lower in height and do not affect the flow of the air mass. Meteorological measurements, especially wind speed and wind direction, were deliberately performed at a height higher than the adjacent tower so as not to contain an artificial bias. While there are several large trees located on the campus and wooded areas in the surrounding region, there is not a significant amount of vegetation as to provide an increased amount of biogenic hydrocarbon emissions.

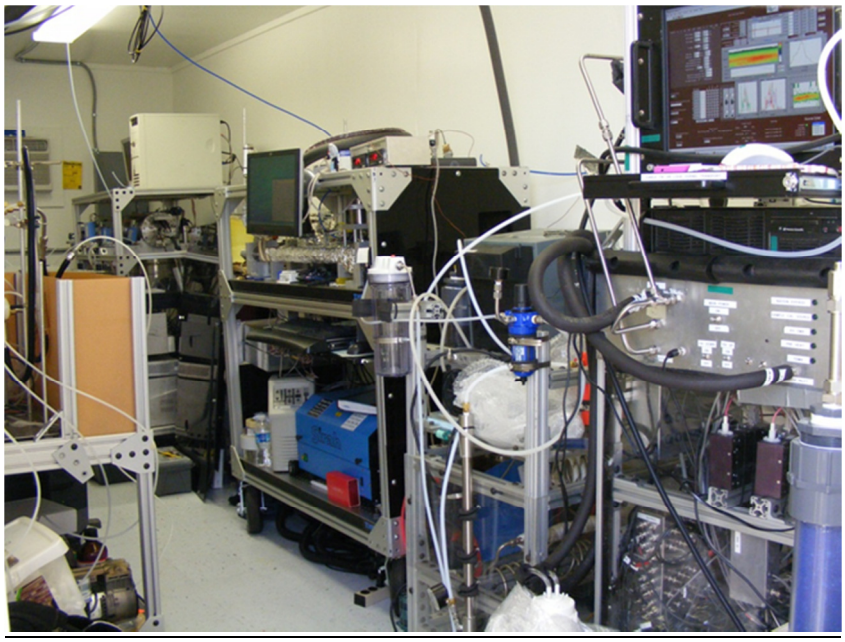

Figure 3.7. Instrumentation located in Trailer 4 during the SHARP campaign. The TAMU CRDS instrument is seen in the center.

III.3 Experimental Methods

N_2O_5 was measured using the Texas A&M cavity ring-down instrument from 15 April 2009 to 31 May 2009. The instrument was located in Trailer 4 in the southeast corner of the North Moody Tower approximately 70 m above ground level. The instruments housed in Trailer 4 were all operated by Texas A&M University researchers, and are pictured in Figure 3.7. All of these instruments were designed and operated by the TAMU Department of Atmospheric Sciences Renyi Zhang and Don Collin's Research Groups, with the exception of the CRDS which was developed and operated by the Department of Chemistry.

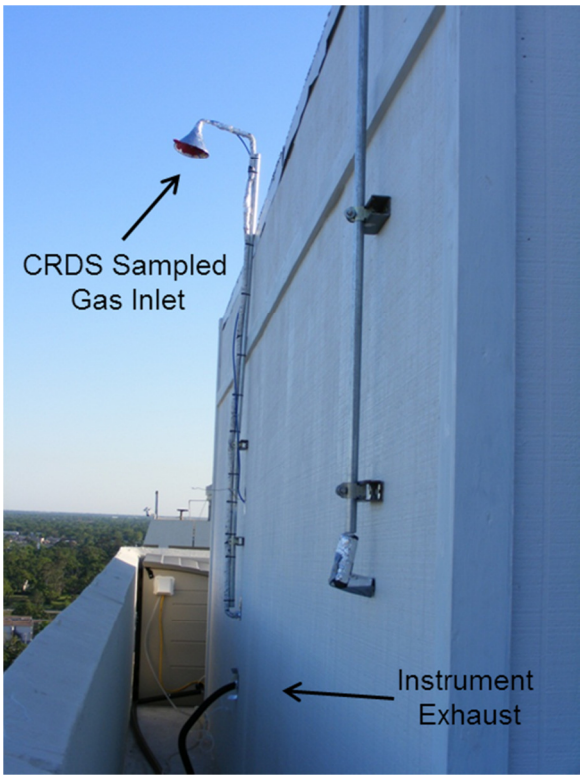

Figure 3.8. Location of sampled gas inlet and instrument exhaust in Trailer 4 on the roof of Moody Tower.

The CRDS instrument both sampled air and exhausted through the back wall of Trailer 4, and both the inlet and the exhaust are pictured in Figure 3.8. The instrument used a 16 ft, 0.125 in I.D. Teflon inlet utilizing a Teflon funnel on the end to prevent the pumping of moisture from rain into the instrument. The inlet was located approximately 0.5 m above the roof of the trailer and 20 cm away from the wall in hopes of minimizing the contact of sampled air with the structure. The instrument exhaust, also shown in Figure 3.8, was connected to a common exhaust line for all instruments located on the roof of Moody Tower, and was pulled to ground level and away from all instrumentation sampling inlets.

The TAMU CRDS instrument was set up to measure N_2O_5 through thermal decomposition followed by absorption of 662 nm light by NO_3. The instrument was automated to perform a measurement of the intrinsic ring-down of the cavity through titration of NO_3 by NO gas for thirty seconds followed by ninety seconds of absorption measurements. The Teflon aerosol filter of the instrument was replaced with a fresh filter manually every 1 hr to ensure minimal losses of N_2O_5 to particles trapped by the filter. The laser was operated at a 10 Hz repetition rate, and data was collected using 50 shot averaging, resulting in a 5 s integration time.

The TAMU CRDS instrument was operated for most nights within the 15 April – 31 May period with the exception of nights experiencing heavy rainfall or thunderstorms with a high probability of lightening. Typically measurements were performed starting from approximately thirty minutes before sunset and continuing to approximately thirty minutes after sunrise. For this time of year this equated to 20:00 to 06:00 Central Standard Time. It is important to note that all data are reported in Central Standard Time as opposed to Central Daylight Time.

III.4 Supporting Measurements

In order to fully understand the nighttime nitrogen chemistry in an urban area, it is necessary to perform measurements of several different species. This allows for the quantification of the partitioning of the nitrogen pathway and the analysis of the nitrogen budget. Many of the analyses presented in this work would not have been possible without the work of several other research groups that participated in the SHARP campaign.

The research group of Prof. Barry Lefer at the University of Houston was responsible for several key measurements during the field study including all meteorological measurements. All wind speed and wind direction measurements as well as the ambient temperature were measured from the roof of the North Moody Tower and adjacent to the N_2O_5 measurement trailer. It was crucial that these measurements be made in close proximity to the N_2O_5 measurements as meteorology in an urban area can exhibit a high spatial variability. The Lefer Research Group also performed measurements of ozone ambient concentration as well as nitrogen dioxide concentration measurements that are included in this chapter. Ozone measurements were performed with a commercially available ozone absorption spectrometer (ThermoFisher) which was calibrated with standard gas and zero air once per day. A commercially available NO_X analyzer (ThermoFisher) utilizing chemiluminesence was used for nitrogen dioxide measurements. These measurements were used in the calculation of the ambient atmospheric lifetime of N_2O_5.

Prof. Jack Dibb of the University of New Hampshire measured the ambient concentration of nitric acid throughout the study duration using the spray mist chamber/ion chromatography technique [*Scheuer et al.*, 2003; *Talbot et al.*, 1990]. In this method, sampled air passes through a small chamber where it is met by a dense, fine mist of water. Any water-soluble gases, including HNO_3, are then collected in the aqueous phase. The sample is then measured for the presence of corresponding soluble ions, in this case NO_3^-, by an ion chromatograph. While this method is extremely accurate and has a low detection limit, the drawback is a longer measurement integration

time. During the SHARP study, the mist chamber recorded HNO_3 in thirty-minute time intervals.

Prof. Greg Huey of Georgia Institute of Technology performed the nitryl chloride measurements using chemical ionization mass spectrometry (CIMS) and the technique has been previously described [*Huey*, 2007; *Kercher et al.*, 2009; *Slusher et al.*, 2004]. In this method, iodide ion-molecule clusters are formed from ambient $ClNO_2$ through the reactions represented in Equations 3.1 and 3.2.

$$I^- + ClNO_2 \rightarrow I(ClNO_2)^- \quad (3.1)$$

$$I^- + ClNO_2 \rightarrow ICl^- + INO_2 \quad (3.2)$$

and the ionized chloride compounds are detected through time-of-flight mass spectrometry which allows for quantization of ambient concentrations.

III.5 Summary of Measurement Period

N_2O_5 was observed during the initial few days of the study preceding a large storm that passed through the region. However, in the month following this frontal passage, no N_2O_5 was observed for nearly thirty consecutive days. Strong winds that led to atypically low ozone concentrations. All nitrogen oxides were measured in low mixing ratios, so this issue was not specific to the TAMU CRDS instrument.

N_2O_5 was observed in elevated concentrations by TAMU CRDS on several occasions, most notably following frontal passages. A large storm system moving through the area is typically followed by stability in the local air mass and a decrease in wind speeds. In a high emission urban area such as Southeastern Texas, this results in the increased concentration of pollutants without a clean air mass to dilute the local

emissions. Elevated concentrations of ozone during the day resulted in atypically high sources of N_2O_5 as nitrogen oxides are removed from the air, and were confirmed through observation of the ambient concentration.

Although the TAMU CRDS system is capable of simultaneously measuring N_2O_5 as well as NO_3, no ambient NO_3 was observed during the time frame of the SHARP campaign on Moody Tower. There are several possible explanations:

1. Losses of NO_3 within the CRDS instrument are greater than expected which caused a bias in the measurement of NO_3 and raised the instrument detection limit higher than calculated. Given the extent of laboratory calibrations as discussed in Chapter II of this work, this explanation is however unlikely.
2. It is more likely that the sampling location was unfavorable for NO_3 detection. As shown in Figure 3.7, the sampling inlet was located immediately adjacent to the instrument trailer without much effort to avoid sampling air that has made contact with the building or trailer itself. It is possible that chimney effects artificially removed any NO_3 from the sampled gas.
3. The final possible cause of the lack of NO_3 detection is that the height of the tower was too low in the NO_3 vertical profile. The Moody Tower is approximately 70 m in height, and several studies into the NO_3 vertical profile have suggested relatively low concentrations at measurement heights lower than 100 m [*Fish et al.*, 1999; *Geyer and Stutz*, 2004; *Stutz et al.*, 2004].

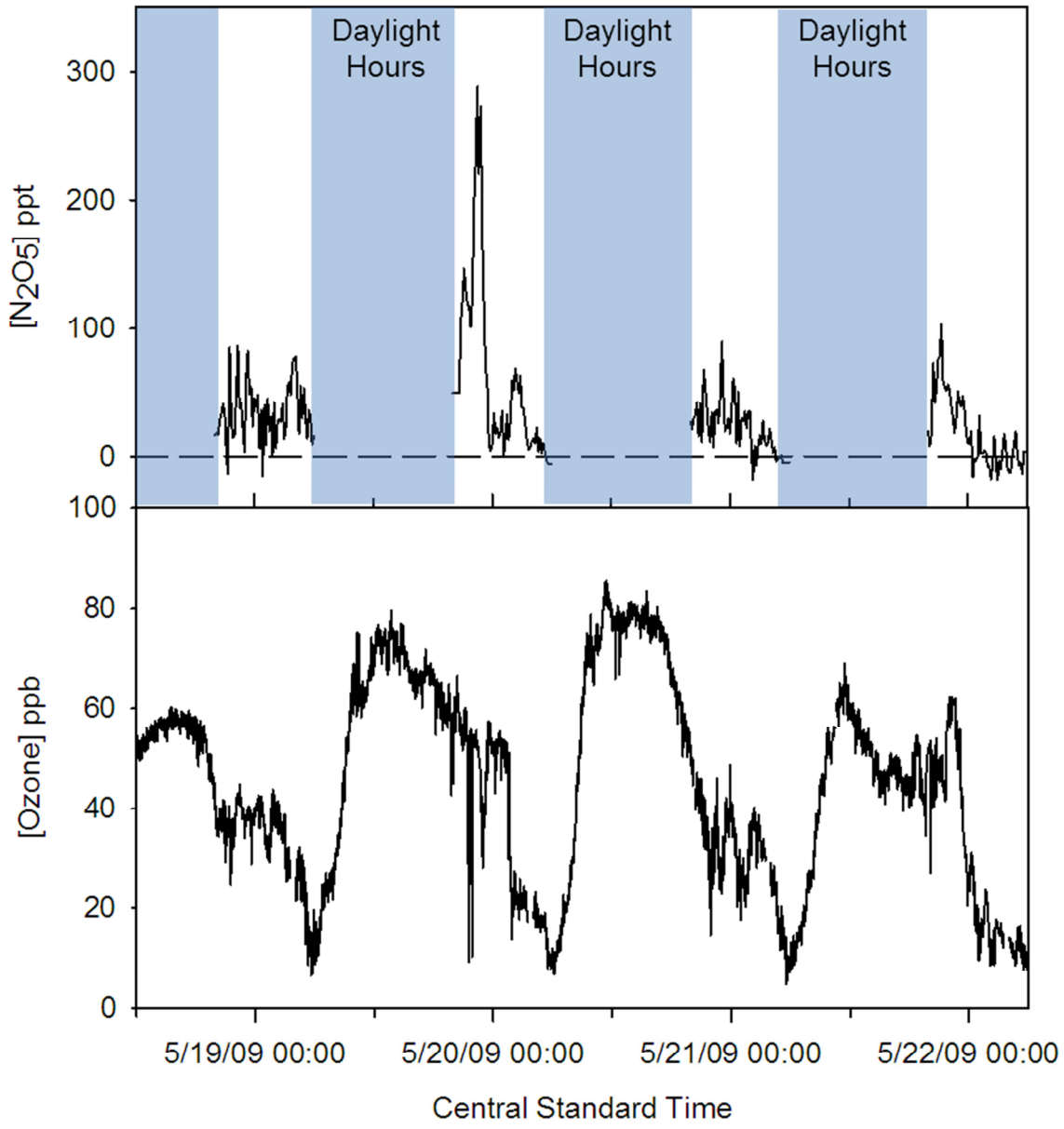

Figure 3.9. N_2O_5 and ozone concentrations from 18-22 May 2009.

III.6 Observations of Nocturnal Ambient Species from 18-22 May 2009

High levels of N_2O_5 were observed after a frontal passage that occurred on May 17, 2009, and the results on the following four evenings are shown in Figure 3.9 along with the ozone profiles observed on Moody Tower. The highest ambient levels of N_2O_5 were on the evening of 19-20 May 2009, and exceeded 300 ppt for a short time between 22:00 and 21:00. Although N_2O_5 was measured consistently at night over the four day period, the concentration was lower on the preceding day and subsequent two days, and never surpassed 100 ppt. The ozone concentration was elevated over all four days, and exceeded the Environmental Protection Agency (EPA) standard of 75 ppb on both 19 May and 20 May 2009.

An important note from the data in Figure 3.9 is that the higher N_2O_5 concentration at night is not dependent simply on the levels of ozone during the day. The highest concentration of ozone during this four-day period was reached on 20 May 2009, however the concentration of N_2O_5 the subsequent evening was less than 100 ppt. On the previous day, 19 May 2009, the ozone concentration was never higher than 80 ppb, a threshold that was passed on 20 May. However, due to the local chemistry of this night in particular, the ambient ozone persisted at high levels long after sundown when ozone concentrations normally begin to show a decrease. In an area with a large amount of chemical and petroleum processing such as Houston, nitrogen oxide emissions continue all night as processing plants are typically fully operational twenty-four hours a day.

With the presence of ozone late into the night and long after sunset, large quantities of N_2O_5 are formed via Equations 3.3 and 3.4.

$$O_3 + NO_2 \rightarrow NO_3 + O_2 \quad (3.3)$$

$$NO_3 + NO_2 \leftrightarrow N_2O_5 \quad (3.4)$$

Without nighttime ozone, the source reactions cannot proceed even if there are significantly high amounts of nitrogen oxides emitted.

Because of the large elevation in the N_2O_5 concentration that occurred on 19-20 May 2009, this data was explored further and is shown in detail with error bars in Figure 3.10. The error is evaluated individually for each data point, and therefore varies throughout the night. We found an average error for the night of 2.90 ppt, which provides good signal-to-noise ratios at the elevated values. Due to the fact that other measurements involving the TAMU CRDS system were being performed on this night, the system did not start measuring ambient air samples until 20:40 which was approximately 1 hour after sunset. The instrument began detecting elevated concentrations immediately, which rose over the course of the next two hours. A maximum N_2O_5 concentration of 303.7± 1.93 ppt was reached at 22:21. At approximately 23:00, a rapid decrease in the concentration was observed with no observable N_2O_5 at approximately 23:45. Small levels were observed for the rest of the night; however, concentrations never exceeded 100 ppt.

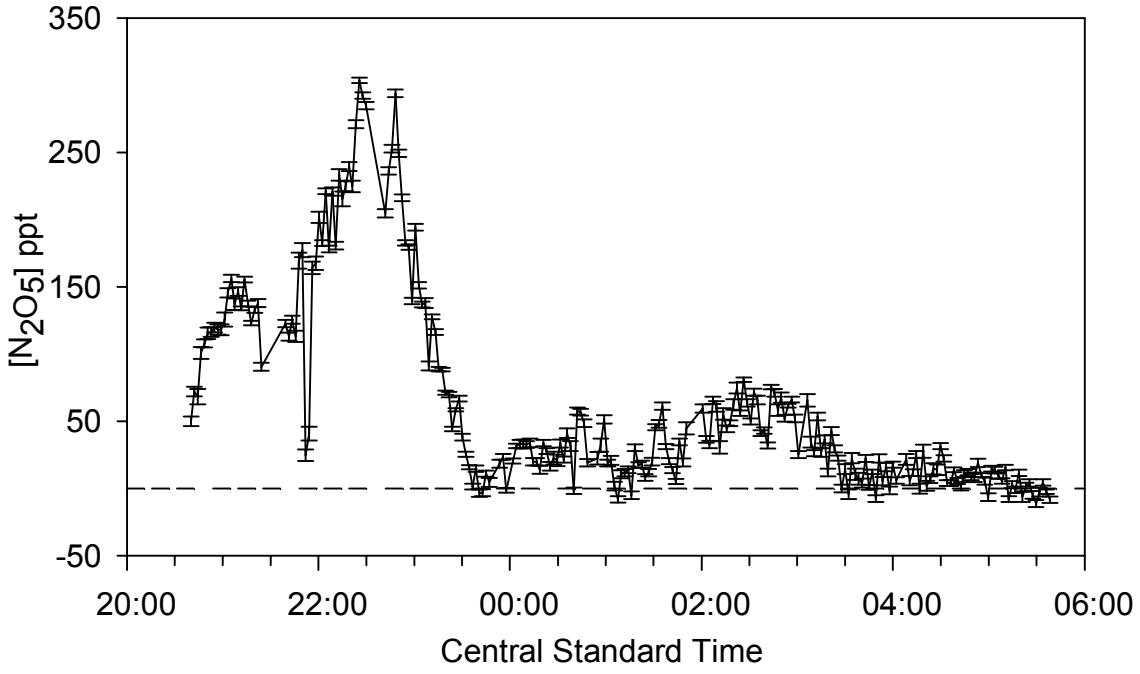

Figure 3.10. Measured N_2O_5 concentration on 19-20 May 2009 showing the measurement uncertainty.

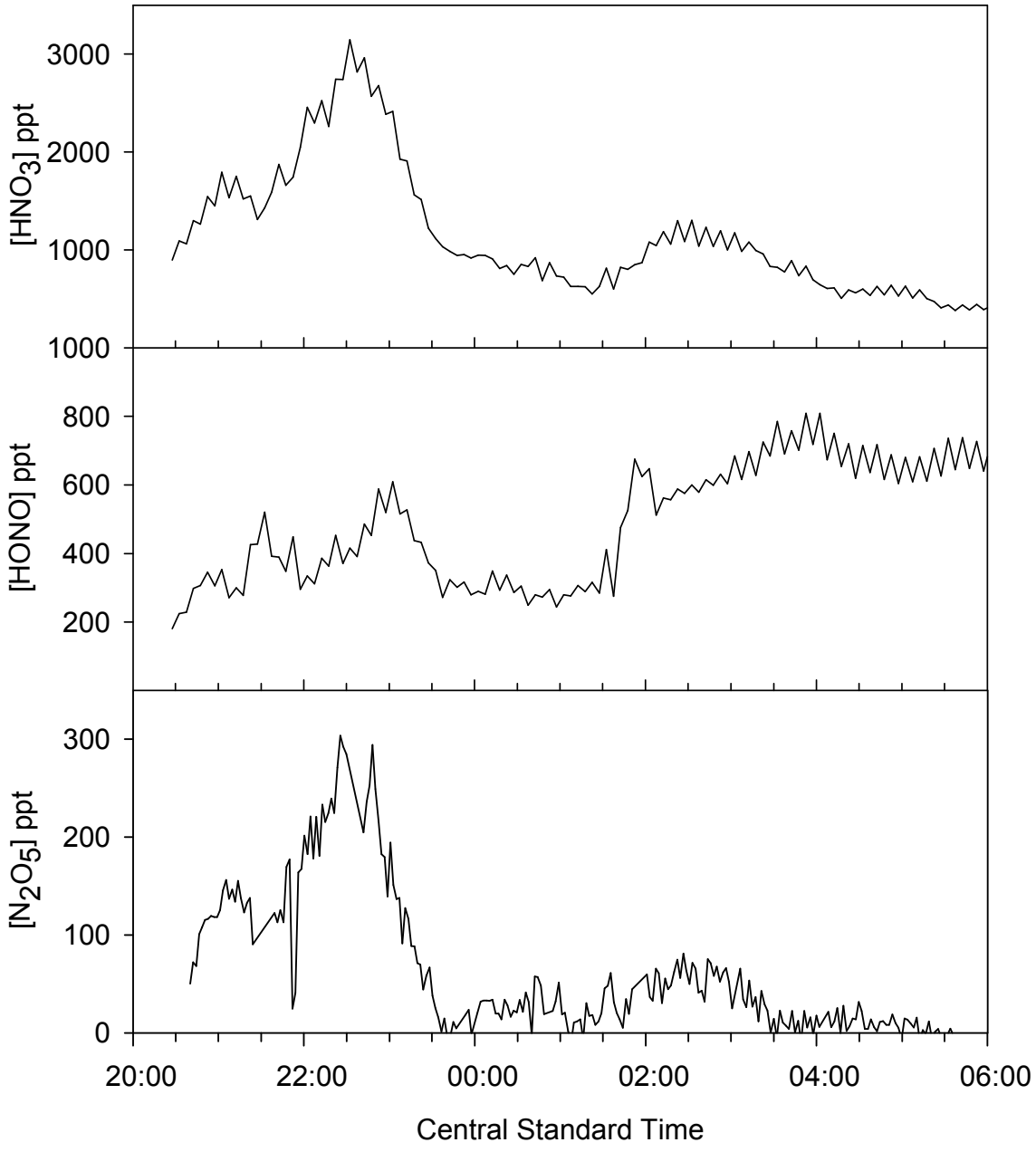

Figure 3.11. Measurements of N_2O_5, HNO_3, and HONO on 19-20 May 2009.

The measurements of three nocturnal nitrogen species, nitrous acid, nitric acid, and N_2O_5, were shown to correspond in similar profiles on the night of 19-20 May. The HONO and HNO_3 measurements were performed by Prof. Dibb of the University of New Hampshire, and are compared with the N_2O_5 measurements by TAMU CRDS in Figure 3.11. As these species are all dependent on emitted nitrogen oxides as a source, similar profiles are to be expected. Multiple previous studies have shown that N_2O_5 is the primary source of nitric acid at night through heterogeneous hydrolysis following Equation 3.5.

$$N_2O_{5(g)} + H_2O_{(l)} \xrightarrow{het} 2HNO_3 \qquad (3.5)$$

The strong correlation of the observed concentrations of N_2O_5 and HNO_3 reinforces the dependence of nitric acid production on the N_2O_5 concentration. Several features observed in the N_2O_5 profile were absent from the HNO_3 measurements, for instance the sudden drop in the N_2O_5 concentration around 22:00, however this is most likely an artifact of the longer integration time of the HNO_3 instrument. The drop in concentration at this time could have several causes. While this could be due to the chemistry, it is more likely the result of a sudden updraft in the wind. If ground level air was carried up the side of the building, reactions with the ground surface would have cause a decrease in reactive species such as ozone and N_2O_5. Unfortunately, vertical wind velocity was not measured on the tower and it is there impossible to know for sure.

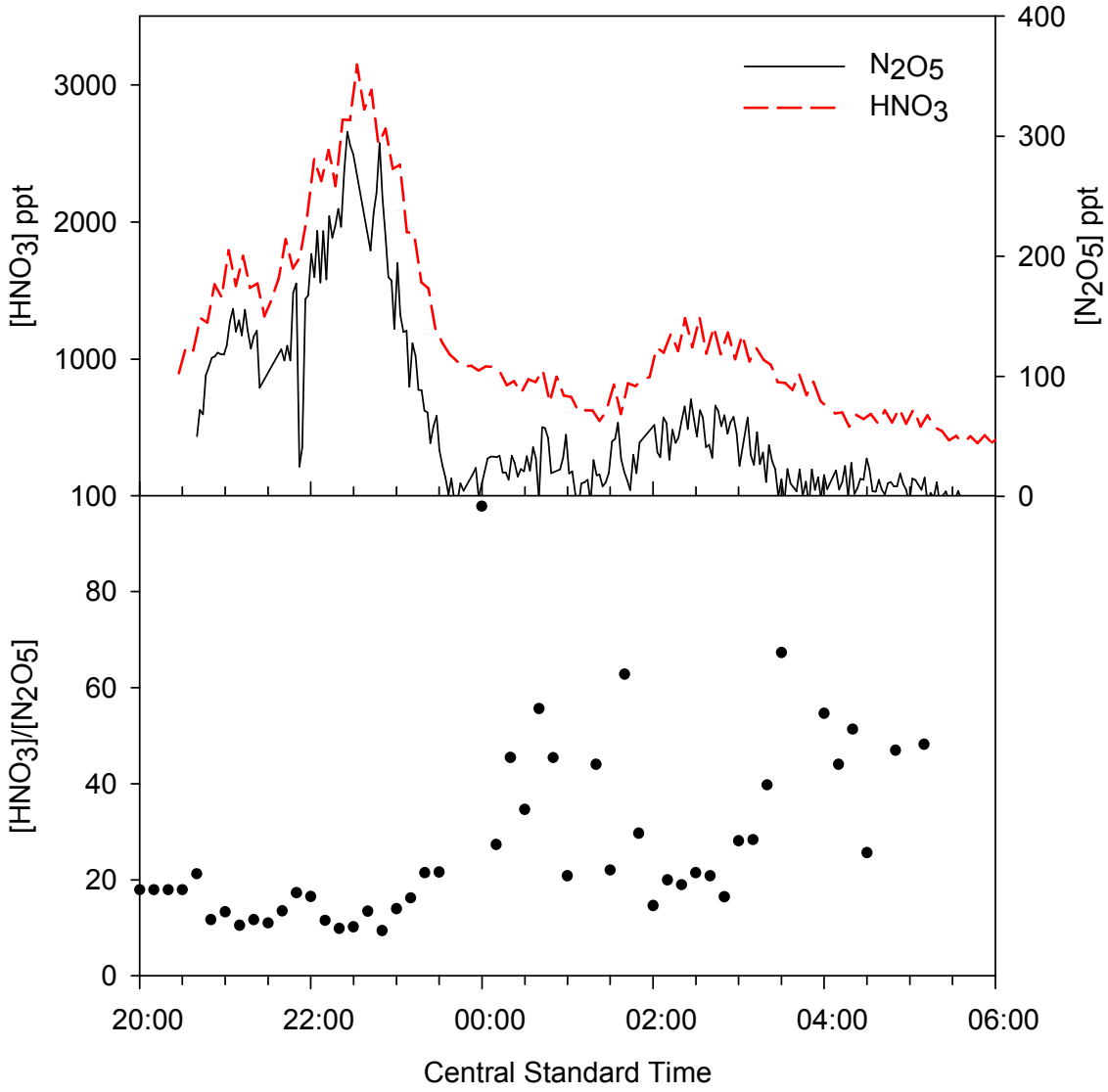

Figure 3.12. Comparison of observed N_2O_5 and HNO_3 along with HNO_3/N_2O_5 ratio on the evening of 19-20 May 2009.

The ratio of HNO_3 to N_2O_5 is an indicator of the degree of N_2O_5 hydrolysis, and the calculated ratio for 19-20 May is shown in Figure 3.12. A larger ratio is representative of an increased rate of conversion of N_2O_5 into HNO_3, and a smaller value for the ratio indicates slow and inefficient N_2O_5 hydrolysis. Typically a HNO_3/N_2O_5 ratio higher than 12 is considered a relatively fast conversion and indicates the dominant nighttime NO_x loss through heterogeneous hydrolysis. As seen in Figure 3.12, the ratio was quite high throughout the night, ranging from 10 to 20 before midnight before rising rapidly to a maximum of 80.

The main source of ambient HONO is through the reaction of NO_2 with hydroxyl radical during the day; however OH is not available at night. Although not yet fully understood, it is thought that the main source of nocturnal HONO is through the heterogeneous reaction of nitrogen dioxide with water on a particle surface as shown in Equation 3.6 [*Finlayson-Pitts et al.*, 2003].

$$2NO_{2(g)} + H_2O_{(l)} \xrightarrow{het} HONO_{(g)} + HNO_{3(g)} \qquad (3.6)$$

Several other mechanisms for HONO formation, including the homogeneous formation of HONO in the gas phase, have been observed in the laboratory. However, these reactions have been shown to be considerably slower and therefore are not thought to be atmospherically significant. While the kinetics of Equation 3.6 continues to be investigated, it is assumed that this reaction dominates the formation of nighttime nitrous acid. While formed through Equation 3.6, the primary source of nitric acid at night is believed to be the heterogeneous hydrolysis of N_2O_5 [*Bertram et al.*, 2009; *Dentener and Crutzen*, 1993]. Therefore, nitric acid, nitrous acid, and N_2O_5 expected to exhibit a very strong correlation, and the concentrations of all three species should be dependent on both nighttime nitrogen emissions and aerosol properties.

The formation of HONO at night relies directly on the presence of nitrogen dioxide as well as the abundance and composition of particulates whereas HNO_3 does not. The formation of HONO and HNO_3 favors similar aerosol conditions, but HONO is directly influenced by rapid changes in NO_2 mixing ratios[*Finlayson-Pitts et al.*, 2003]. As seen in Figure 3.11, around 02:00 the HONO and HNO_3 profiles began to deviate. While HNO_3 correlated with the availability of N_2O_5 and declined in concentration, the measured concentration of HONO increased from 275 ppt to 675 ppt.

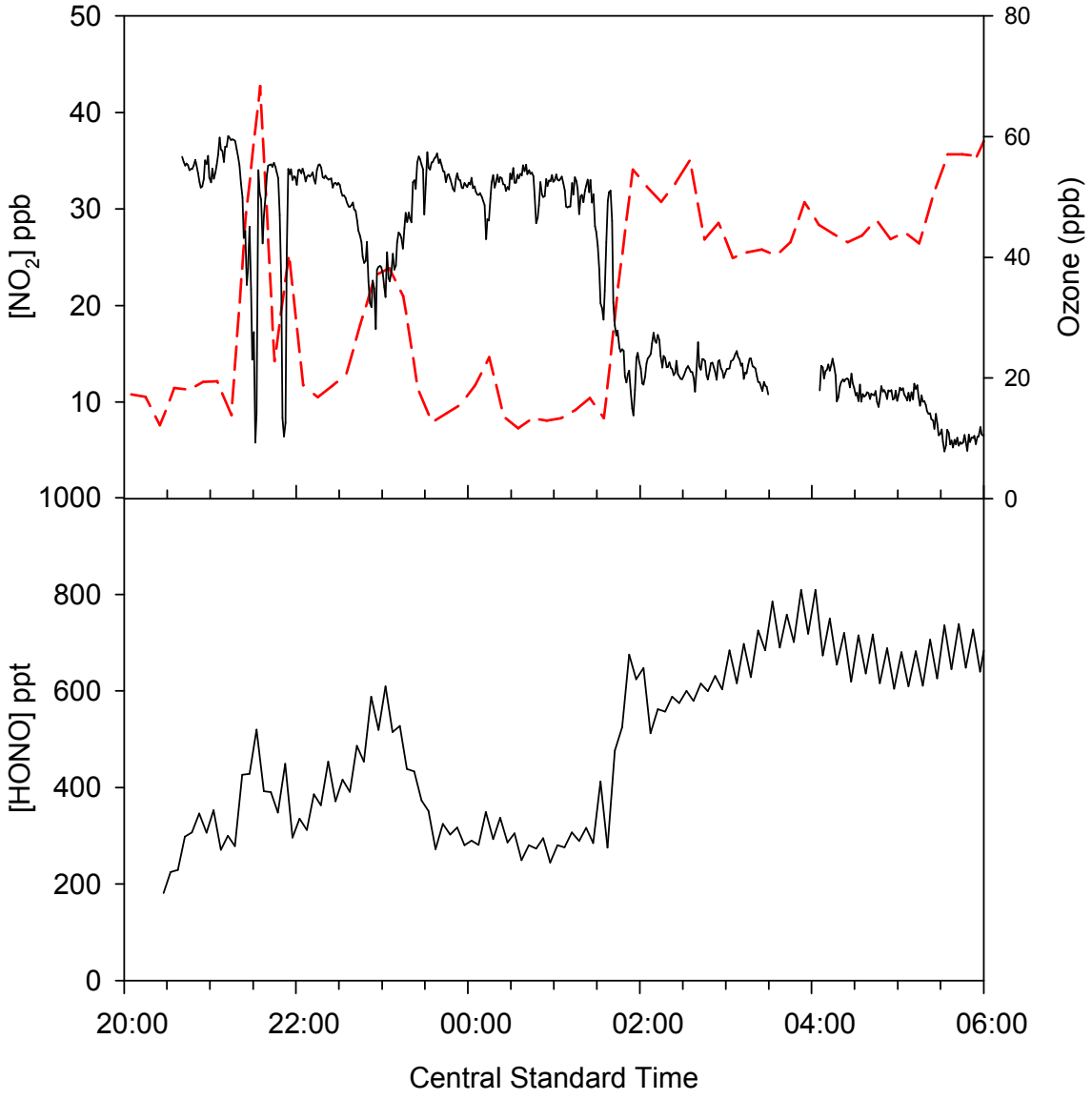

Figure 3.13. Ozone, nitrogen dioxide, and HONO measured at Moody Tower on the night of 19-20 May 2009.

There was a sudden increase in the nitrogen dioxide concentration around 02:00 on 20 May, explaining the deviation of in the profile of the mixing ratio nitrous acid from the other two nitrogen compounds. The observed nitrogen dioxide and ozone concentrations compared to measured ambient HONO concentration are shown in Figure 3.13. Also of note in this figure is the rapid formation of HONO in response to the increase availability of source compounds, indicating a fast hydrolysis of NO_2 on aerosol particles [*Finlayson-Pitts et al.*, 2003]. As nitrogen dioxide is only a direct source for HONO and not HNO_3 or N_2O_5, it is expected that a fast change in the nitrogen dioxide concentration will affect HONO formation more rapidly than the other two compounds. The formation nitric acid and N_2O_5 are also reliant on the presence of ozone. A sudden increase in NO_2 is nearly always associated with a large and rapid decrease in the ozone concentration as ozone is no longer present to suppress the nitrogen dioxide concentration through titration.

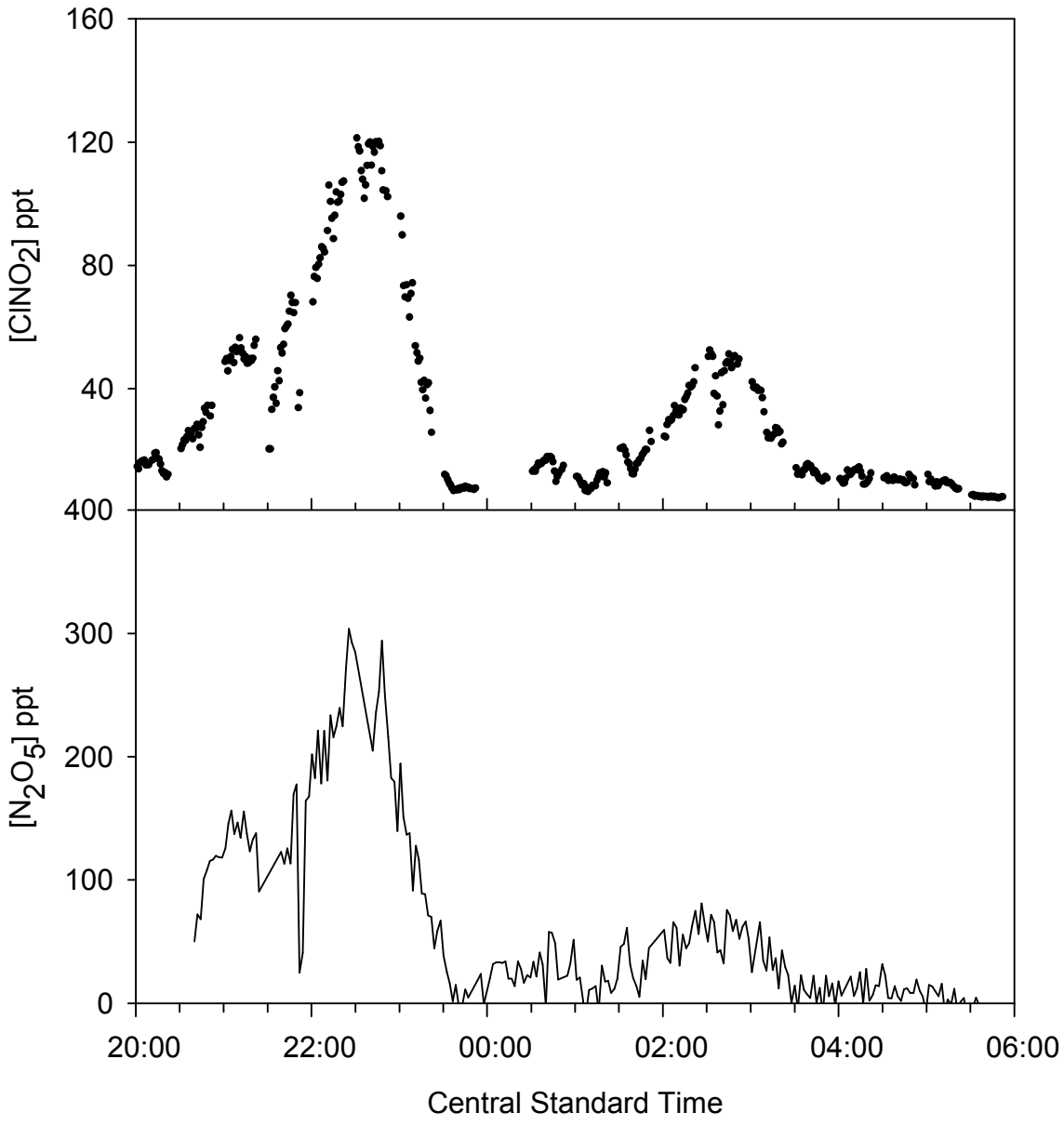

Figure 3.14. Comparison of $ClNO_2$ and N_2O_5 measurements on 19-20 May 2009 at Moody Tower.

Nitryl chloride measurements performed at the Moody Tower by the Rice University group also showed a strong correlation to the TAMU N_2O_5 measurements, and the comparison is presented in Figure 3.14. The two compounds show a similar profile, which is expected as N_2O_5 is the primary source of $ClNO_2$ through Equation 3.7.

$$N_2O_5 + Cl^- \xrightarrow{het} ClNO_2 + NO_3^- \qquad (3.7)$$

The hydrolysis of N_2O_5 to form $ClNO_2$ is a heterogeneous process and relies both on aerosol concentrations and properties [*Kercher et al.*, 2009; *Osthoff et al.*, 2008]. The heterogeneous chemistry observed in Houston during the SHARP study in relation to nitric acid and nitryl chloride will be discussed further in Section III.9 of this chapter.

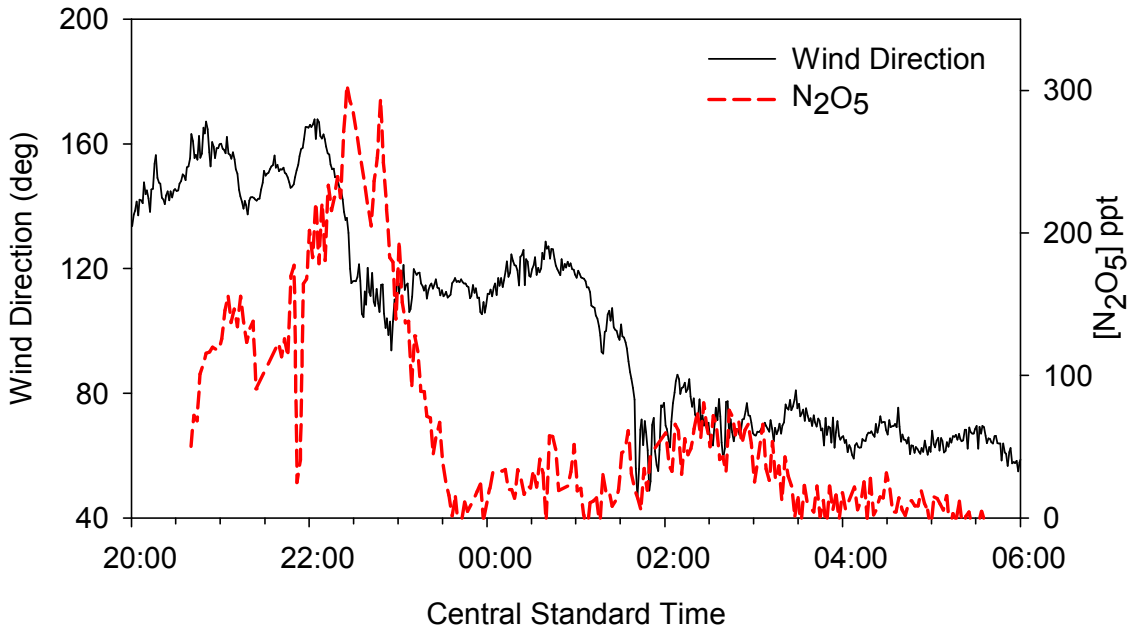

Figure 3.15. Measured N_2O_5 compared to wind direction over the night of 19-20 May 2009.

The geography of the emission sources in Houston in relation to Moody Tower creates a strong dependence of the observed pollutants to the wind direction. The majority of emissions are located along the Galveston Bay and Gulf of Mexico coastline to the South and Southeast of the measurement site and along the ship channel to the East. Air masses from the North and West will typically be much cleaner due to the lack of industrial sources and only the presence of primarily vehicular emissions. The N_2O_5 concentration compared to the wind direction over time is shown in Figure 3.15. There were two major shifts in the wind direction throughout the course of the night occurring at approximately 22:00 and 01:00. Prior to 22:00, the wind was predominantly from the south-southeast, and centered around 150° followed by a wind shift to the east-southeast and centered around 120°. The wind direction remained relatively constant for the next four hours, with a shift to approximately 70° from the east-northeast direction just before 02:00 on 20 May 2009. The wind continued from this direction for the remainder of the night.

The wind shifts were followed by changes in the species observed on Moody Tower which indicates the measurement of separate air mass. As shown in Figure 3.15, after the change in wind direction at 22:00, there was a sudden drop from very high N_2O_5 concentrations around 300 ppt to observed levels barely above the instrument detection limit. There was an increase in the N_2O_5 after the shift in wind direction at 02:00, however the N_2O_5 decreased without a major change in the wind direction at approximately 03:00. Without a shift in the wind, this drop must be a result of the chemistry and not the measurement of a separate air mass.

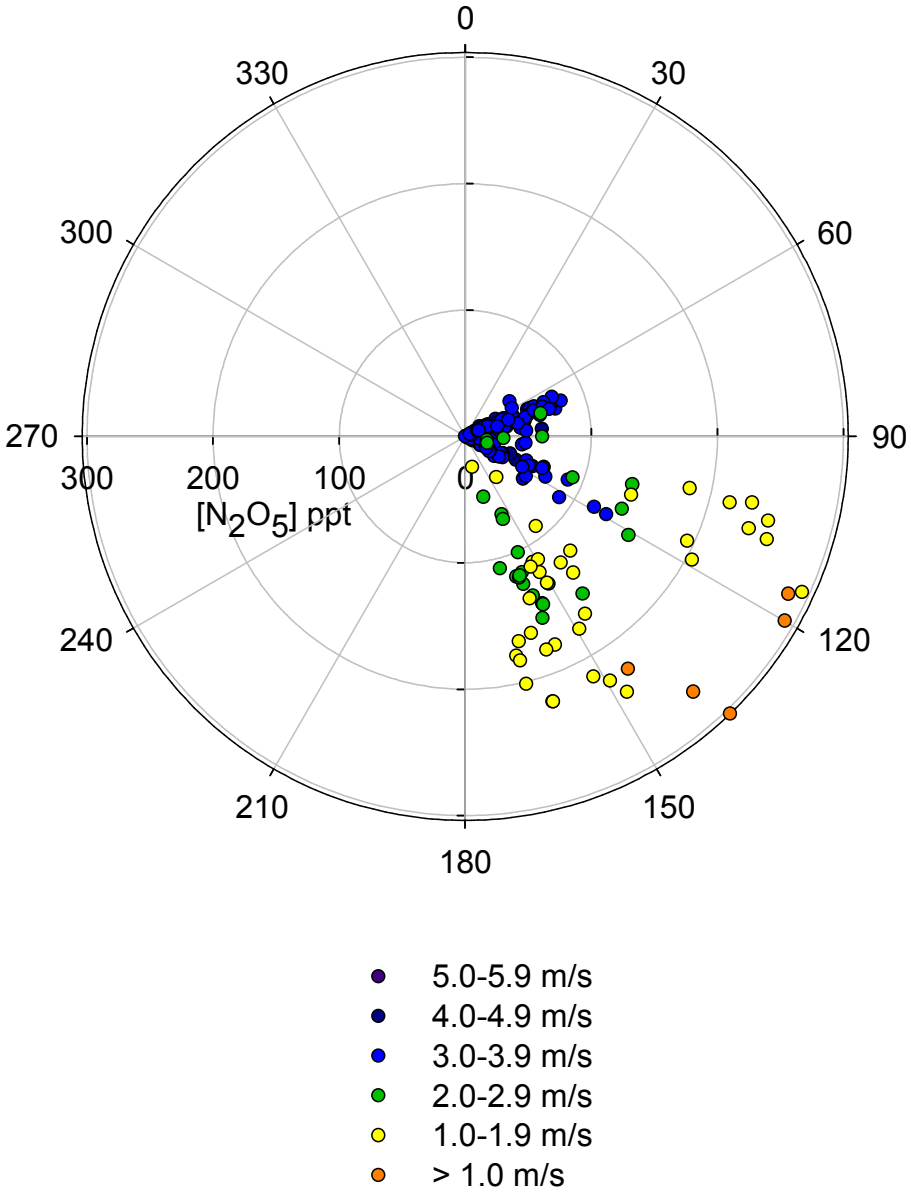

Figure 3.16. N_2O_5 concentration plotted by wind direction with wind speed in m/s indicated by color on the night of 19-20 May 2009.

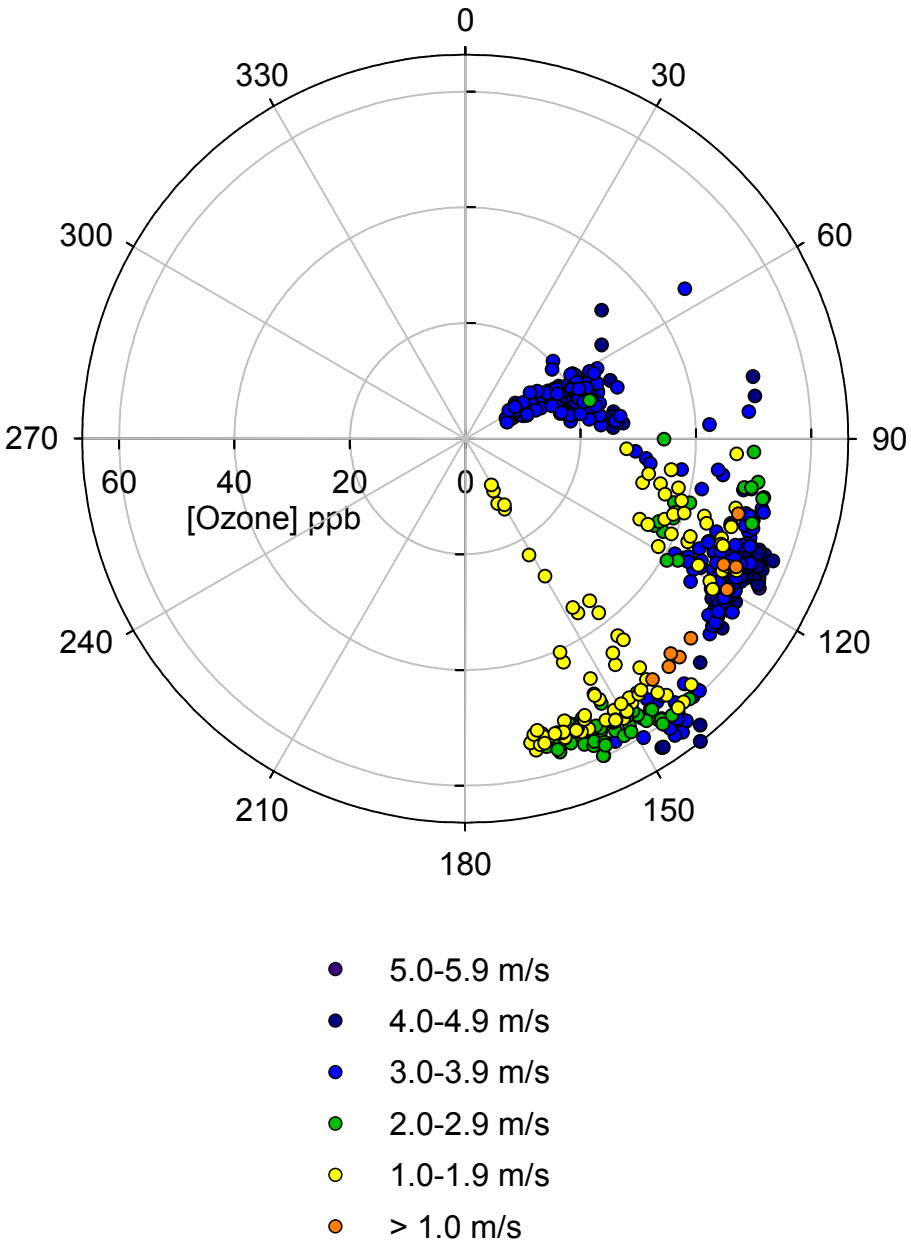

Figure 3.17. Ozone concentration plotted by wind direction with wind speed in m/s indicated by color on the night of 19-20 May 2009.

Shown in Figure 3.16 is the measured N_2O_5 concentration on 19-20 May 2009 as a function of the wind direction, with the wind speed reflected in the color, and a similar plot reflecting ozone concentration is represented in Figure 3.17. Several interesting trends are of note in Figure 3.16, and perhaps most apparent of which is that the highest concentration of N_2O_5 was observed from southeasterly winds and is representative of a more polluted air mass coming from that direction. Much lower ambient levels of N_2O_5 and ozone when the wind direction shifted east-northeasterly. A more subtle feature is the gradient in the wind speed, with faster winds correlating to a lower N_2O_5 concentration and slower winds corresponding to a higher N_2O_5 concentration. As stated earlier, N_2O_5 is an aged product of NO_X and ozone emissions. A significant time period is needed for NO_2 and ozone reaction to occur and form the nitrate radical, an N_2O_5 precursor, via Equation 3.8 [*Sander et al.*, 2006].

$$\begin{gathered} NO_2 + O_3 \rightarrow NO_3 + O_2 \\ k_1 = 3.5 \times 10^{-17} cm^3 s^{-1} \end{gathered} \tag{3.8}$$

Under typical atmospheric conditions, Equation 3.8 proceeds quite slowly. Using pseudo first-order kinetics and treating the ozone concentration as relatively constant, the reaction time of Equation 3.8 can be approximated using the observed levels of nitrogen dioxide by Equation 3.9 resulting in an observed reaction time of 11.8 hours.

$$\tau = \frac{1}{k[NO_2]} \tag{3.9}$$

The sampling site is located approximately 65 km from the coastline of the Gulf of Mexico. Ignoring any significant ship emissions in the Gulf, the measurements are performed at least that far from the emission sources. A fast wind speed of 5.0 m s^{-1} only

allows a maximum of 3.6 hours for the precursor molecules to react, and is much slower than the 11.8 hour reaction time. However, a slower wind speed of 1.0 m s^{-1} gives the air mass approximately 18 hours to age before reaching the Moody Tower. The slower winds allow the precursor molecules from emissions time to form N_2O_5 before being measured at the tower, whereas the faster wind speeds do not. This observation also implies that had the measurement site been located further inland and farther from the emission sources a higher concentration of N_2O_5 would likely have been observed.

An opposite trend in the correlation between wind speed and concentration is in the ozone plot in Figure 3.17, however on a much smaller scale. The ozone concentration is in the range of parts per billion, and therefore several orders of magnitude larger than nitrate species discussed. Only a very small fraction of total ozone is reacted nitrogen dioxide to form N_2O_5. Yet, the aging of the air mass as ozone is titrated out during the course of the night is reflected in the inverse relationship shown between ozone concentration and wind speed. Similar is the high concentrations observed from the southeasterly direction and lower concentrations of ozone from the east-northeasterly direction.

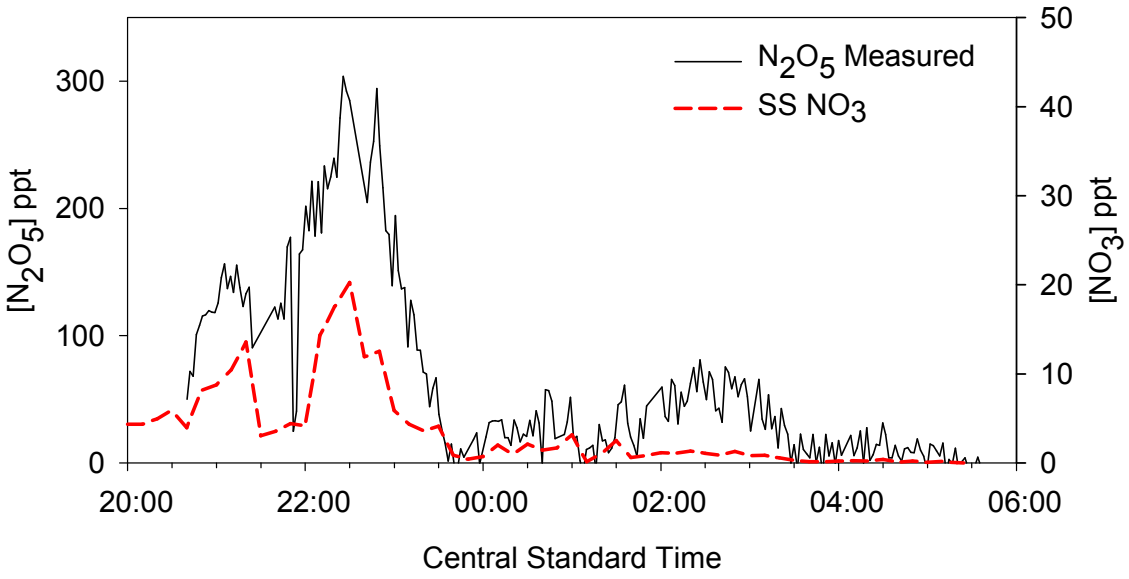

Figure 3.18. Calculated steady-state NO_3 concentration based on measured N_2O_5 on the night of 19-20 May 2009.

Several studies have suggested that it may take several hours to reach steady-state equilibrium between NO_3 and N_2O_5, and especially in an urban region with high emissions similar to those observed during the SHARP study. Rapid changes in the concentration of N_2O_5, such as those observed on 19-20 May, suggest an inhomogeneous mixture of gases and a system that has not reached a steady-state equilibrium. However, assuming equilibrium of Equation 3.4 is established, the steady-state concentration of NO_3 can be calculated based on Equations 3.10 and 3.11 [*Brown et al.*, 2003a].

$$[NO_3]_{SS} = \frac{[N_2O_5]}{K_{eq}(T)[NO_2]} \tag{3.10}$$

$$K_{eq}(T) = (2\times10^{-27})\exp\left(\frac{10990}{T}\right) \tag{3.11}$$

The concentration of NO_3 calculated from observed N_2O_5 on 19-20 May is shown in Figure 3.18. The maximum steady-state concentration of NO_3 was 20.2 ppt at approximately 22:30. As this number is higher than the calculated detection limit of the TAMU CRDS instrument, either the equilibrium deviated far from steady-state or, more likely, there was an issue with the NO_3 sampling. It is notable however that during most of this night the calculated steady-state NO_3 was below 5 ppt, the approximate detection limit. This indicates that observable NO_3, if adhering to the established steady-state, would only have persisted for a short period of time.

III.7 Observations of Nocturnal Ambient Species on 29-30 May 2009

A low pressure front passed through the Houston area on 28 May 2009 causing a drastic decrease in the movement of air through the region. This resulted in the elevation in the ambient concentration of ozone and therefore elevated levels of N_2O_5 and other species. Ozone levels were extremely high, maintaining a concentration of 80 ppb until 21:00, exceeding the 75 ppb NAAQS standard. The meteorological conditions resulted in the recirculation of air throughout the Houston area on the 29-30 of May. Recirculation events typically lead to elevated levels of all emitted species, and therefore ground level ozone, due to the lack of a new clean air mass diluting emissions.

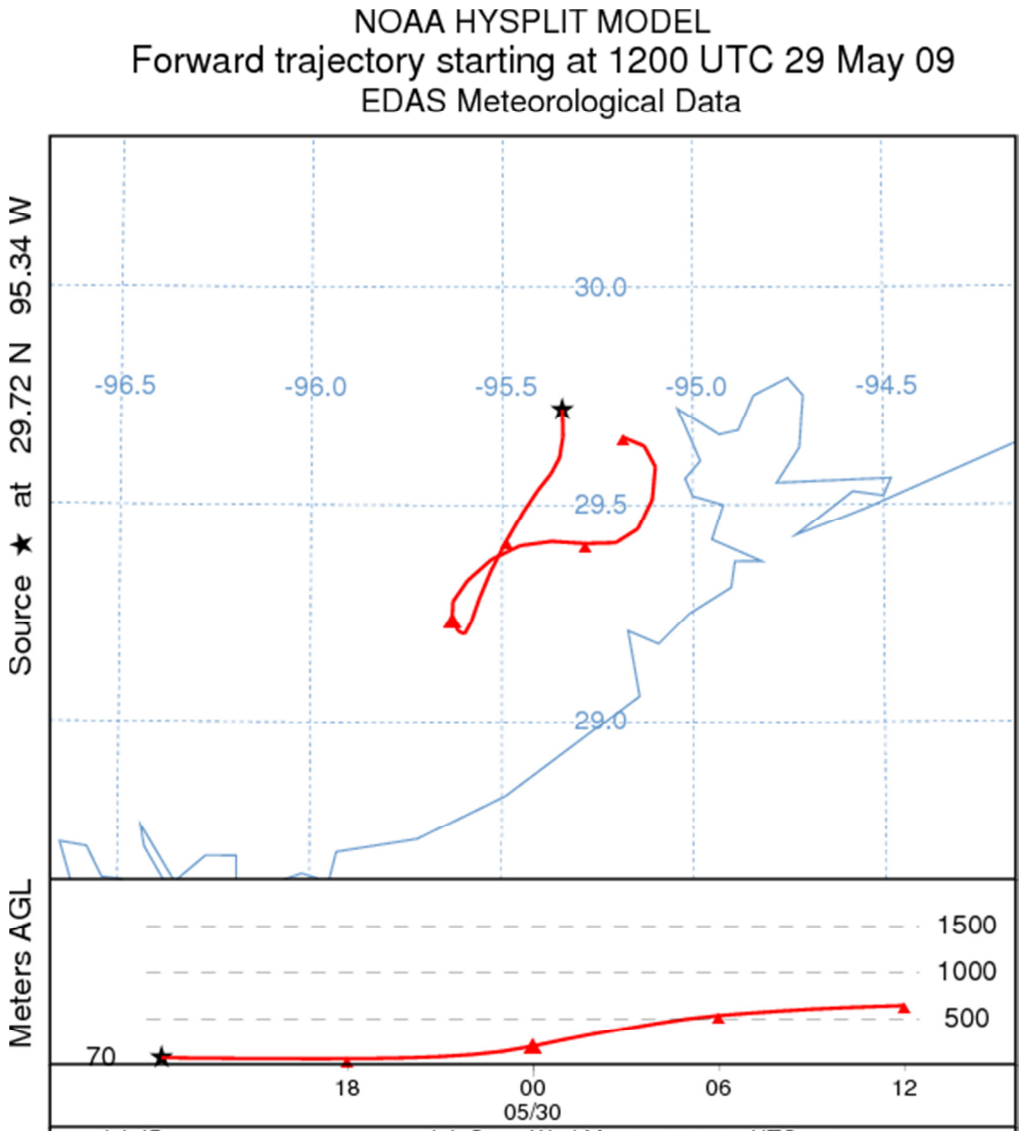

Figure 3.19. NOAA HYSPLIT 24 hour forward trajectory starting at Moody Tower at 17:00 on 29 May 2009. Markers indicate six hour time intervals and trajectory path shows recirculation of air in Southeastern Texas.

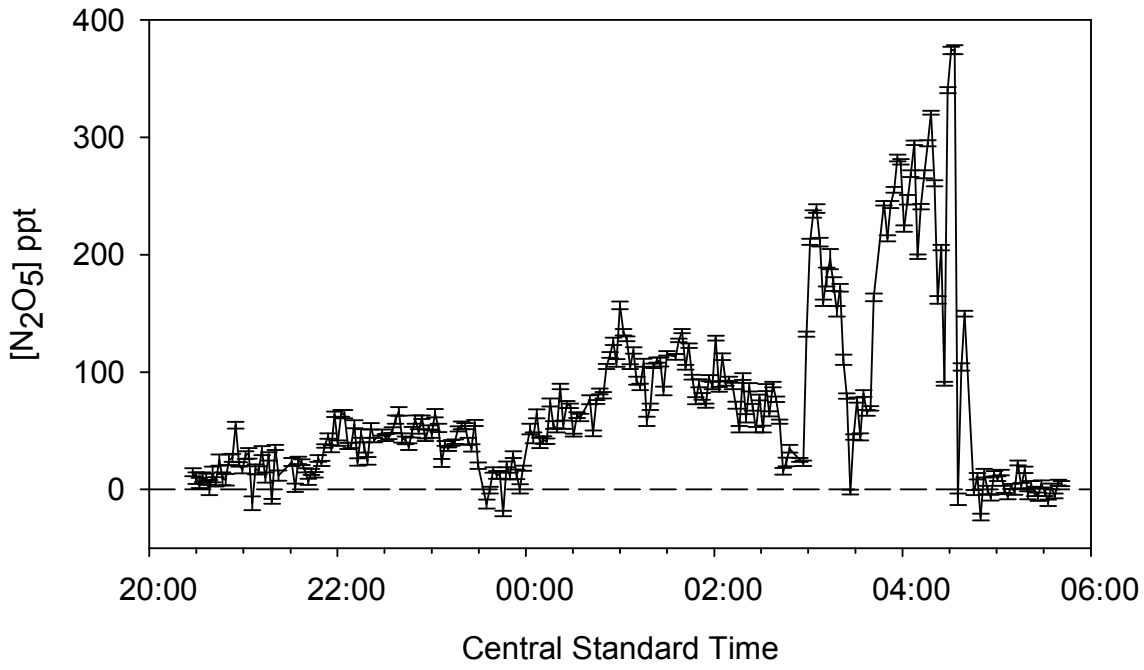

Figure 3.20. Measured N_2O_5 concentration on 29-30 May 2009, with error bars indicating the sensitivity of the measurement.

Figure 3.19 shows the forward meteorological trajectory starting at the Moody Tower at 12:00 on 29 May and continuing for twenty-four hours. The trajectory was modeled using the NOAA Hybrid Single-Particle Lagrangian Integrated Trajectory (HYSPLIT) model with the EDAS data set [*Draxler and Rolph*, 2011; *Rolph*, 2011]. This model uses observed meteorological conditions to model air movement with a 40 km resolution. Because of the low geographical resolution, it is important only to interpret the results qualitatively. However, the modeled trajectory clearly shows a recirculation in the air mass with a slow vertical rising. This indicates that the same air mass was present around the sampling site through the afternoon and through the night

of 29 May 2009, and that the wind direction cannot be taken as an indication of the origin of the emissions.

The ambient N_2O_5 concentration observed by TAMU CRDS on 29-30 May 2009 is shown in Figure 3.20 along with measurement error. The average detection limit for this time period was 2.97 ppt, with a minimum of 1.14 ppt and a maximum of 8.50 ppt. The concentration of N_2O_5 on this day was the highest observed during the Houston campaign time period, reaching a maximum of 374 ppt at approximately 04:00. The profile of N_2O_5 on 29-30 May is the reverse of what was seen on 19-20 May, with low levels barely above the instrument detection limit early on and gradually increasing throughout the night. At approximately 03:00 there was a rapid increase in the observed N_2O_5 level followed by a sudden drop and recovery in the concentration. The drop in the concentration lasted for approximately 20 minutes from 03:20 to 03:40. This drop occurred while a single filter was in place, and therefore is unlikely that it is simply an artifact of the instrument or measurement technique. After this time period, the N_2O_5 concentration remained high, reaching maximum observed values for the night, followed by a rapid drop around 04:30. At this time the concentration decreased dramatically, and given the instrumental error, the observed mixing ratio was not statistically above the instrumental detection limit.

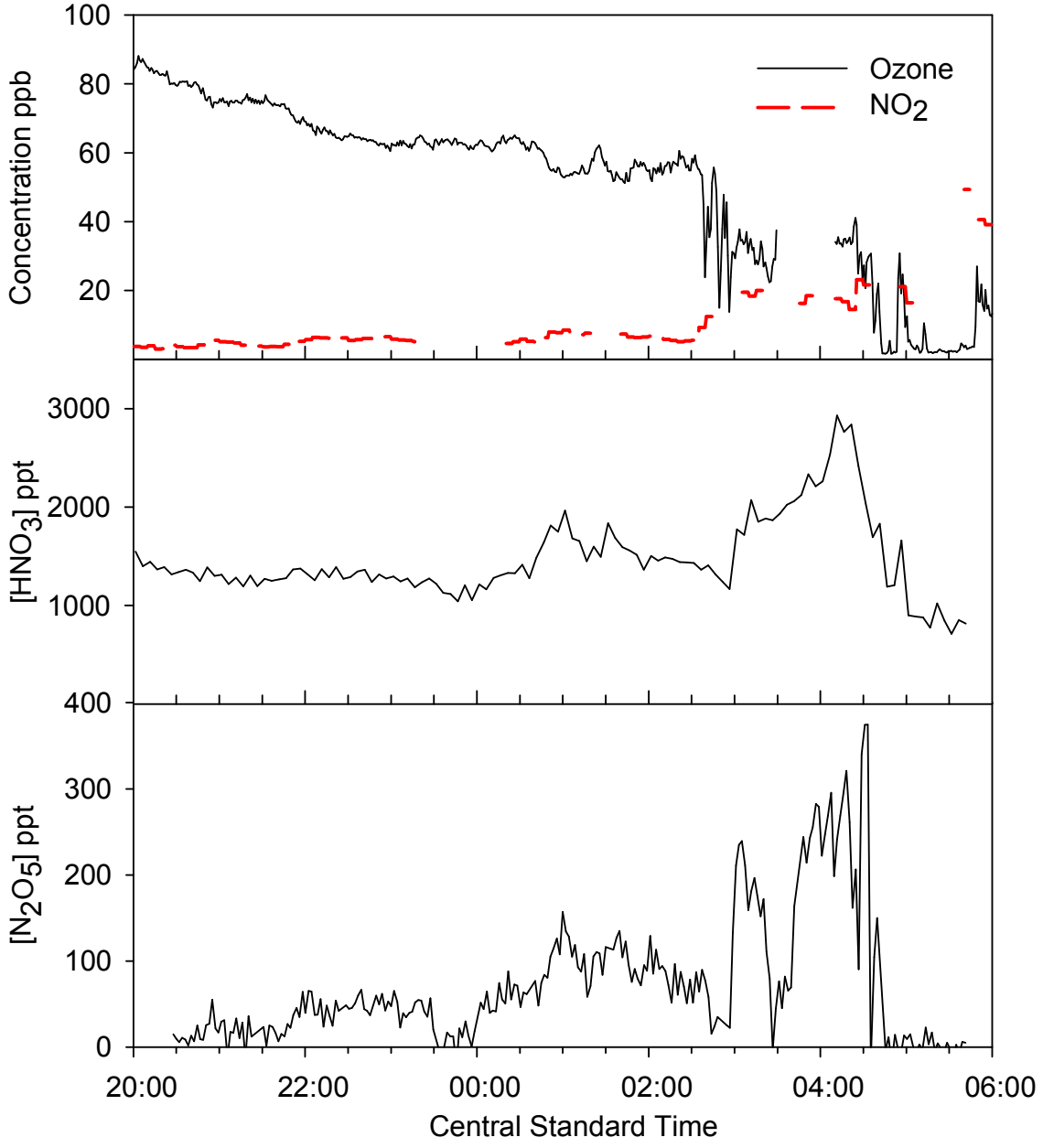

Figure 3.21. Comparison of ozone, nitrogen dioxide, nitric acid, and N_2O_5 on the night of 29-30 May 2009 observed at Moody Tower.

The ozone, nitrogen dioxide, nitric acid, and N_2O_5 concentration profiles for the night of 29-30 May is compared in Figure 3.21. As seen in the top panel, a high ozone level was maintained throughout most of the night without any remarkable features. It is however unusual to observe ozone concentrations at this high for this period of time, and is likely the result of the slow wind speeds through the night. The absence of ozone data from 03:30 to 04:00 is due to the calibration of the instrument during this time period, and is typical for the ozone analyzer operation. The ozone concentration began decreasing at approximately 02:30, and was removed completely at roughly 05:00. Unfortunately, there were technical issues with the nitrogen dioxide analyzer on the night of the measurements, so only sporadic data was available for analysis as depicted in Figure 3.20.

The middle and bottom panels of Figure 3.21 compare the observed HNO_3 and N_2O_5 concentrations. Similar to 19-20 May, both show a strong correlation in profile. The lack of sharp features in the nitric acid concentration compared to the N_2O_5 concentration is a result of the longer thirty minute integration time in the HNO_3 measurements compared to the 5 second N_2O_5 instrument integration time. This difference is the likely reason that the nitric acid concentration showed a more gradual increase around 03:00 compared with the sharp rise in N_2O_5 levels. The difference in the integration times could also explain why the sudden drop in N_2O_5 concentration around

03:20 was not also observed in the HNO_3 profile. Unfortunately, this time period also coincided with calibration of the ozone analysis instrument, so it is unknown if there was a change in ozone at this time. It is likely that the ozone concentration remained consistent as there was no sudden rise in the nitrogen dioxide levels. Typically a sudden decrease in ozone will lead to a sudden rise in NO_2 as there is a loss of the titrating species.

As shown in Figure 3.22, the ratio of nitric acid to N_2O_5 was consistently high enough to indicate and fast hydrolysis of N_2O_5 during the earlier part of the night. Although not as high as on 19-20 May, HNO_3/N_2O_5 was above 50 in the initial hours of measurement, and steadily declined throughout the night. The ratio remained above twelve until approximately 2:00 am, after which time the observed ratio was measured to be between six and twelve with few exceptions. This is indicative of a decrease in the speed of heterogeneous processing of N_2O_5, and most likely is a result of the aging particles as the same air mass was being observed.

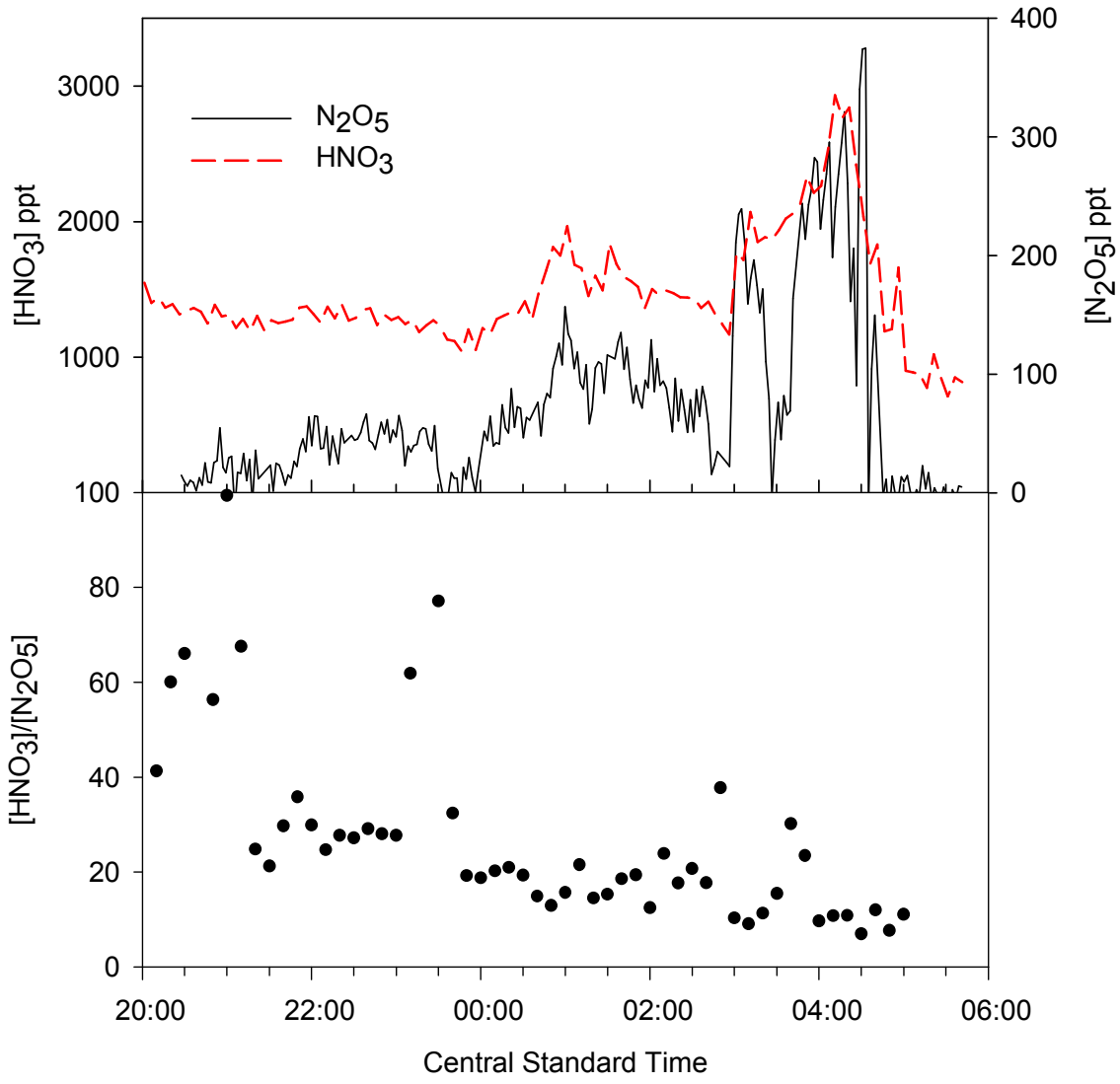

Figure 3.22. Comparison of observed N_2O_5 and HNO_3 along with HNO_3/N_2O_5 ratio on the evening of 29-30 May 2009.

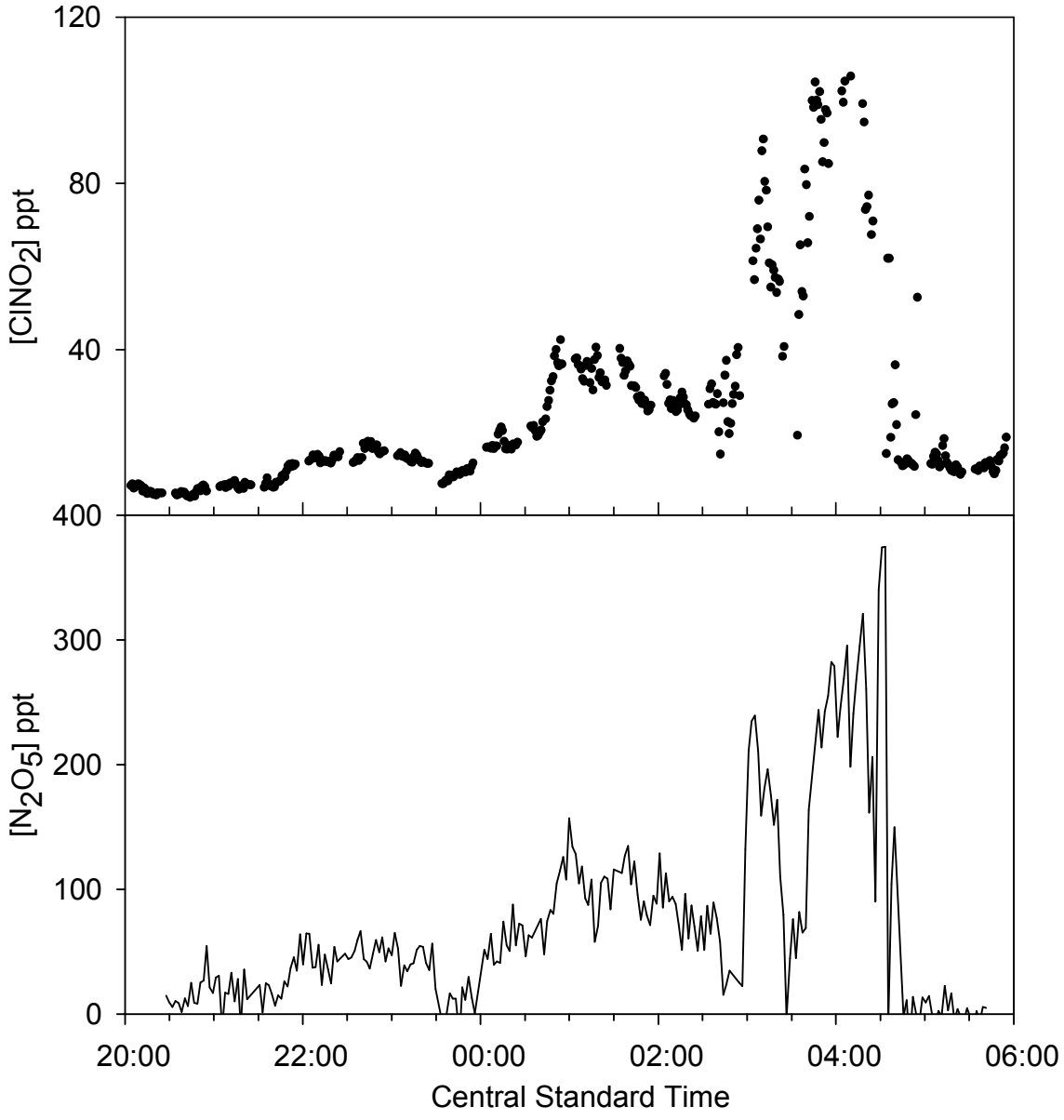

Figure 3.23. Comparison of nitryl chloride and N_2O_5 measurements on 29-30 May 2009.

Detectable levels of $ClNO_2$ were observed by Rice University from Moody Tower on the night of 29-30 May 2009 and results are compared to the N_2O_5 measurements in Figure 3.23. Similar to the measurements of 19-20 May, the two species show near identical profiles. It is notable that there is also a dramatic drop in the $ClNO_2$ concentration during the time period that a drop in N_2O_5 was observed. This further reinforces the notion that there was a decrease in the HNO_3 concentration at this time that was missed due to the extended integration time. The maximum observed concentration of nitryl chloride was 106 ppt, compared to374 ppt of N_2O_5 at this time. The observed $ClNO_2$ mixing ratio was much lower than in the 2006 TexAQS II study where concentrations were in excess of 2 ppb.

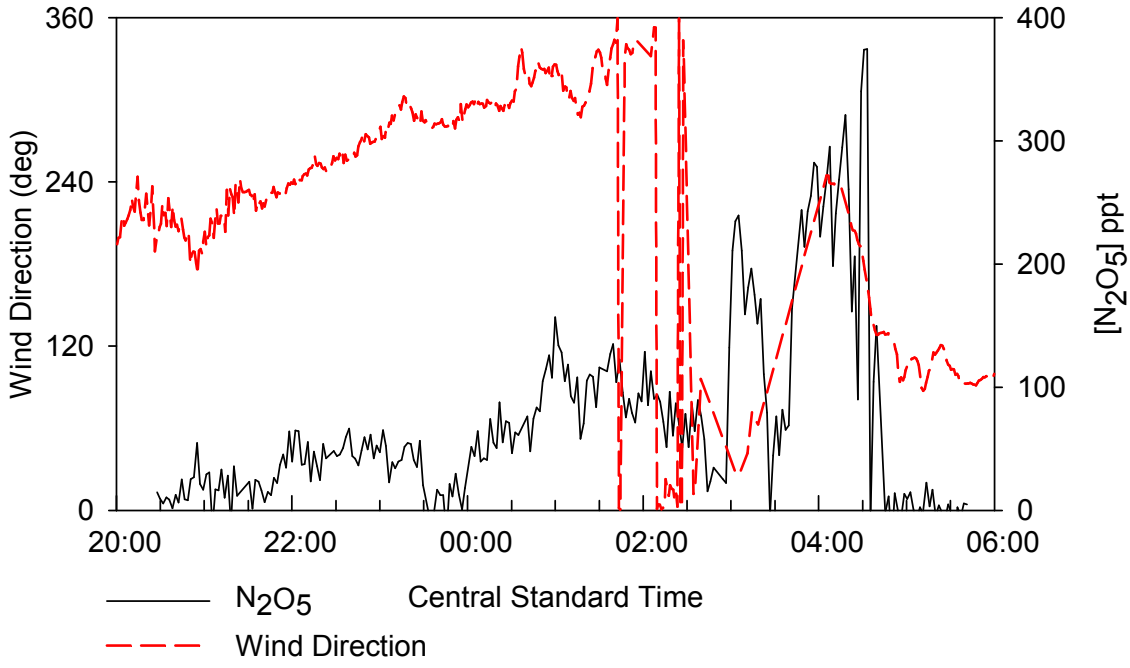

Figure 3.24. Wind direction and N_2O_5 concentration observed at Moody Tower on 29-30 May 2009.

The post-frontal winds on the evening of 29-30 May were much slower than average and had resulted in the recirculation of air as depicted in Figure 3.19. The wind direction over time as compared to the N_2O_5 concentration profile is shown in Figure 3.24. The wind direction is plotted in degrees, where 0° and 360° corresponds to winds originating due North and 180° corresponds to southerly wind flows. The wind on this night slowly rotated, originating from southwesterly to northerly in clockwise direction from 20:00 to approximately 03:00. The wind direction over the next hour shifted to a southwesterly flow and then shifted back to southeasterly. All wind direction changes over this night were quite gradual, indicating a single air mass was being observed. The rapid rise in ambient N_2O_5 concentration at approximately 03:00 was accompanied by a change in the wind direction, however the increase in the N_2O_5 concentration was much faster. This can be contrast with the sudden, simultaneous changes in wind direction and N_2O_5 concentration seen on 19-20 May and depicted in Figure 3.15.

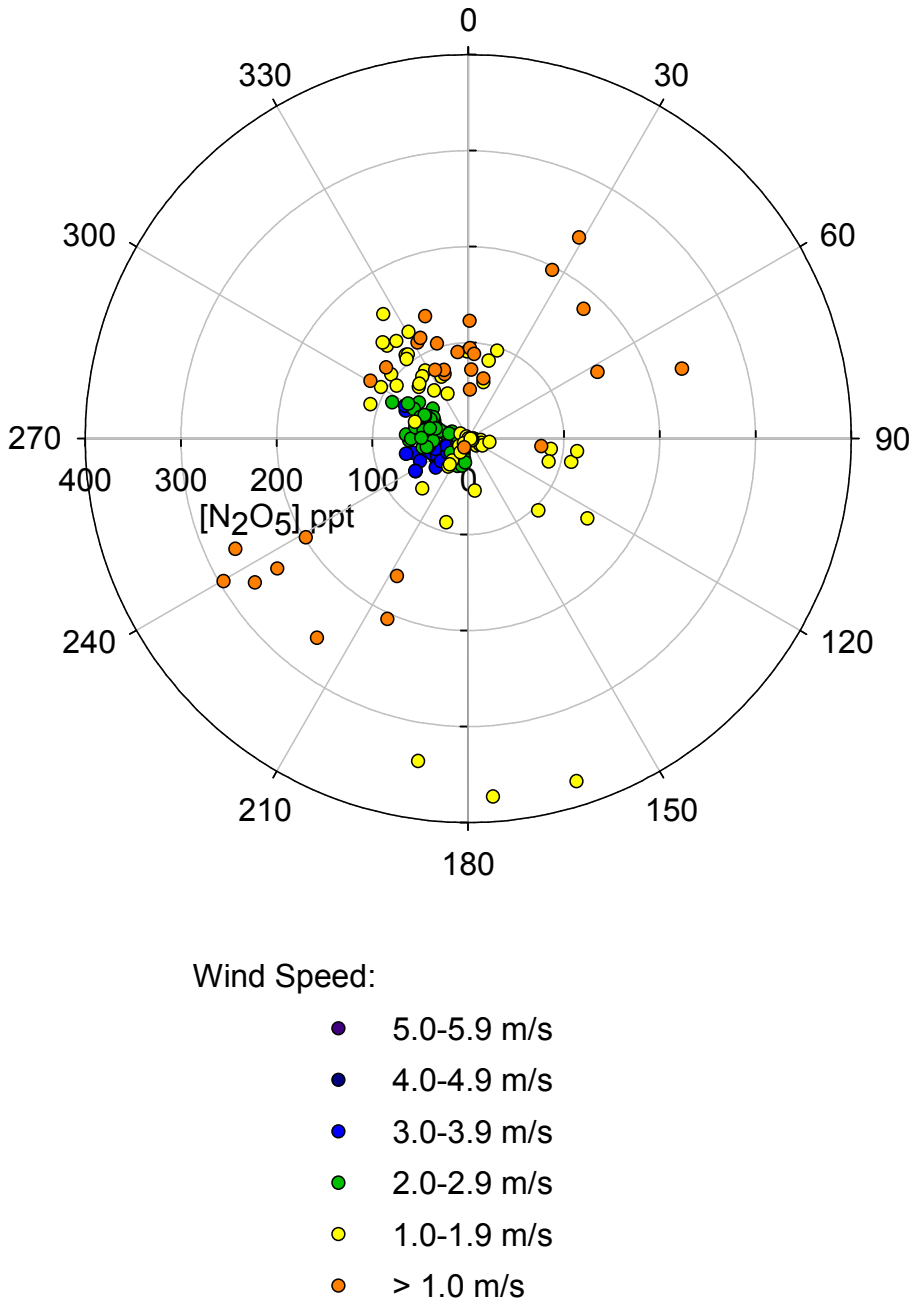

Figure 3.25. N_2O_5 concentration plotted by wind direction on 29-30 May 2009, where color of the points is representative of the wind speed.

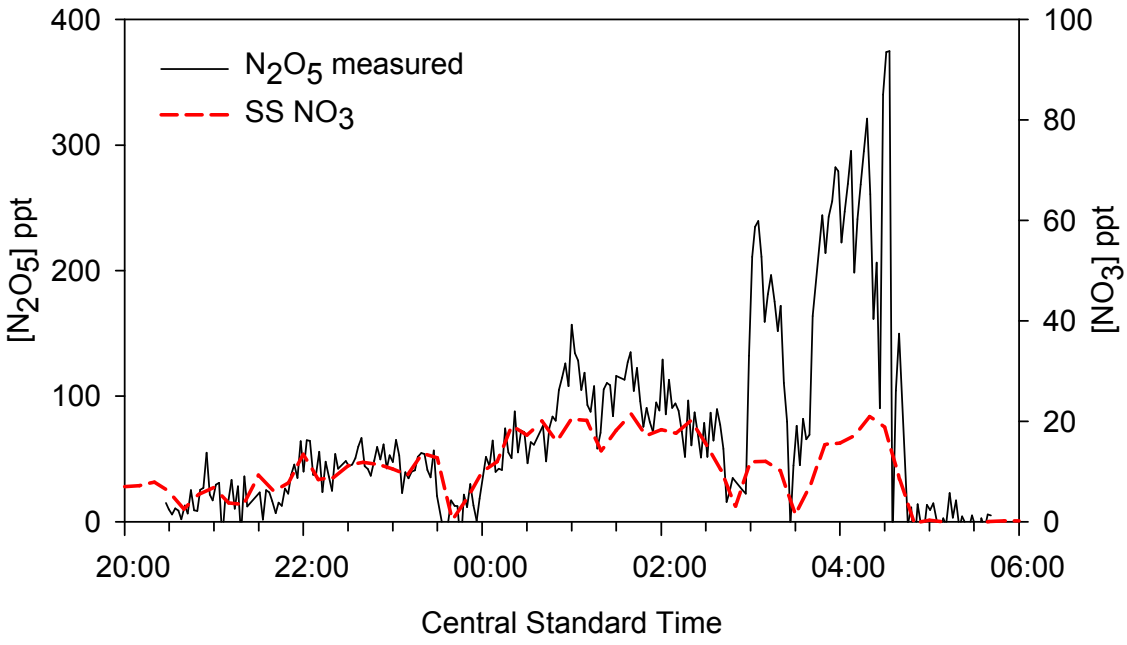

Figure 3.26. N_2O_5 concentration measured on 29-30 May 2009, shown in black, compared with calculated NO_3 concentration, shown in red, based on the steady-state ratio.

The relationship between the wind speed and direction and the N_2O_5 concentration on 29-30 May 2009 is depicted in Figure 3.25. Similarly to the data shown in Figure 3.15, higher N_2O_5 concentrations showed a correlation to slower wind speeds allowing time for source species to react. However, this night differs in that the wind speed after approximately 01:00 was extremely slow and the same air mass was being observed as it aged. High concentrations of N_2O_5 were observed in winds originating from nearly every direction; however this was at very low wind speeds.

The steady-state concentration of NO_3 was calculated for 29-30 May through Equation 3.9 using the measured N_2O_5, ozone, and nitrogen dioxide concentrations. The data with corresponding N_2O_5 concentration are presented in Figure 3.26. The steady-state NO_3 concentration on this evening was found to be low and never exceeding 22 ppt. There was a consistent concentration of NO_3 throughout most of the night, and given the steady-state assumption is accurate for this data set, the TAMU CRDS instrument should have detected the ambient NO_3 at these levels if present.

III.8 Correlations with Nocturnal Nitrogen Compounds and Ozone

As discussed throughout this chapter, there were strong correlations noted between the observed concentrations of several species measured by other researchers to N_2O_5 measured by TAMU CRDS. It is therefore helpful to determine the degree of correlation to help explain the nocturnal loss pathway of nitrogen.

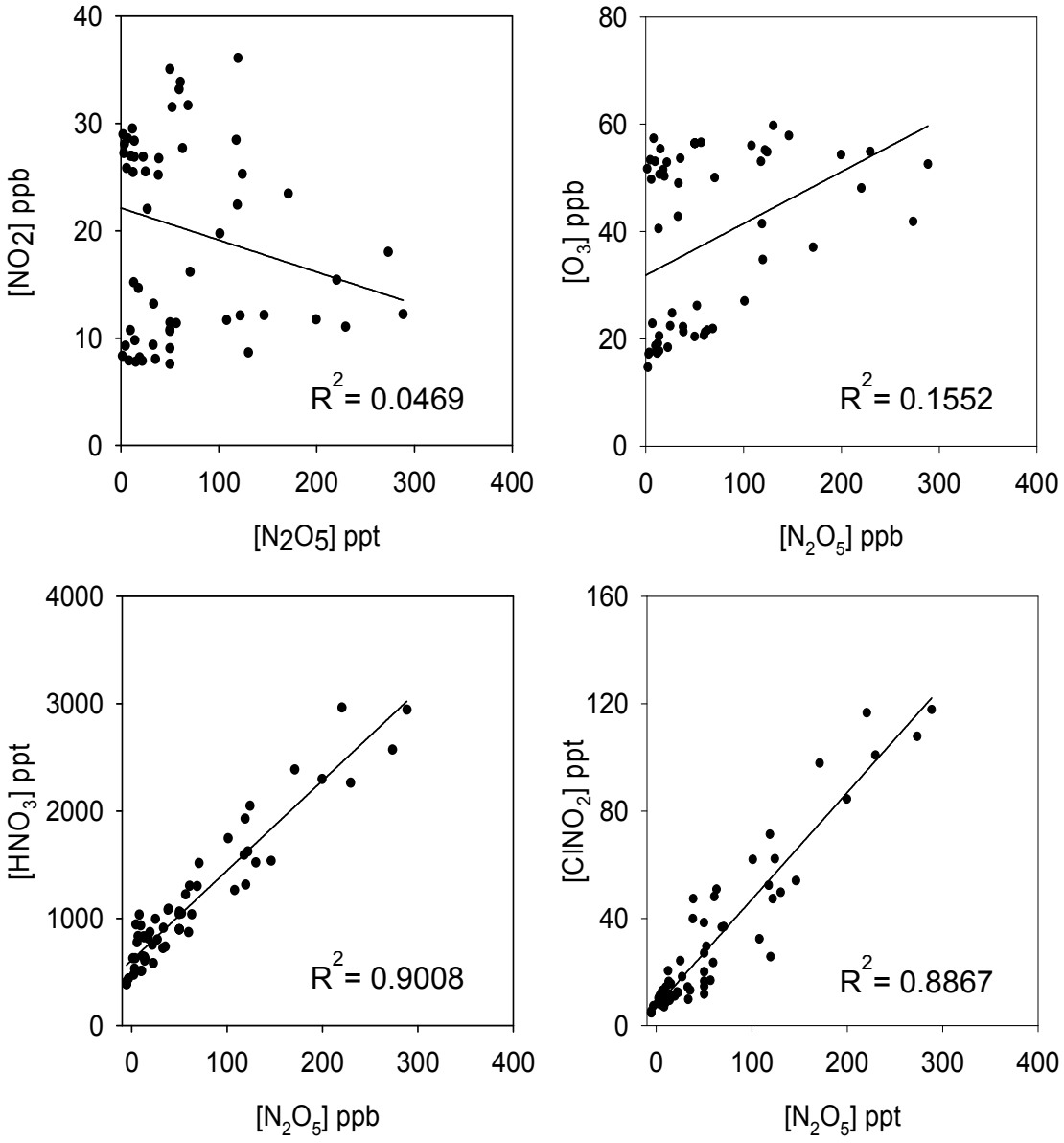

Figure 3.27. Scatter plots showing the correlations of mixing ratios of N_2O_5 to NO_2, O_3, HNO_3, and $ClNO_2$ on 19-20 May 2009.

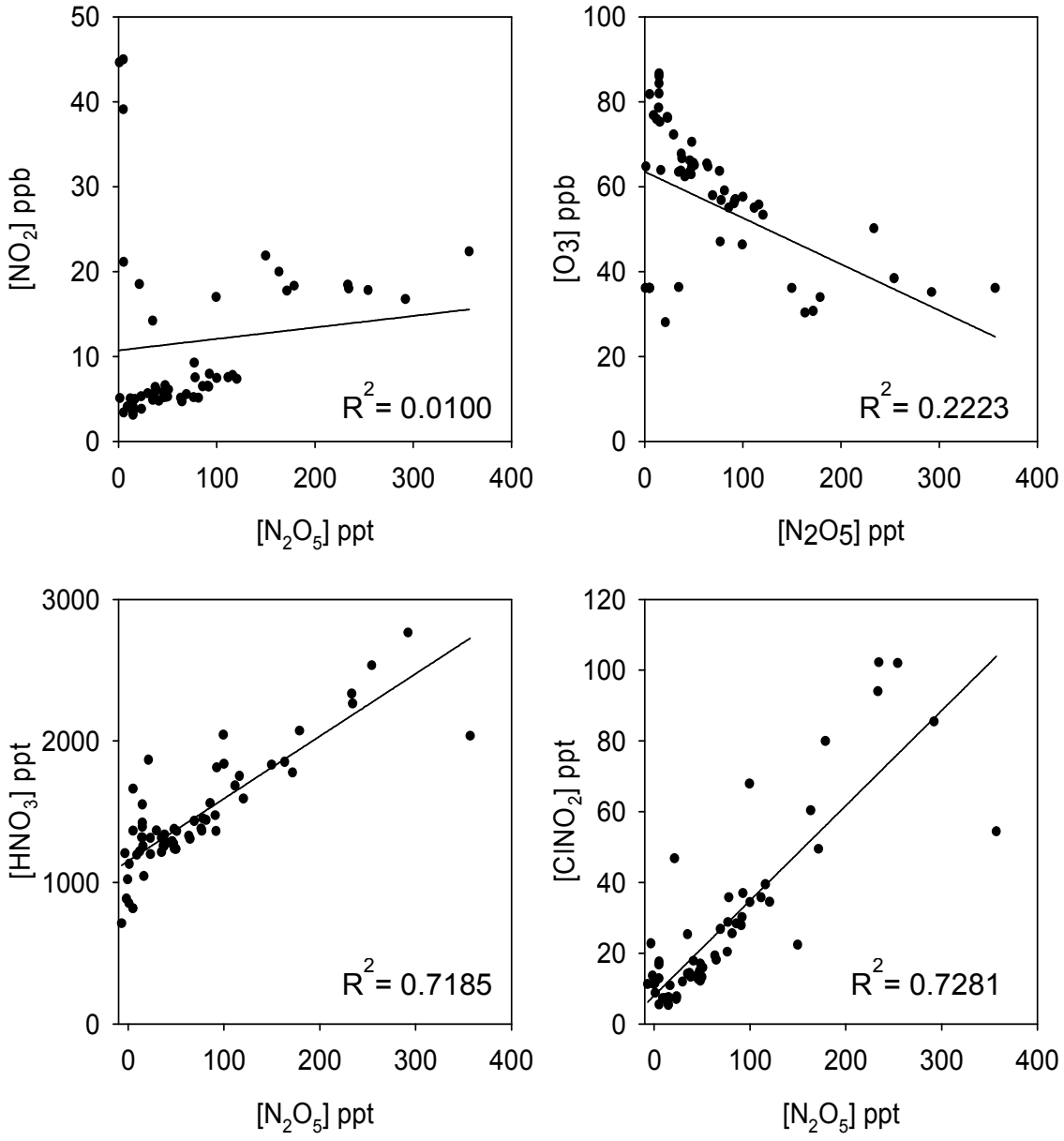

Figure 3.28. Scatter plots showing the correlations of mixing ratios of N_2O_5 to NO_2, O_3, HNO_3, and $ClNO_2$ on 29-30 May 2009.

The correlation of N_2O_5 with supporting measurements of nitrogen dioxide, ozone, nitric acid, and nitryl chloride are shown in Figures 3.27 and 3.28 for 19 May and 29 May, respectively. The data was interpolated in ten minute time increments from 20:00 to 06:00 for all measurements. On both the nights of 19 May and 29 May, a strong positive correlation was observed between N_2O_5 and both HNO_3 and $ClNO_2$, and reinforces the assumption that N_2O_5 was the major source of both species. A slight positive correlation in the concentration of NO_2 and ozone to N_2O_5 was observed on the evening of 19-20 May. While both NO_2 and ozone are the main sources of N_2O_5, only a slight correlation indicates that there are several other significant pathways. Nitrogen dioxide and ozone both were measured to be in the parts-per-billion range, several orders of magnitude higher than measured N_2O_5 which occurs in parts-per-trillion mixing ratios. While a significant portion of NO_X is removed through the pathway at night, only a very small percentage of all ambient nitrogen oxides exist as N_2O_5 at a single point in time. During the measurement campaign, N_2O_5 was typically less than one percent of total measured nitrogen oxides. Similar trends were observed with nitrogen dioxide and ozone on 29 May.

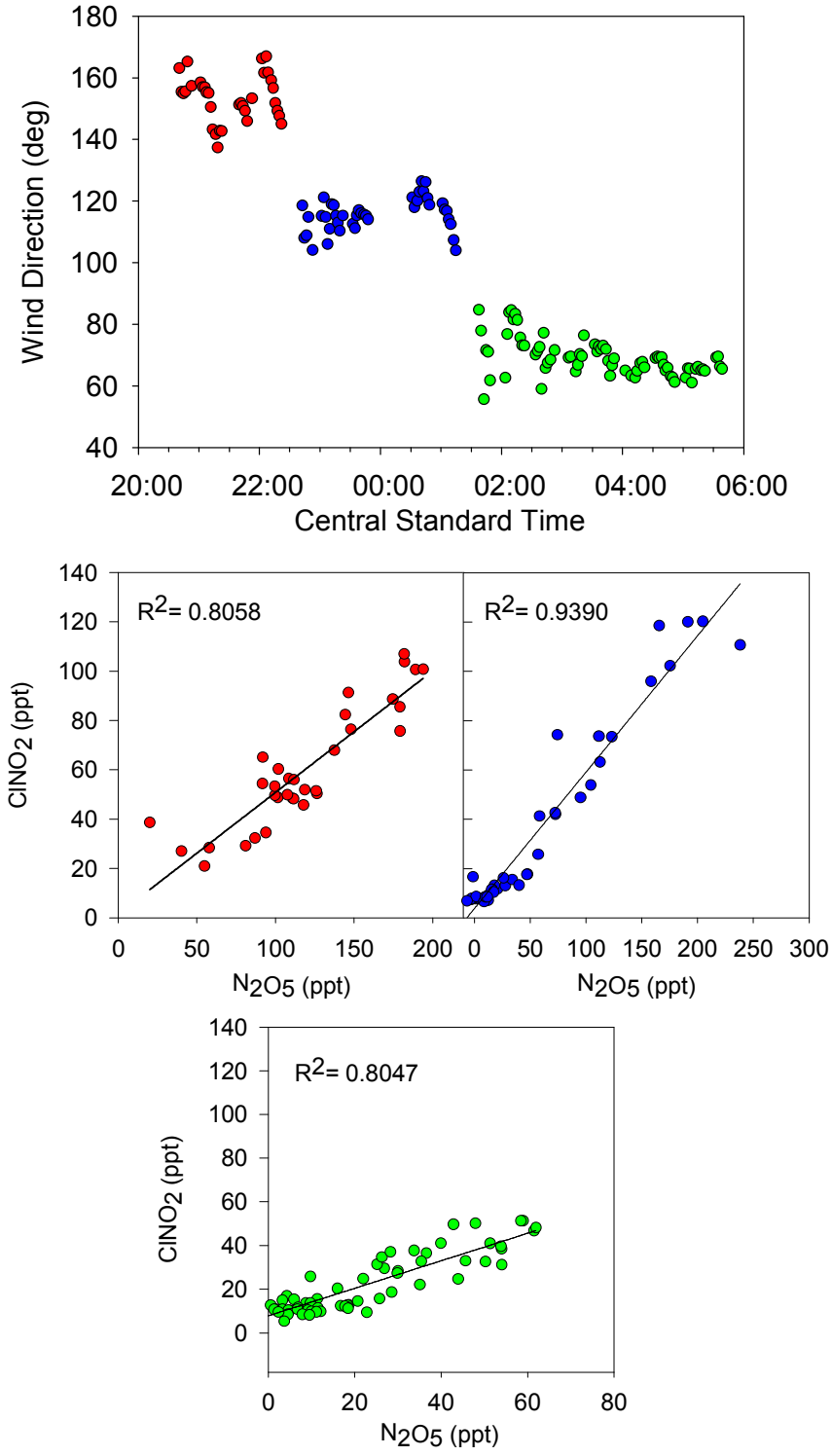

Figure 3.29. Correlations of $ClNO_2$ and N_2O_5 on 19-20 May 2009 as observed during three distinct wind direction changes.

The conversion of N_2O_5 to nitryl chloride is dependent on the presence of heterogeneous chlorine most commonly derived from sea salt aerosol [*Chang et al.*, 2011; *Osthoff et al.*, 2008]. While sea salt measurements made at Moody Tower were not available for the SHARP study, it is well known that the abundance of sea salt is highly dependent on winds originating from marine areas [*Finlayson-Pitts and Pitts*, 1999]. This leads to the hypothesis that the measurement of samples with an origination over the Gulf of Mexico should show a stronger N_2O_5 to $ClNO_2$ correlation than samples traveling over land. While very slow winds with variable directions were observed on the night of May 29, faster wind speeds with a definitive origin were measured on May 19-20. As shown in Figure 3.29, this night can be divided into three sections with three distinct points of origin. The early and late part of the night, as indicated in red and green respectively, corresponded to wind directions that indicate the air mass traveled over land for over two hours before reaching the measurements site at Moody Tower. These two periods also showed a good correlation in the N_2O_5 and $ClNO_2$, with R^2 values of approximately 0.080. However, the middle portion of the night, indicated in Figure 3.29 in blue, showed a very high correlation between N_2O_5 and $ClNO_2$ (R^2=0.09390) and, as indicated by the wind direction, was the shortest distance from the Gulf of Mexico to the sampling site.

III.9 Observed Atmospheric Lifetimes and Implications to Heterogeneous Chemistry

The calculation of the atmospheric lifetime of N_2O_5 provides an indication as to the reactivity and characteristics of atmospheric particulates as well as the magnitude of

sources and sinks of nitrogen oxides. The major loss pathway for N_2O_5 in urban areas has been shown to be heterogeneous hydrolysis to nitric acid following Equation 3.6. The pathway depends strongly on the specific composition of aerosol particles, particularly water adsorbed onto the particle surface.

Because there has been significant debate over the time period to establish the steady-state equilibrium between N_2O_5 and NO_3, both the steady-state, τ_{SS}, and non-steady-state, τ^*, atmospheric lifetime was calculated for N_2O_5 using the data collected on 19-20 May 2009. The steady-state and non-steady-state lifetime of N_2O_5 can be calculated based on observed levels of N_2O_5, O_3, and NO_2 [*Brown et al.*, 2003a].

$$\tau_{SS} = \frac{[N_2O_5]}{k_1[O_3][NO_2]} \tag{3.12}$$

$$\tau^* = \frac{[N_2O_5]}{k_1[O_3][NO_2] - \frac{d[N_2O_5]}{dt}} \tag{3.13}$$

where k_1 is the rate constant of the reaction between ozone and nitrogen dioxide. A ten minute time increment was used in the calculation of the differential for the non-steady-state lifetime, as well as the interpolation of the ambient measurements.

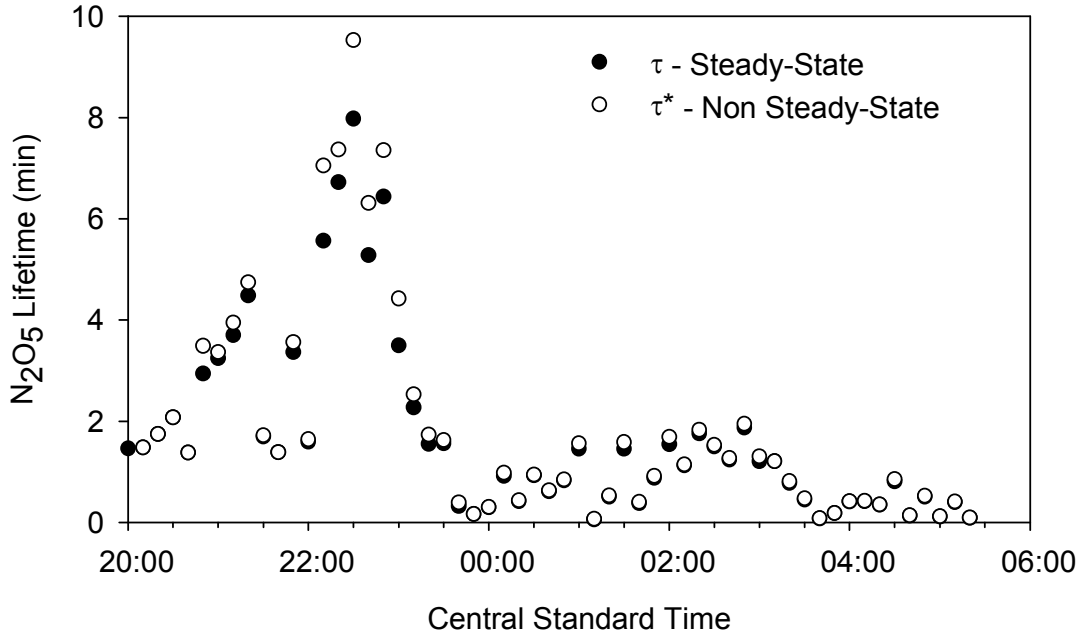

Figure 3.30. Comparison of the calculated steady-state and non-steady-state atmospheric lifetimes of N_2O_5 on 19-20 May 2009.

As shown in Figure 3.30, there was a small difference between the calculated steady-state and non-steady-state lifetimes for N_2O_5 on 19-20 May 2009. The steady-state lifetime was a maximum of 21% higher than the calculated non-steady-state lifetime throughout the night, and a negligible difference was found in the second half of the night when N_2O_5 concentrations were lower. This data indicates that while N_2O_5 and NO_3 are in equilibrium, a steady-state may not have been reached until at least several hours into the night. The atmospheric lifetime calculated for N_2O_5 ranged between several seconds up to ten minutes throughout the night of 19-20 May. Based on literature data, the observed lifetime is short but typical for urban measurements [*Benton et al.*, 2010; *Osthoff et al.*, 2008; *Stutz et al.*, 2004].

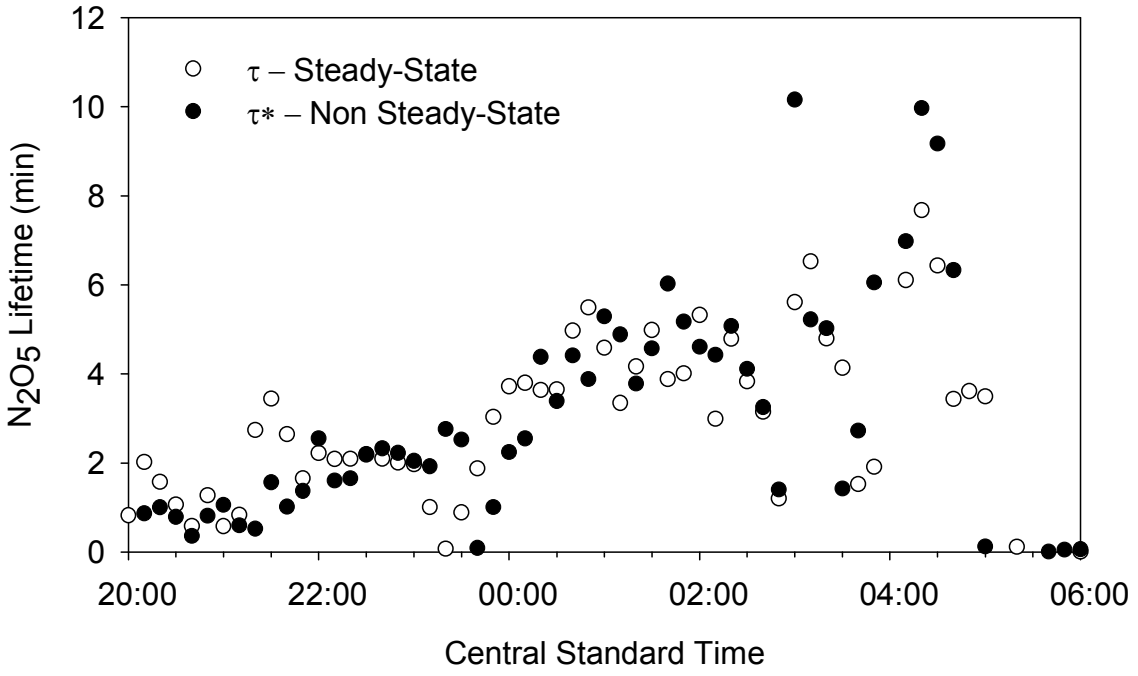

Figure 3.31. Comparison of the calculated steady-state and non-steady-state atmospheric lifetimes of N_2O_5 on 29-30 May 2009.

The calculated steady-state and non-steady-state lifetime for N_2O_5 on 29-30 May 2009 is shown in Figure 3.31. A larger difference in the two calculated lifetime was observed on this night, and was seen both when N_2O_5 concentrations were small, in the early evening, and large just before sunrise. This indicates a possible significant deviation from $N_2O_5 – NO_3$ steady-state equilibrium, and suggesting that the calculated NO_3 values shown in Figure 3.25 may not be accurate. The deviation is likely the result of the high variation in the N_2O_5 concentration over short periods of time that occurred on this night. The length of the N_2O_5 atmospheric lifetime on 29 May was similar to 19 May, ranging from approximately 30 seconds to ten minutes.

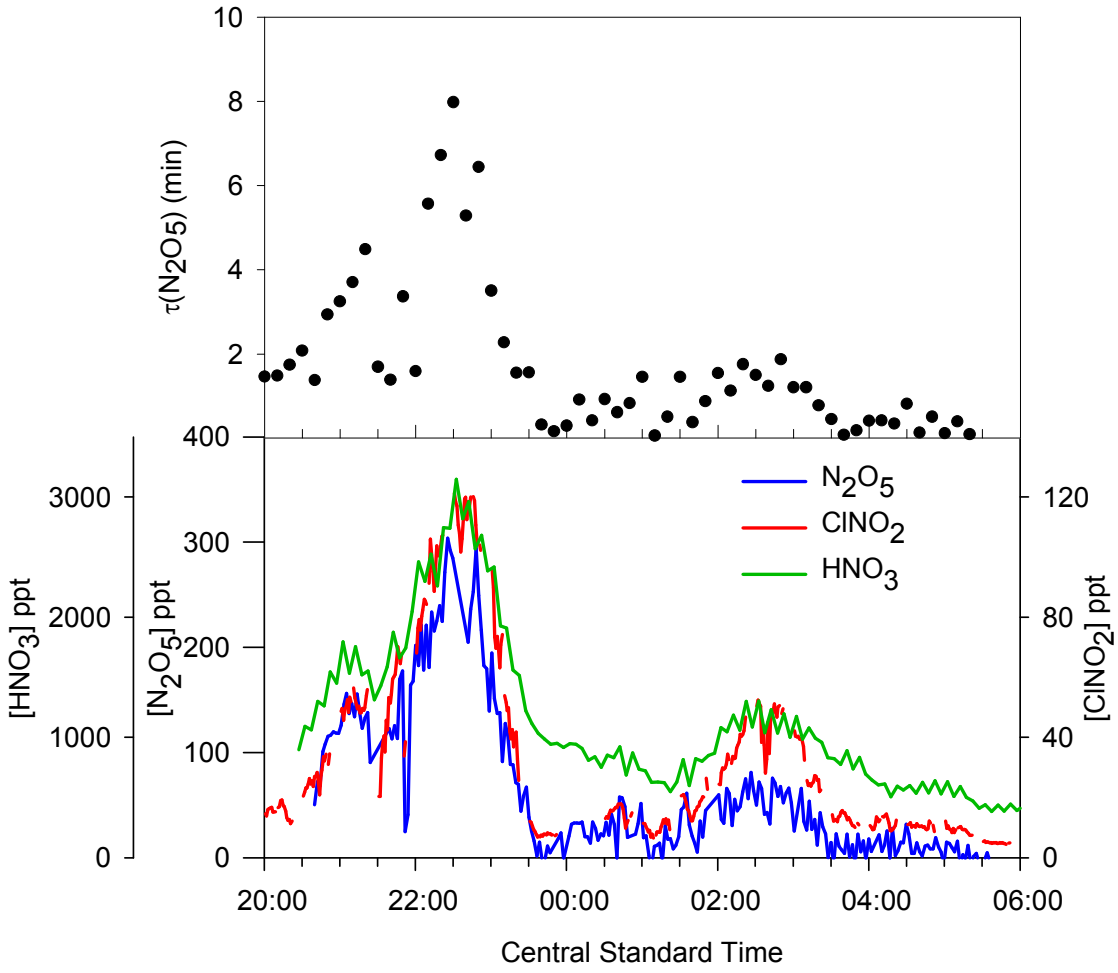

Figure 3.32. Comparison of N_2O_5 atmospheric lifetime and observed mixing ratios of N_2O_5, HNO_3, and $ClNO_2$ on 19-20 May 2009.

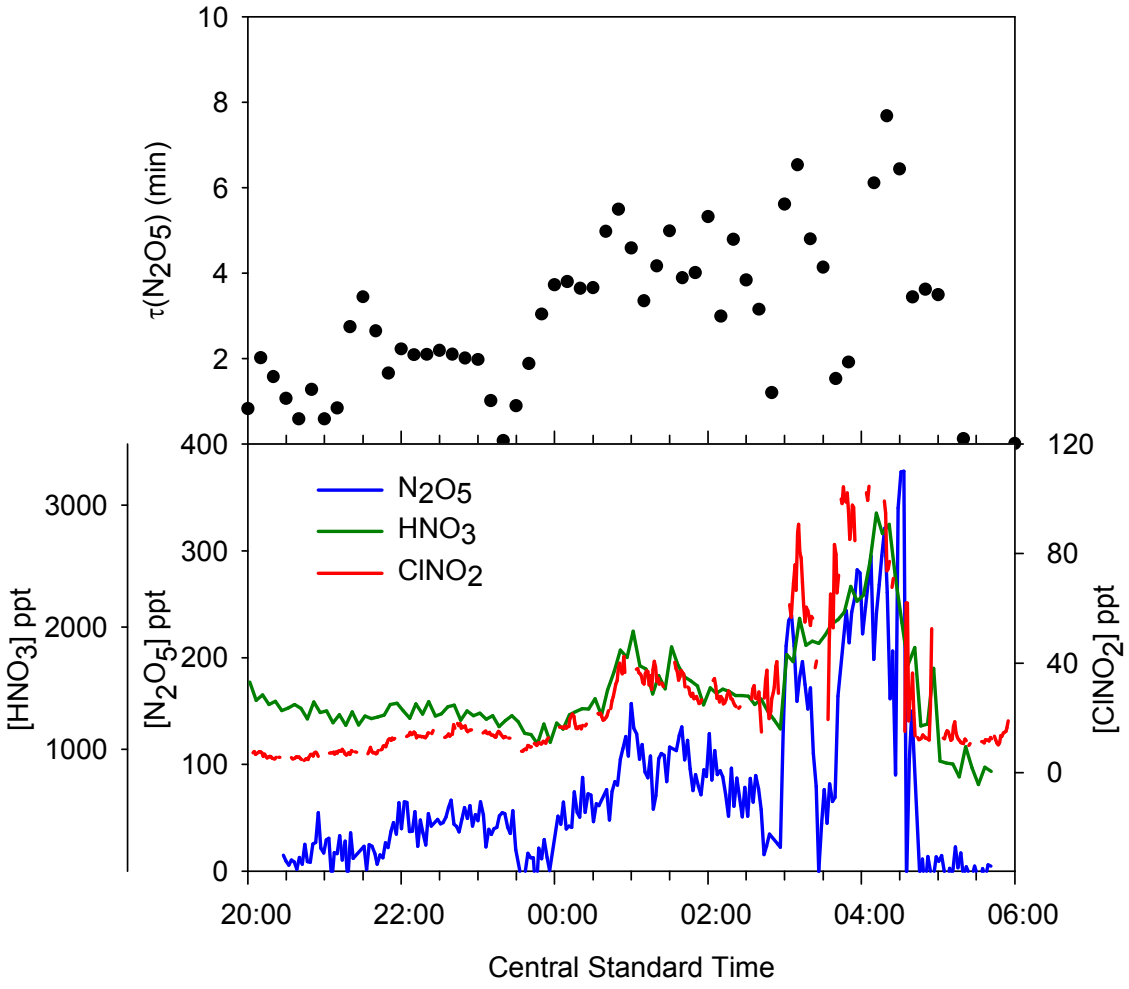

Figure 3.33. Comparison of N_2O_5 atmospheric lifetime and observed mixing ratios of N_2O_5, HNO_3, and $ClNO_2$ on 29-30 May 2009.

As shown in Figure 3.32 and 3.33, the atmospheric lifetime of N_2O_5 throughout both nights discussed exhibits very similar profiles to N_2O_5, HNO_3, and $ClNO_2$ concentrations. As the calculation of the lifetime is dependent on the source terms of N_2O_5, and nitric acid and nitryl chloride are both N_2O_5 sinks, the agreement between these three species is expected. It is also of note that the HNO_3/N_2O_5 ratio decreased while the N_2O_5 atmospheric lifetime increased at the night progressed on 19-20 May 2009. This is predicted, as a faster heterogeneous hydrolysis of N_2O_5 is indicated by a large HNO_3/N_2O_5 ratio and would result in a short atmospheric lifetime. While expected, this is significant because the calculation of the lifetime relies on source concentrations whereas the ratio relies on sink concentrations. Having the ability to calculate from both sources and sinks was an advantage during this study, and the fact that the results of both calculations are analogous provides an increase in the confidence of the measurements.

III.10 Comparisons Between 19-20 May and 29-30 May

It is significant that opposite profiles in both measured N_2O_5 mixing ratio and atmospheric lifetime were observed on the nights of 19-20 May and 29-30 May on Moody Tower. On 19 May, large concentrations of N_2O_5 were observed initially in the early evening and generally decreased throughout the night. In contrast to this, on 29 May, N_2O_5 was measured in low concentrations during the beginning of the night and gradually increased in concentration until sunrise. This signifies that there is no general or expected profile for N_2O_5, and is concentration is completely dependent on the specific chemistry of a certain day. Depending on the ozone and NO_X emissions, the N_2O_5 concentration will be highly variable.

III.11 Conclusions from SHARP Campaign

The SHARP field study in 2009 was the first successful deployment of the TAMU CRDS system for the measurement of N_2O_5 in a national and well-represented field campaign. While the instrument collected a significant amount of N_2O_5 data, the experiment was unsuccessful in regard to obtaining NO_3 measurements. Improvements must be made in this area in order to make simultaneous NO_3 and N_2O_5 measurements.

It is worth noting that the percentage of N_2O_5 compared to total NO_X never exceeded two percent at night throughout the entire measurement campaign, and was typically less than one percent. This indicates that a relatively small fraction of total NO_X is at any one point within the N_2O_5-NO_3 equilibrium. It was shown that N_2O_5 provides the dominant mechanism for the nighttime removal of NO_X, which then requires then a fast processing of nocturnal nitrogen.

It was also determined that there is up to a 20 percent difference in the calculated steady-state and non-steady-state atmospheric lifetime of N_2O_5 as observed during the study, and that this difference in greatest when the N_2O_5 concentration is large. This could be an indication that a steady-state equilibrium is not established between N_2O_5 and NO_3 in the Houston area when NO_X and ozone concentrations are high. It is, however, necessary to perform direct, simultaneous measurements of both NO_3 and N_2O_5 in order to be certain. The large concentration of ambient particulates common in Houston can also be a contribution to the fast processing of N_2O_5 and therefore NO_X.

CHAPTER IV

ANALYSIS OF NOCTURNAL NITROGEN CHEMISTRY IN RURAL TEXAS

IV.1 Motivation

Lick Creek Park is a public park in the city of College Station in central Texas, and has been the focus of several atmospheric chemistry studies by Texas A&M University. Although a rural area, this location is known for having poorer than expected air quality due to urban outflow from Houston or a high background ozone level when the wind direction is from the north [*Schaede*, 2010]. The current ozone NAAQS is scheduled to be decreased in the summer of 2011 by the EPA. This will possibly result in ozone exceedance days in the Brazos Valley as a result of urban outflow from the Houston area. Currently, there are efforts to determine the difference in the chemistry occurring in College Station in relation to more well-studied, urban areas.

Previous studies of N_2O_5 in rural areas have shown concentrations ranging from 0-150 ppt, and typically averaging 20-30 ppt [*Ayers and Simpson*, 2006; *Nakayama et al.*, 2008; *Wood et al.*, 2005]. Measurements of N_2O_5 in rural areas can be difficult because concentrations are often low and near or below the instrumental detection limit. Higher sensitivity is often achieved by increasing the integration time of data collection which in turn sacrifices temporal resolution.

IV.2 Site Description

The measurement trailer was located in south College Station, TX in the Equestrian Parking Lot of Lick Creek Park (30° 34’ 23.5” N, 96° 12’ 55.44” W). College Station is a rural location in eastern central Texas approximately 100 km northwest of Houston, TX and 150 km east of Austin, TX. The area was chosen due to its close proximity to Texas A&M University along with the availability of measurement space and electrical power. The location of Lick Creek Park within the state of Texas is shown in Figure 4.1.

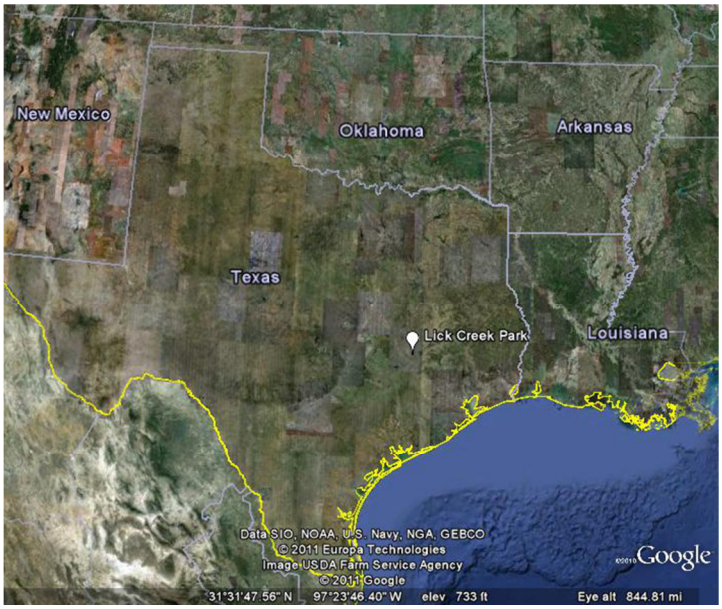

Figure 4.1. Location of the measurement site, Lick Creek Park, in eastern central Texas.

Figure 4.2. Measurement trailer located in the Equestrian Parking Lot of Lick Creek Park in College Station, TX.

Figure 4.3. The measurement trailer located in Lick Creek Park in College Station, TX.

As shown in Figures 4.2 and 4.3, the measurement trailer was located in a rural area within the equestrian parking lot. This was separate from the main entrance and parking lot, and was used solely by the researchers involved in the study and rarely park guests with horse trailers. The park is located on a low traffic road in a mainly residential and ranch area, and the trailer was set approximately 30 m from the road. The low traffic in the area should not produce a significant amount of local emissions to affect the measurements.

The park itself is little developed, and contains only several cleared dirt hiking trails. There are a significant number of post oak trees in the area, and it is assumed that a high level of isoprene and other biogenic VOC emissions are present. However, these levels have not been measured.

IV.3 Instrument and Sampling Description

The TAMU CRDS instrument was located at Lick Creek Park for approximately a one year time period from Fall 2009 to Fall 2010.Measurements were performed for over 80 days throughout this time period, and days were chosen based on meteorological conditions and current ozone levels. The instrument was located at the rear wall of the measurement trailer, as seen in Figure 4.4, with inlet ports cut through the wall facing northeast. A 0.125 in I.D. FEP Teflon inlet line with a length of 5.5 m was employed for the CRDS instrument. Temperature regulation was important within the measurement trailer as there is a large ambient temperature change throughout the year. Both heating and cooling systems were present in the trailer, and care was taking to carefully insulate the sampling lines with fiberglass insulation. Additionally, both the main inlet and the

ambient temperature cell had to be heated to prevent water condensation when the ambient temperature exceeded the indoor temperature. This was accomplished by using fiberglass heat tape and Variac controllers. Typically, the inlet and ambient temperature cell were kept 3-4 °C warmer than ambient to ensure there was no water condensation.

Figure 4.4. The TAMU CRDS instrument located at the rear wall of the measurement trailer in Lick Creek Park.

Ambient measurements of ozone, nitrogen dioxide, and nitric oxide were also performed at the measurement site simultaneously. Two commercially available NO_X and ozone analyzers (ThermoFisher Scientific, 42*i* and 49*i*) were housed in the measurement trailer alongside the CRDS instrument and are pictured in Figure 4.5. These instruments were both calibrated prior to deployment at the Lick Creek Park site, and the data monitored for abnormalities. Values for ozone, NO, and total NO_x were recorded every minute as observed by the instruments.

Figure 4.5. The NO_x and ozone analyzers located in the measurement trailer at Lick Creek Park.

Figure 4.6. Sampling inlets for the NO_X and ozone analyzers in addition to the CRDS instrument.

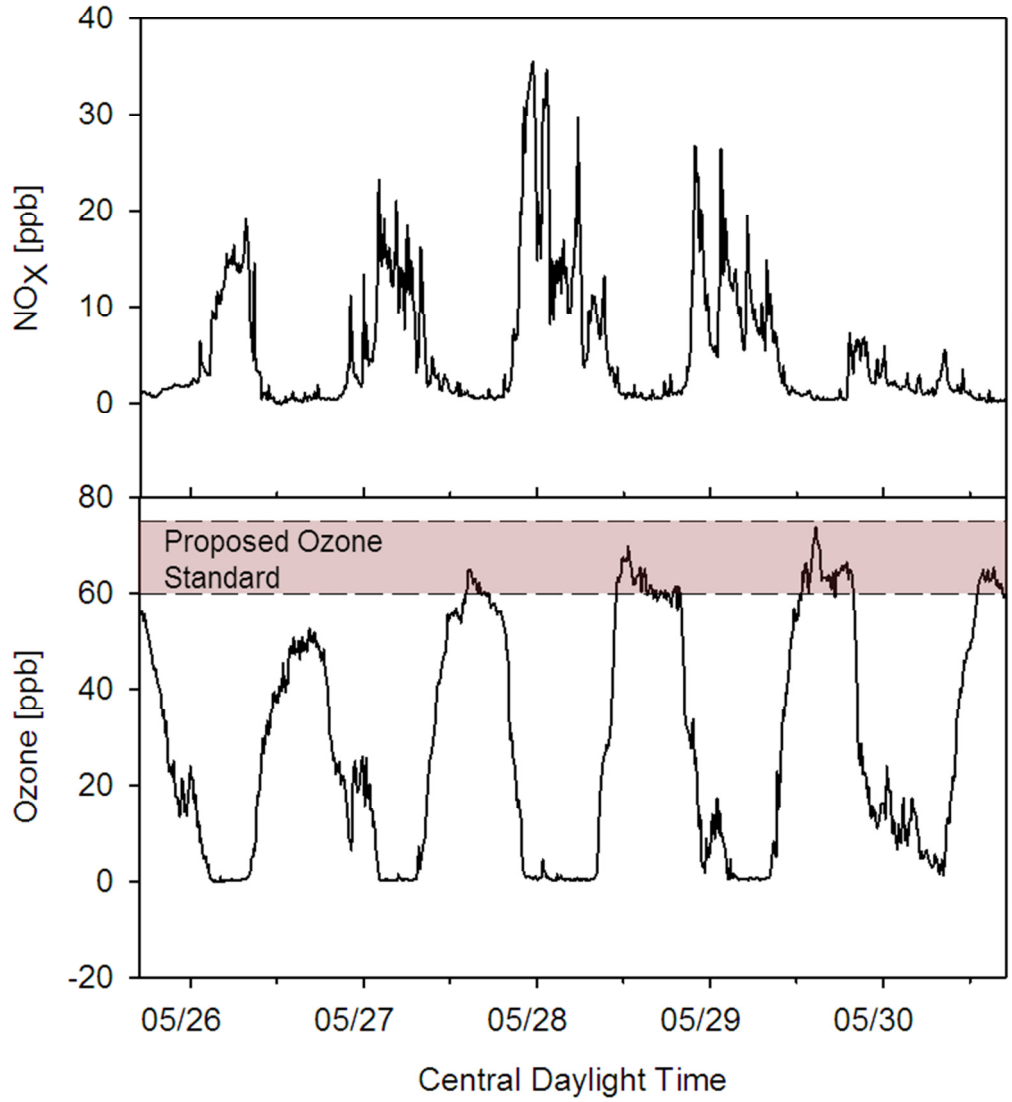

Figure 4.7. Measurements of NO_x and ozone at the Lick Creek Park site from 26-30 May 2010.

While the NO_x, ozone, and CRDS instruments each had their own sampling inlet line, the three lines were positioned immediately adjacent to each other on the same conduit support. The three inlets are shown in Figure 4.6, along with the FEP Teflon funnels (Welch Fluorocarbon) that were used to shield the inlet from rain and prevent

moisture from entering the system. Originally, the three sampling lines were placed at a height corresponding to the roof of the trailer; however, this was problematic for two reasons. First, there were additional research groups occupying the measurement site, and their equipment involved two large acrylic sampling chambers that were placed in front of the trailer. A chained link fence was erected around the chambers because of security issues. However, the location of the fencing and chambers prevented free air from reaching the CRDS sampling inlets and caused recirculation of air from the ground, chamber, and trailer walls. This would make an artificial bias in the measurement as both ozone and N_2O_5 are very reactive on the metal fence and trailer surface. Secondly, after several security issues occurred in the park, a floodlight was installed on the trailer near the sampling inlet. Because measurements are performed at night, this would attract a significant number of insects and beetles that would often be entrapped by the instrument flow thus contaminating the system. Both of these problems were rectified by extending the height of the inlets to approximately 4 ft above the height of the trailer and 12 ft from the ground.

Measurements of NO_x and ozone from 26-30 May 2010 at the Lick Creek Park site are shown in Figure 4.7. This was atypically high concentrations for this area as a result of high level of background ozone travelling from the Houston area. Ozone concentrations exceeded 60 ppb and could possibly result in an ozone exceedance of the NAAQS with the proposed lowering of the standard to 60-75 ppb in the summer of 2011.

IV.4 Observations of N_2O_5 and Atmospheric Lifetime

N_2O_5 was only observed a few days over the one year measurement period, and never for length of an entire night. The instrument detection limit was calculated to range from 2 to 10 ppt, indicating that levels of N_2O_5 in the College Station area are extremely low.

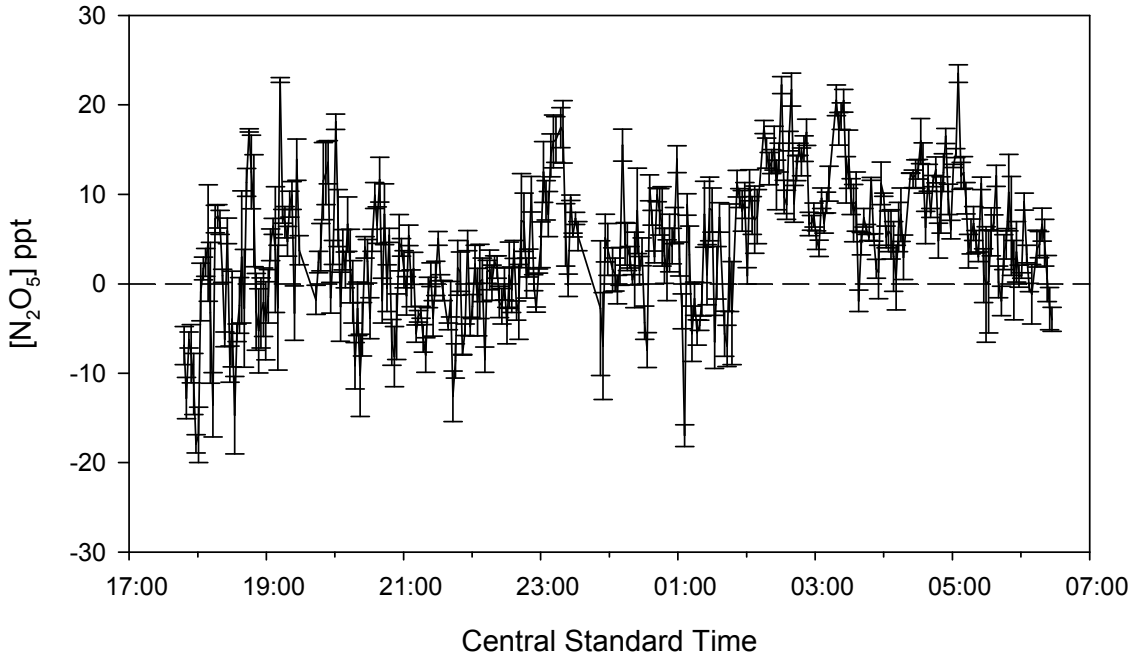

Figure 4.8. N_2O_5 observed at Lick Creek Park on 10-11 November 2009 showing the uncertainty in the measurement.

Observed N_2O_5 mixing ratios for the night of 10-11 November 2009 are shown in Figure 4.8. Because of the low levels, a 100 shot, or 10 s, average of the data was calculated resulting in an average uncertainty for the night of 2.2 ppt. However, given the maximum concentration observed of 20 ppt, this still results in a poor signal-to-noise ratio. Until approximately 23:00, there was no N_2O_5 observed consistently that cannot be

distinguished from the instrument noise. N_2O_5 was observed for approximately 30 min between 23:00 and 23:30 at a maximum concentration of 16.12 ± 2.57 ppt. There was little statistically significant data observed until approximately 01:45 when N_2O_5 was measured for several hours until 05:30. During this time the concentration ranged from 2-20 ppt and reached a maximum for the night of 23.50 ± 0.99 ppt at 05:05.

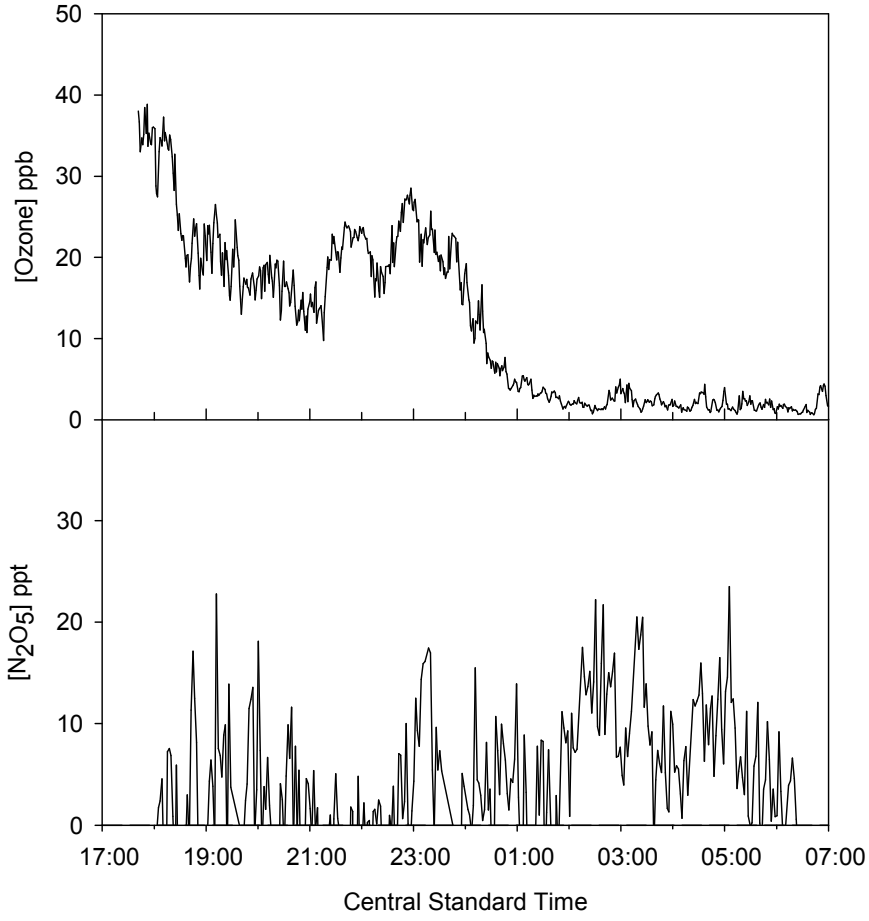

Figure 4.9. Measured N_2O_5 and ozone at Lick Creek Park on 10-11 November 2009.

The ozone concentration on this night, compared with observed N_2O_5 in Figure 4.9, was shown to follow a typical nighttime trend. Decreasing concentrations were seen after sundown reaching values below the instrument detection limit in the early morning hours. No obvious correlation is seen with the N_2O_5 measurements, however with low N_2O_5 concentrations observed trends are difficult to discern. Unfortunately, the NO_x analyzer was undergoing repairs at this time and NO_2 data from Lick Creek Park is therefore unavailable.

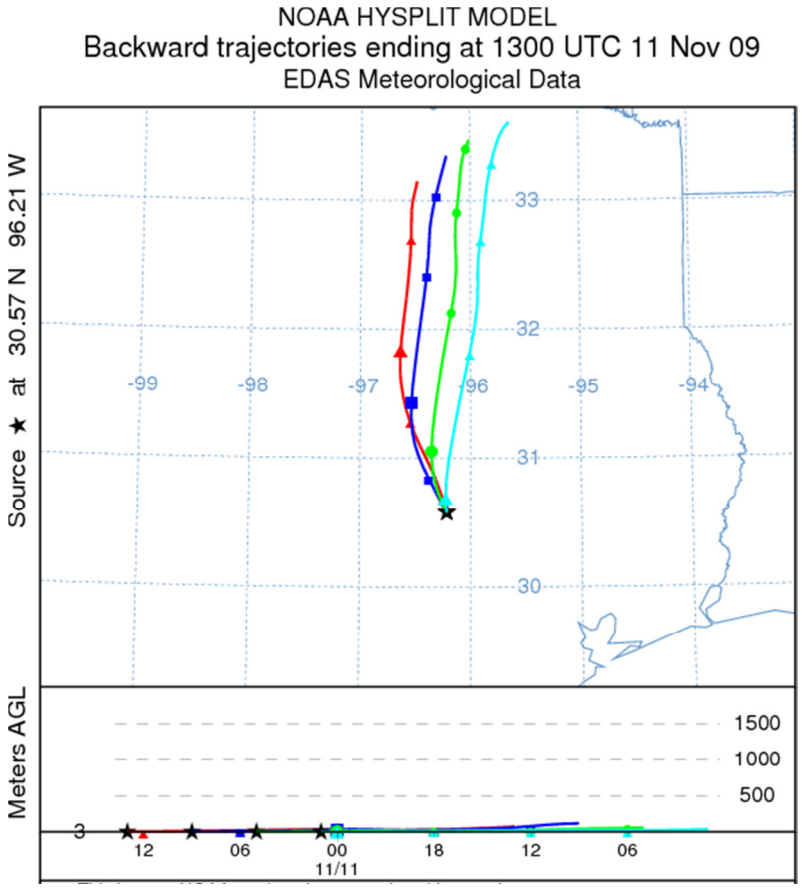

Figure 4.10. NOAA HYSPLIT backward trajectory for Lick Creek Park. Trajectories shown are 24-hour simulations for air arriving at the measurement site at 20:00 Nov 10, 00:00, 04:00, and 08:00 Nov 11 CST (01:00, 05:00, 09:00, and 13:00 UTC). Markers indicate six-hour time intervals.

Analysis was performed to determine any correlations between meteorological conditions and the measured species. 24-hour backward air trajectories were simulated using the NOAA HYSPLIT model with the EDAS data set and the results are shown in Figure 4.10 [*Draxler and Rolph*, 2011; *Rolph*, 2011]. The model specifies a similar trajectory and point of origin for air arriving throughout the course of the night and indicates that similar emission sources in all paths.

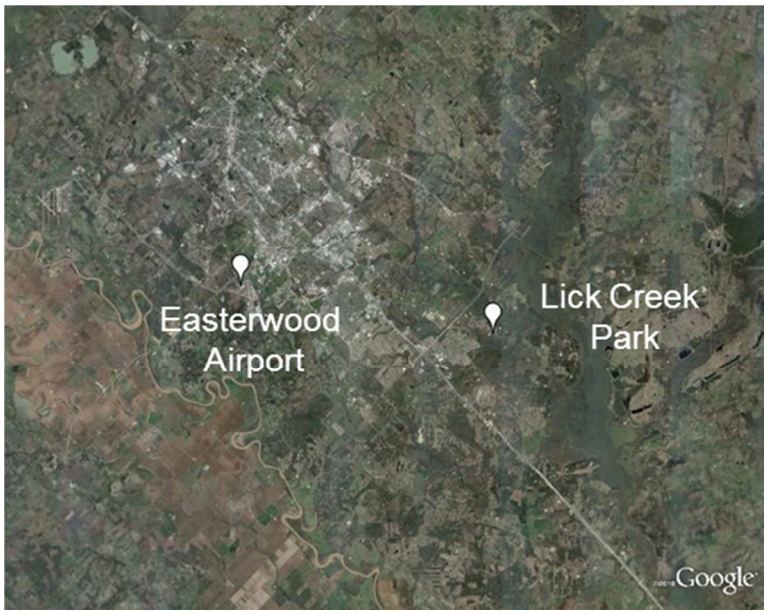

Figure 4.11. Location of Easterwood Airport relative to the measurement site approximately 14.75 km to the east.

Because wind direction and wind speed data were not available at the measurement site, the N_2O_5 concentration had been compared to the wind direction and wind speed measured at Easterwood Airport located approximately 14.75 km to the west. The location of the airport relative to Lick Creek Park is shown in Figure 4.11. The

monitoring station at Easterwood Airport is maintained by The National Weather Service (NWS). Wind speed and direction is averaged and recorded for one hour time periods by the NWS.

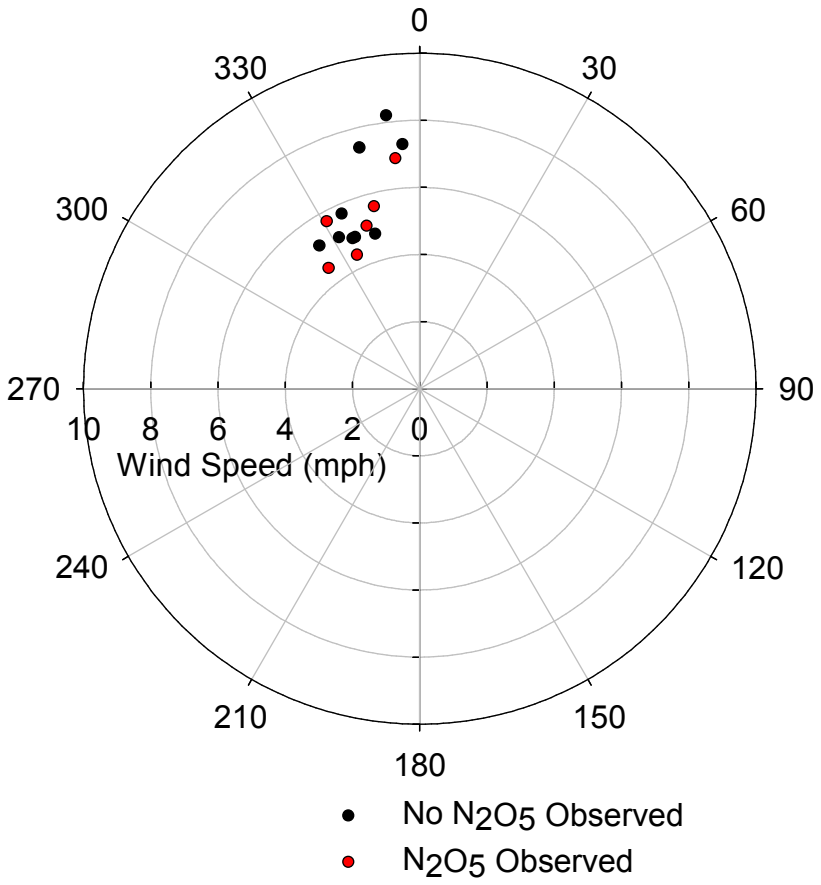

Figure 4.12. The wind speed and direction at Easterwood Airport on the night of 10-11November 2009 compared to the presence of N_2O_5 indicated by color.

As shown in Figure 4.12, the wind speed and direction was relatively consistent for the night of November 10-11, 2009 with no clear correlations to N_2O_5 presence. The criteria for whether N_2O_5 was present were determined through if N_2O_5 was observed for at least 50 percent of the 1 hour period of wind measurements.

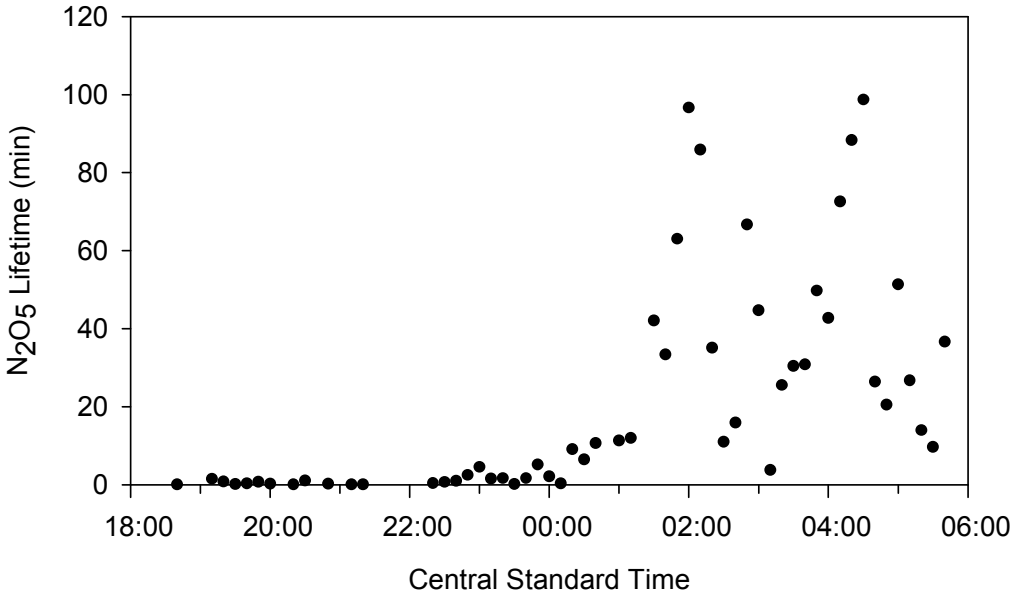

Figure 4.13. Atmospheric lifetime measurements for N_2O_5 from the night of 10-11 November 2009.

Similar to the lifetime measurements presented in Chapter III, the lifetime was calculated for N_2O_5 on the evening of 10-11 November 2009 and results are shown in Figure 4.13. Nitrogen dioxide data from the TCEQ monitoring site in Huntsville, TX was used for the purpose of calculations. Data before 00:00 is not valid given the lack of measurements, however the time period from approximately 01:30 to 05:30 gives some indication of the N_2O_5 atmospheric lifetime. While there was a lot of variation, the lifetime ranged from several minutes up to 100 minutes, which is consistent with other measurements in more rural areas [*McLaren et al.*, 2004; *Nakayama et al.*, 2008; *Wood et al.*, 2005]. The longer lifetime observed in College Station than Houston could also indicate that the presence of heterogeneous water on aerosols is lower in the Central Texas region.

IV.5 Implications and Future Measurements

The Lick Creek Park study was met with limited success in measuring N_2O_5, as there were only a handful of days over a one year measurement period in which N_2O_5 was observed. Improvements must be made to the detection limit of the instrument in order to consistently observe N_2O_5. However, considering the detection limit of the instrument ranged from 2-10 ppt throughout the course of the study, it is now established that the concentration N_2O_5 in the College Station area is extremely low. Even if N_2O_5 had been measured, it would be difficult to observe trends when the values are so small. It may also be advantageous to extend the height of the sampling inlet to avoid surface interactions and be at a more favorable height in the N_2O_5 vertical profile.

It is possible that the large quantity of post oak trees, and therefore biogenic emissions, in the area are creating a large NO_3 sink and shifting the equilibrium of NO_3 with N_2O_5. Nitrate radical has been shown to react quickly ($k=7x10^{-13}$ cm^3 $molecule^{-1}$ s^{-1}) with isoprene leading to secondary organic aerosol formation [*Ng et al.*, 2008]. Ambient measurements have shown a decline in the concentration after sunset, and some studies have attributed this to reaction with NO_3 [*Steinbacher et al.*, 2005; *Stroud et al.*, 2002]. This could explain the lack of observation of N_2O_5 and the presumed very low mixing ratios. However, previous measurements of N_2O_5 in rural areas were reported at appreciable concentrations averaging between 20-30 ppt [*McLaren et al.*, 2004; *Nakayama et al.*, 2008; *Simpson*, 2003; *Wood et al.*, 2005]. It would be necessary to measure isoprene and possibly other VOCs at the Lick Creek site in order to determine the effect of biogenic emissions.

CHAPTER V

CONCLUSIONS

V.1 Conclusions from Laboratory and Field Measurements

This dissertation represents the calibration and characterization as well as field measurements of N_2O_5 performed with the Texas A&M cavity ring-down spectrometer. The instrument was calibrated and characterized to ensure the quantitative measurement of N_2O_5. A system was developed for the automatic titration of the ambient gas with NO for accurate background measurements. This was integrated with the data collection software to ensure the accurate recording of the timing. The instrument flow was well characterized to determine the length of time it takes the sample to reach the detection axis. As NO_3 is an extremely reactive species, its losses on the sampling inlet and instrument walls were determined through simultaneous measurements with a known concentration of solid synthesized N_2O_5.

Measurements during the SHARP field study were successful in quantizing concentrations of N_2O_5 in the Houston area. Elevated mixing ratios of N_2O_5 exceeding 300 ppt were observed on days following atypical ozone events in Houston. The concentration was shown to be strongly dependent on both the wind speed and direction, and was shown to have strong correlations with both HNO_3 and $ClNO_2$. This is suggestive of a fast hydrolysis of N_2O_5 on aerosol particles that are known to be abundant in the Houston area. Short atmospheric lifetimes of N_2O_5 ranging from several

seconds to several minutes were calculated, agreeing with the suggestion of fast reaction on aerosols.

The Lick Creek Park measurements in College Station were only of limited success. N_2O_5 was only observed on several occasions in low concentrations only reaching approximately 20 ppt. This was in agreement with several published rural N_2O_5 studies, and could possibly be due a large amount of biogenic emissions in the area shifting the equilibrium between NO_3 and N_2O_5. The atmospheric lifetime was much longer than observed in Houston, ranging up to several hours and indicating a smaller number of N_2O_5 sinks.

V.2 Future Directions

There are still many improvements to be made to the TAMU CRDS system. One major goal is the full automation of the instrument. We have developed an automatic filter changer to replace the Teflon filter on the inlet on the instrument. The filter changer has been programmed and integrated with the data collection software and has been tested in the laboratory. However, it is still necessary to develop a way to stop instrument flow in the event of the failure of the filter. Unfiltered air entering the instrument will introduce aerosols to the detection cavities, creating additional reactive losses and contaminating the system. There is also the risk of sharp particles damaging the cell mirrors. Because the start and stop of the instrument flow is not currently integrated into the software, a technique to control this with the computer must be determined before the filter changer can safely be used. The instrument cannot be operated without a researcher present until a filter failure mechanism is present.

Improvements are also needed for simultaneous NO_3 detection. It is still unknown as to whether the lack of NO_3 measurements is due to the instrument sensitivity or poor sampling techniques. The extent of laboratory measurements performed indicate that we are not falsely under calculating the NO_3 detection limit, so further investigation into the sampling techniques is needed. It is possible that the sampling inlet has been placed too close to the structures housing the instrument, and therefore it may be necessary to extend the inlet height or employ and sampling tower.

The dependence of the N_2O_5concentration on the wind speed observed in Houston, TX during the SHARP campaign is suggestive of higher concentrations of N_2O_5 further downwind of the measurement site. It would be interesting to perform N_2O_5 measurements in other locations father from the Houston Ship Channel to determine the evolution of source compounds over a longer length of time.

We would also like to further investigate the differences on NO_x losses in urban and rural areas. As very low concentrations of N_2O_5 were observed in the College Station area, it is desirable to measure VOC concentrations and determine the effect of NO_3-initiated oxidation on the equilibrium between NO_3 and N_2O_5. We are interested in seeing if we are able to model the NO_3 and N_2O_5 losses in order to estimate the concentration and atmospheric lifetime of N_2O_5 below the instrumental detection limit.

REFERENCES

Alicke, B., A. Geyer, A. Hofzumahaus, F. Holland, S. Konrad, H. W. Patz, J. Schafer, J. Stutz, A. Volz-Thomas, and U. Platt (2003), OH formation by HONO photolysis during the BERLIOZ experiment, *J. Geophys. Res.-Atmos.*, *108*(D4).

Allan, B. J., J. M. C. Plane, H. Coe, and J. Shillito (2002), Observations of NO_3 concentration profiles in the troposphere, *J. Geophys. Res.-Atmos.*, *107*(D21).

Allen, D., M. Estes, J. Smith, and H. Jeffries (2001), Accelerated science evaluation of ozone formation in the Houston-Galveston area, *Report of the Texas Comission for Environmental Quality,* Retrieved at http://www.utexas.edu/research/ceer/.

Asaf, D., E. Tas, D. Pedersen, M. Peleg, and M. Luria (2010), Long-term measurements of NO_3 radical at a semiarid urban site: 2. Seasonal trends and loss mechanisms, *Environ. Sci. Technol.*, *44*(15), 5901-5907.

Atkinson, D. B. (2003), Solving chemical problems of environmental importance using cavity ring-down spectroscopy, *Analyst*, *128*(2), 117-125.

Atkinson, R. (2000), Atmospheric chemistry of VOCs and NO_x, *Atmospheric Environment*, *34*(12-14), 2063-2101.

Atkinson, R., D. L. Baulch, R. A. Cox, J. N. Crowley, R. F. Hampson, R. G. Hynes, M. E. Jenkin, M. J. Rossi, and J. Troe (2004), Evaluated kinetic and photochemical data for atmospheric chemistry: Volume 1 - gas phase reactions of O_X, HO_X, NO_X, and SO_X species, *Atmospheric Chemistry and Physics*, *4*(6), 1461-1738.

Ayers, J. D., and W. R. Simpson (2006), Measurements of N_2O_5 near Fairbanks, Alaska, *J. Geophys. Res.*, *111*(D14), D14309.

Benton, A. K., J. M. Langridge, S. M. Ball, W. J. Bloss, M. Dall'Osto, E. Nemitz, R. M. Harrison, and R. L. Jones (2010), Night-time chemistry above London: Measurements of NO_3 and N_2O_5 from the BT Tower during REPARTEE-II, *Atmospheric Chemistry and Physics*, *10*(20), 9781-9795.

Bertram, T. H., and J. A. Thornton (2009), Toward a general parameterization of N_2O_5 reactivity on aqueous particles: The competing effects of particle liquid water, nitrate and chloride, *Atmospheric Chemistry and Physics*, *9*(21), 8351-8363.

Bertram, T. H., J. A. Thornton, T. P. Riedel, A. M. Middlebrook, R. Bahreini, T. S. Bates, P. K. Quinn, and D. J. Coffman (2009), Direct observations of N_2O_5 reactivity on ambient aerosol particles, *Geophysical Research Letters*, *36*.

Brasseur, G. P., J. J. Orlando, and G. S. Tyndall (1999), *Atmospheric Chemistry and Global Change*, Oxford University Press, New York.

Brown, S. S., H. Stark, S. J. Ciciora, and A. R. Ravishankara (2001), In-situ measurement of atmospheric NO_3 and N_2O_5 via cavity ring-down spectroscopy, *Geophysical Research Letters*, *28*(17), 3227-3230.

Brown, S. S., H. Stark, S. J. Ciciora, R. J. McLaughlin, and A. R. Ravishankara (2002a), Simultaneous *in situ* detection of atmospheric NO_3 and N_2O_5 via cavity ring-down spectroscopy, *Review of Scientific Instruments*, *73*(9), 3291-3301.

Brown, S. S., H. Stark, and A. R. Ravishankara (2002b), Cavity ring-down spectroscopy for atmospheric trace gas detection: Application to the nitrate radical (NO_3), *Applied Physics B*, *75*(2-3), 173-182.

Brown, S. S., H. Stark, and A. R. Ravishankara (2003a), Applicability of the steady-state approximation to the interpretation of atmospheric observations of NO_3 and N_2O_5, *Journal of Geophysical Research*, *108*(D17), 4359.

Brown, S. S., H. Stark, T. B. Ryerson, E. J. Williams, D. K. N. Jr., M. Trainer, F. C. Fehsenfeld, and A. R. Ravishankara (2003b), Nitrogen oxides in the nocturnal boundary layer: Simultaneous in situ measurements of NO_3, N_2O_5, NO_2, NO, and O_3, *Journal of Geophysical Research*, *108*(D9), 4299-4310.

Brown, S. S. (2003), Absorption spectroscopy in high-finesse cavities for atmospheric studies, *Chem. Rev.*, *103*(12), 5219-5238.

Brown, S. S., J. E. Dibb, H. Stark, M. Aldener, M. Vozella, S. Whitlow, E. J. Williams, B. M. Lerner, R. Jakoubek, A. M. Middlebrook, J. A. DeGouw, C. Warneke, P. D. Goldan, W. C. Kuster, W. M. Angevine, D. T. Sueper, P. K. Quinn, T. S. Bates, J. F. Meagher, F. C. Fehsenfeld and A. R. Ravishankara (2004), Nighttime removal of NOx in the summer marine boundary layer, *Geophysical Research Letters*, *31*(7).

Brown, S. S., T. B. Ryerson, A. G. Wollny, C. A. Brock, R. Peltier, A. P. Sullivan, R. J. Weber, W. P. Dube, M. Trainer, J. F. Meagher, F. C. Fehsenfeld and A. R. Ravishankara (2006), Variability in nocturnal nitrogen oxide processing and its role in regional air quality, *Science*, *311*(5757), 67-70.

Brown, S. S., W. P. Dubé, H. D. Osthoff, D. E. Wolfe, W. M. Angevine, and A. R. Ravishankara (2007a), High resolution vertical distributions of NO_3 and N_2O_5 through the nocturnal boundary layer, *Atmospheric Chemistry and Physics*, *7*(1), 139-149.

Brown, S. S., W. P. Dubé, H. D. Osthoff, J. Stutz, T. B. Ryerson, A. G. Wollny, C. A. Brock, C. Warneke, J. A. de Gouw, E. Atlas, J. A. Neuman, J. S. Holloway, B. M. Lerner, E. J. Williams, W. C. Kuster, P. D. Goldan, W. M. Angevine, M. Trainer, F. C. Fehsenfeld and A. R. Ravishankara (2007b), Vertical profiles of NO_3 and N_2O_5 measured from aircraft: Results from the NOAA P-3 and surface platforms during the New England Air Quality Study 2004, *Journal of Geophysical Research*, *112*(D22304).

Brown, S. S., W. P. Dube, H. Fuchs, T. B. Ryerson, A. G. Wollny, C. A. Brock, R. Bahreini, A. M. Middlebrook, J. A. Neuman, E. Atlas, J. M. Roberts, H. D. Osthoff, M. Trainer, F. C. Fehsenfeld and A. R. Ravishankara (2009), Reactive uptake coefficients for N_2O_5 determined from aircraft measurements during the Second Texas Air Quality Study: Comparison to current model parameterizations, *J. Geophys. Res.-Atmos.*, *114*.

Cantrell, C. A., J. A. Davidson, R. E. Shetter, B. A. Anderson, and J. G. Calvert (1987), The temperature invariance of the NO_3 absorption cross-section in the 662-nm region, *Journal of Physical Chemistry*, *91*(23), 5858-5863.

Chang, W. L., P. V. Bhave, S. S. Brown, N. Riemer, J. Stutz, and D. Dabdub (2011), Heterogeneous Atmospheric Chemistry, Ambient Measurements, and Model Calculations of N_2O_5: A Review, *Aerosol Sci. Technol.*, *45*(6), 655-685.

Crowley, J. N., G. Schuster, N. Pouvesle, U. Parchatka, H. Fischer, B. Bonn, H. Bingemer, and J. Lelieveld (2010), Nocturnal nitrogen oxides at a rural mountain-site in south-western Germany, *Atmospheric Chemistry and Physics*, *10*(6), 2795-2812.

Dentener, F. J., and P. J. Crutzen (1993), Reaction of N_2O_5 on tropospheric aerosols - Impact on the global distributions of NO_X, O_3, and OH *J. Geophys. Res.-Atmos.*, *98*(D4), 7149-7163.

Doran, J. C., C. M. Berkowitz, R. L. Coulter, W. J. Shaw, and C. W. Spicer (2003), The 2001 Phoenix sunrise experiment: Vertical mixing and chemistry during the morning transition in Phoenix, *Atmospheric Environment*, *37*(17), 2365-2377.

Draxler, R. R., and G. D. Rolph (2011), HYSPLIT (HYbrid Single-Particle Langrangian Intergrated Trajectory) Model access via NOAA ARL READY Website (http://ready.arl.noaa.gov/HYSPLIT.php). NOAA Air Resources Laboratory, Silver Spring, MD.

Dubé, W. P., S. S. Brown, H. D. Osthoff, M. R. Nunley, S. J. Ciciora, M. W. Paris, R. J. McLaughlin, and A. R. Ravishankara (2006), Aircraft instrument for simlutaneous, *in situ* measurement of NO_3 and N_2O_5 via pulsed cavity ring-down spectroscopy, *Review of Scientific Instruments*, *77*(3), 034101.

Evans, M. J., and D. J. Jacob (2005), Impact of new laboratory studies of N_2O_5 hydrolysis on global model budgets of tropospheric nitrogen oxides, ozone, and OH, *Geophysical Research Letters*, *32*(9).

Finlayson-Pitts, B. J., and J. N. Pitts (1999), *Chemistry of the Upper and Lower Atmosphere: Theory, Experiments, and Applications*, Academic Press, San Diego, CA.

Finlayson-Pitts, B. J., L. M. Wingen, A. L. Sumner, D. Syomin, and K. A. Ramazan (2003), The heterogeneous hydrolysis of NO_2 in laboratory systems and in outdoor and indoor atmospheres: An integrated mechanism, *Physical Chemistry Chemical Physics*, *5*(2), 223-242.

Fish, D. J., D. E. Shallcross, and R. L. Jones (1999), The vertical distribution of NO_3 in the atmospheric boundary layer, *Atmospheric Environment*, *33*(5), 687-691.

Fuchs, H., W. P. Dubé, S. J. Ciciora, and S. S. Brown (2008), Determination of Inlet Transmission and Conversion Efficiencies for in Situ Measurements of the Nocturnal Nitrogen Oxides, NO_3, N_2O_5, and NO_2, via Pulsed Cavity Ring-Down Spectroscopy, *Analytical Chemistry*, *80*(15), 6010-6017.

Geyer, A., and J. Stutz (2004), Vertical profiles of NO_3, N_2O_5, O_3, and NO_x in the nocturnal boundary layer: 2. Model studies on the altitude dependence of composition and chemistry, *Journal of Geophysical Research*, *109*, D12307.

Griffiths, P. T., C. L. Badger, R. A. Cox, M. Folkers, H. H. Henk, and T. F. Mentel (2009), Reactive uptake of N_2O_5 by aerosols containing dicarboxylic acids. Effect of particle phase, composition, and nitrate content, *J. Phys. Chem. A*, *113*(17), 5082-5090.

Hallquist, M., D. J. Stewart, S. K. Stephenson, and R. A. Cox (2003), Hydrolysis of N_2O_5 on sub-micron sulfate aerosols, *Physical Chemistry Chemical Physics*, *5*(16), 3453-3463.

Hanson, D. R., and A. R. Ravishankara (1991), The reaction probabilities of $ClONO_2$ and N_2O_5 on 40-percent to 75-percent sulfuric acid solutions, *J. Geophys. Res.-Atmos.*, *96*(D9), 17307-17314.

Heard, D. E. (2006), *Analytical Techniques for Atmospheric Measurements*, Blackwell Publishing, Oxford, UK.

Herbelin, J. M., J. A. McKay, M. A. Kwok, R. H. Ueunten, D. S. Urevig, D. J. Spencer, and D. J. Benard (1980), Sensitive measurement of photon lifetime and true reflectances in an optical cavity by a phase-shift method, *Appl. Optics*, *19*(1), 144-147.

Huey, L. G. (2007), Measurement of trace atmospheric species by chemical ionization mass spectrometry: Speciation of reactive nitrogen and future directions, *Mass Spectrometry Reviews*, *26*, 166-184.

Ide, T., T. Nakayama, K. Takahashi, and Y. Matsumi (2008), Thermal decomposition rate of N_2O_5 measured by cavity ring-down spectroscopy, *International Journal of Chemical Kinetics*, *40*(10), 679-684.

Kercher, J. P., T. P. Riedel, and J. A. Thornton (2009), Chlorine activation by N_2O_5: Simultaneous, in situ detection of $ClNO_2$ and N_2O_5 by chemical ionization mass spectrometry, *Atmospheric Measurement Techniques*, *2*(1), 193-204.

Kim, B. S., P. L. Hunter, and H. S. Johnston (1992), NO_3 radical studied by laser-induced fluorescence, *J. Chem. Phys.*, *96*(6), 4057-4067.

Marinelli, W. J., D. M. Swanson, and H. S. Johnston (1982), Absorption cross-sections and line-shape for the NO_3 (0-0) band, *J. Chem. Phys.*, *76*(6), 2864-2870.

Matsumoto, J., N. Kosugi, H. Imai, and Y. Kajii (2005), Development of a measurement system for nitrate radical and dinitrogen pentoxide using a thermal conversion/laser-induced fluorescence technique, *Review of Scientific Instruments*, *76*(6), 064101-064101-11.

McLaren, R., R. A. Salmon, J. Liggio, K. L. Hayden, K. G. Anlauf, and W. R. Leaitch (2004), Nighttime chemistry at a rural site in the Lower Fraser Valley, *Atmospheric Environment*, *38*(34), 5837-5848.

McLaren, R., P. Wojtal, D. Majonis, J. McCourt, J. D. Halla, and J. R. Brook (2010), NO_3 radical measurements in a polluted marine environment: Links to ozone formation, *Atmospheric Chemistry and Physics*, *10*(9), 4187-4206.

Mentel, T. F., M. Sohn, and A. Wahner (1999), Nitrate effect in the heterogeneous hydrolysis of dinitrogen pentoxide on aqueous aerosols, *Physical Chemistry Chemical Physics*, *1*(24), 5451-5457.

Morris, E. D., and H. Niki (1973), Reaction of dinitrogen pentoxide with water, *Journal of Physical Chemistry*, *77*(16), 1929-1932.

Mozurkewich, M., and J. G. Calvert (1988), Reaction probability of N_2O_5 on aqueous aerosols, *J. Geophys. Res.-Atmos.*, *93*(D12), 15889-15896.

Nakayama, T., T. Ide, F. Taketani, M. Kawai, K. Takahashi, and Y. Matsumi (2008), Nighttime measurements of ambient N_2O_5, NO_2, NO, and O_3 in a sub-urban area, Toyokawa, Japan, *Atmospheric Environment*, *42*, 1995-2006.

Ng, N. L., A. J. Kwan, J. D. Surratt, A. W. H. Chan, P. S. Chhabra, A. Sorooshian, H. O. T. Pye, J. D. Crounse, P. O. Wennberg, R. C. Flagan and J. H. Seinfeld (2008), Secondary organic aerosol (SOA) formation from reaction of isoprene with nitrate radicals (NO_3), *Atmospheric Chemistry and Physics*, *8*(14), 4117-4140.

Noxon, J. F., R. B. Norton, and W. R. Henderson (1978), Observation of atmospheric NO_3, *Geophysical Research Letters*, *5*(8), 675-678.

O'Keefe, A., and D. A. G. Deacon (1988), Cavity ring-down optical spectrometer for absorption measurements using pulsed laser sources, *Review of Scientific Instruments*, *59*(12), 2544-2551.

Orphal, J., C. E. Fellows, and P. M. Flaud (2003), The visible absorption spectrum of NO_3 measured by high-resolution Fourier transform spectroscopy, *J. Geophys. Res.-Atmos.*, *108*(D3), 4077.1-4077.11.

Osthoff, H. D., M. J. Pilling, A. R. Ravishankara, and S. S. Brown (2007), Temperature dependence of the NO_3 absorption cross-section above 298 K and determination of the equilibrium constant for $NO_3 + NO_2 \leftrightarrow N_2O_5$ at atmospherically relevant conditions, *Physical Chemistry Chemical Physics*, *9*(43), 5785-5793.

Osthoff, H. D., J. M. Roberts, A. R. Ravishankara, E. J. Williams, B. M. Lerner, R. Sommariva, T. S. Bates, D. Coffman, P. K. Quinn, J. E. Dibb, H. Stark, J. B. Burkholder, R. K. Talukdar, J. Meagher, F. C. Fehsenfeld and S. S. Brown (2008), High levels of nitryl chloride in the polluted subtropical marine boundary layer, *Nat. Geosci.*, *1*(5), 324-328.

Parrish, D. D., D. T. Allen, T. S. Bates, M. Estes, F. C. Fehsenfeld, G. Feingold, R. Ferrare, R. M. Hardesty, J. F. Meagher, J. W. Nielsen-Gammon, R. B. Pierce, T. B. Ryerson, J. H. Seinfeld and E. J. Williams (2009), Overview of the Second Texas Air Quality Study (TexAQS II) and the Gulf of Mexico Atmospheric Composition and Climate Study (GoMACCS), *J. Geophys. Res.-Atmos.*, *114*.

Platt, U. F., D. Perner, G. W. Harris, A. M. Winer, and J. N. Pitts (1980), Observations of nitrous acid in an urban atmosphere by differential optical absorption, *Nature*, *285*(5763), 312-314.

Platt, U. F., A. M. Winer, H. W. Biermann, R. Atkinson, and J. N. Pitts (1984), Measurement of nitrate radicals in continental air, *Environ. Sci. Technol.*, *18*(5), 365-369.

Ravishankara, A. R., and E. R. Lovejoy (1994), Atmospheric lifetime, its application and its determination - CFC-substitutes as a case-study, *J. Chem. Soc.-Faraday Trans.*, *90*(15), 2159-2169.

Riemer, N., H. Vogel, B. Vogel, B. Schell, I. Ackermann, C. Kessler, and H. Hass (2003), Impact of the heterogeneous hydrolysis of N_2O_5 on chemistry and nitrate aerosol formation in the lower troposphere under photosmog conditions, *J. Geophys. Res.-Atmos.*, *108*(D4), 4414.1-4414.21.

Robinson, G. N., D. R. Worsnop, J. T. Jayne, C. E. Kolb, and P. Davidovits (1997), Heterogeneous uptake of $ClONO_2$ and N_2O_5 by sulfuric acid solutions, *J. Geophys. Res.-Atmos.*, *102*(D3), 3583-3601.

Rolph, G. D. (2011), Real-time Environmental applications and display system (READY) Website (http://ready.arl.noaa.gov). NOAA Air Resources Laboratory, Silver Spring, MD.

Russell, A. G., G. J. McRae, and G. R. Cass (1985), The dynamics of nitric acid production and the fate of nitrogen oxides, *Atmospheric Environment*, *19*(6), 893-903.

Ryerson, T. B., M. Trainer, J. S. Holloway, D. D. Parrish, L. G. Huey, D. T. Sueper, G. J. Frost, S. G. Donnelly, S. Schauffler, E. L. Atlas, W. C. Kuster, P. D. Goldan, G. Hubler, J. F. Meagher and F. C. Fehsenfeld (2001), Observations of ozone formation in power plant plumes and implications for ozone control strategies, *Science*, *292*(5517), 719-723.

Sander, S. P. (1986), Temperature dependence of the NO_3 absorption spectrum, *Journal of Physical Chemistry*, *90*(17), 4135-4142.

Sander, S. P., A. R. Ravishankara, D. M. Golden, C. E. Kolb, M. J. Kurylo, M. J. Molina, G. K. Moortgat, B. J. Finlayson-Pitts, P. H. Wine, and R. E. Huie (2006), Chemical kinetics and photochemical data for use in atmospheric studies, *JPL Publication 06-2*.

Schaede, G. (2010), *Personal Communication*.

Scherer, J. J., J. B. Paul, A. Okeefe, and R. J. Saykally (1997), Cavity ringdown laser absorption spectroscopy: History, development, and application to pulsed molecular beams, *Chem. Rev.*, *97*(1), 25-51.

Scheuer, E., R. W. Talbot, J. E. Dibb, G. K. Seid, L. DeBell, and B. Lefer (2003), Seasonal distributions of fine aerosol sulfate in the North American Arctic basin during TOPSE, *J. Geophys. Res.*, *108*(D4), 8370.

Simpson, W. R. (2003), Continuous wave cavity ring-down spectroscopy applied to in situ detection of dinitrogen pentoxide (N_2O_5), *Review of Scientific Instruments*, *74*(7), 3442-3452.

Singh, H. B., M. Kanakidou, P. J. Crutzen, and D. J. Jacob (1995), High concentrations and photochemical fate of oxygenate hydrocarbons in the global troposphere, *Nature*, *378*(6552), 50-54.

Singh, H. B., L. Salas, D. Herlth, R. Kolyer, E. Czech, M. Avery, J. H. Crawford, R. B. Pierce, G. W. Sachse, D. R. Blake, R. C. Cohen, T. H. Bertram, A. Perring, P. J. Wooldridge, J. Dibb, G. Huey, R. C. Hudman, S. Turquety, L. K. Emmons, F. Flocke, Y. Tang, G. R. Carmichael and L. W. Horowitz (2007), Reactive nitrogen distribution and partitioning in the North American troposphere and lowermost stratosphere, *J. Geophys. Res.-Atmos.*, *112*(D12).

Slusher, D. L., L. G. Huey, D. J. Tanner, F. M. Flocke, and J. M. Roberts (2004), A thermal dissociation - chemical ionization mass spectrometry (TD-CIMS) technique for the simultaneous measurement of peroxyacyl nitrates and dinitrogen pentoxide, *J. Geophys. Res.*, *109*(D19), D19315.

Snyder, J. A., D. Hanway, J. Mendez, A. J. Jamka, and F. M. Tao (1999), A density functional theory study of the gas-phase hydrolysis of dinitrogen pentoxide, *J. Phys. Chem. A*, *103*(46), 9355-9358.

Stark, H., B. M. Lerner, R. Schmitt, R. Jakoubek, E. J. Williams, T. B. Ryerson, D. T. Sueper, D. D. Parrish, and F. C. Fehsenfeld (2007), Atmospheric in situ measurement of nitrate radical (NO_3) and other photolysis rates using spectroradiometry and filter radiometry, *J. Geophys. Res.-Atmos.*, *112*(D10).

Steinbacher, M., J. Dommen, C. Ordonez, S. Reimann, F. Gruebler, J. Staehelin, S. Andreani-Aksoyoglu, and A. S. H. Prevot (2005), Volatile organic compounds in the Po Basin. Part B: Biogenic VOCs, *J. Atmos. Chem.*, *51*(3), 293-315.

Stroud, C. A., J. M. Roberts, E. J. Williams, D. Hereid, W. M. Angevine, F. C. Fehsenfeld, A. Wisthaler, A. Hansel, M. Martinez-Harder, H. Harder, W. H. Brune, G. Hoenninger, J. Stutz and A. B. White (2002), Nighttime isoprene trends at an urban forested site during the 1999 Southern Oxidant Study, *J. Geophys. Res.-Atmos.*, *107*(D16).

Stull, R. B. (1988), *An Introduction to Boundary Layer Meteorology*, 666 pp., Kluwer Academic Press, Dordrecht, The Netherlands.

Stutz, J., B. Alicke, R. Ackermann, A. Geyer, A. White, and E. Williams (2004), Vertical profiles of NO_3, N_2O_5, O_3, and NO_x in the nocturnal boundary layer: 1. Observations during the Texas Air Quality Study 2000, *Journal of Geophysical Research*, *109*, D12306.

Stutz, J., K. W. Wang, L. Lawrence, L. Ziemba, J. H. Flynn, B. Rappenglück, and B. Lefer (2009), Nocturnal NO_3 radical chemistry in Houston, TX, *Atmospheric Environment*, *44*(33), 4099-4106.

Talbot, R. W., A. S. Vijgen, and R. C. Harriss (1990), Measuring tropospheric HNO_3 - problems and prospects for nylon filter and mist chamber techniques, *J. Geophys. Res.-Atmos.*, *95*(D6), 7553-7561.

Vallance, C. (2005), Innovations in cavity ringdown spectroscopy, *New J. Chem.*, *29*(7), 867-874.

Wahner, A., T. F. Mentel, M. Sohn, and J. Stier (1998), Heterogeneous reaction of N_2O_5 on sodium nitrate aerosol, *J. Geophys. Res.-Atmos.*, *103*(D23), 31103-31112.

Wang, S., R. Ackermann, and J. Stutz (2006), Vertical profiles of O-3 and NOx chemistry in the polluted nocturnal boundary layer in Phoenix, AZ: I. Field observations by long-path DOAS, *Atmospheric Chemistry and Physics*, *6*, 2671-2693.

Wängberg, I., T. Etzkorn, I. Barnes, U. Platt, and K. H. Becker (1997), Absolute determination of the temperature behavior of the $NO_2+NO_3+(M)\leftrightarrow N_2O_5+(M)$ equilibrium, *J. Phys. Chem. A*, *101*(50), 9694-9698.

Wayne, R. P., I. Barnes, P. Biggs, J. P. Burrows, C. E. Canosamas, J. Hjorth, G. Lebras, G. K. Moortgat, D. Perner, G. Poulet, G. Restelli and H. Sidebottom (1991), The nitrate radical - physics, chemistry, and the atmosphere, *Atmospheric Environment Part a-General Topics*, *25*(1), 1-203.

Wood, E. C., P. J. Wooldridge, J. H. Freese, T. Albrecht, and R. C. Cohen (2003), Prototype for in situ detection of atmospheric NO_3 and N_2O_5 via laser-induced fluorescence, *Environ. Sci. Technol.*, *37*(24), 5732-5738.

Wood, E. C., T. H. Bertram, P. J. Wooldridge, and R. C. Cohen (2005), Measurements of N_2O_5, NO_2, and O_3 east of the San Francisco Bay, *Atmospheric Chemistry and Physics*, *5*, 483-491.

Yokelson, R. J., J. B. Burkholder, R. W. Fox, R. K. Talukdar, and A. R. Ravishankara (1994), Temperature dependence of the NO_3 absorption spectrum, *Journal of Physical Chemistry*, *98*(50), 13144-13150.

Zheng, J., et al. (2008), Measurements of HNO_3 and N_2O_5 using ion drift-chemical ionization mass spectrometry during the MILAGRO/MCMA-2006 campaign, *Atmospheric Chemistry and Physics*, *8*(22), 6823-6838.

VITA

Name:	Justine Nicole Geidosch
Address:	Texas A&M University, Department of Chemistry, Mail Stop 3255, College Station, TX 77843
Email Address:	jgeidosch@chem.tamu.edu
Education:	B.S., Chemistry, Duquesne University, 2006 Ph.D., Chemistry, Texas A&M University, 2011